Increased sensitivity for lateral flow immunoassays through signal amplification methods

Koji Abe

A dissertation

submitted in partial fulfillment of the

requirements for the degree of

Doctor of Philosophy

University of Washington

2018

Reading Committee:

Paul Yager, Chair

Xiaohu Gao

Daniel Ratner

Program Authorized to Offer Degree:

Bioengineering

University of Washington

Abstract

Increased sensitivity for lateral flow immunoassays through signal amplification methods

Koji Abe

Chair of the Supervisory Committee:
Professor Paul Yager
Bioengineering

The simple and inexpensive sandwich-immunoassay-based lateral flow tests (LFTs, also known as lateral flow immunoassays, LFIAs, and rapid diagnostic tests, RDTs) are one of the general approaches for detection of disease targets (e.g. nucleoprotein of the influenza virus). However, the use of these LFTs is limited because of their well-recognized lack of sensitivity. To improve the sensitivity of LFTs for influenza diagnosis while maintaining a simple and rapid assay procedure, we proposed signal enhancement methods of antigen detection using three approaches: (1) increasing the absorbance of gold nanoparticles using gold enhancement and silver enhancement solutions, (2) enzymatic creation and precipitation of visible dyes, and (3) nucleic acid amplification test (NAAT)-based signal enhancement. Using the enzymatic amplification-based detection, we developed a prototype of a point-of-care (POC) device

including a dry conjugate pad and the assay sensitivity was compared with a commercially available kit. Since reagent delivery format is also a key factor to improve the sensitivity, we investigated two formats: premixed and sequential delivery. An improved reagent delivery format achieved better assay sensitivity. To elucidate the underlying mechanism related to the reagent delivery format, a preliminary model using experimental data was developed to predict assay performance and potential minimum limit of detection (LOD). Finally, to further improve the sensitivity, we developed a NAAT-based protein detection method (i.e. immuno-NAAT) that can be performed on nitrocellulose. These methods were demonstrated using the assay stack for influenza nucleoprotein as a model analyte. The NAAT-based method showed ~10,000-fold better LOD compared to conventional gold nanoparticle-based LFT; this is the first study of immuno-NAAT performed on nitrocellulose, which is a feasible platform for POC diagnostics.

TABLE OF CONTENTS

LIST OF FIGURES

LIST OF TABLES

ACKNOWLEDGEMENTS

This work would not have been possible without the support and advice provided by Professor Paul Yager, who was the principal investigator of the whole project and the primary supervisor for the work as a PhD student in the Department of Bioengineering at the University of Washington. I faced challenging situations a few times as both a graduate and an international student that led to the delay of my research, but Professor Yager always helped me with his generosity. In addition to his scientific prowess, creativity and curiosity, I have been inspired by how he managed the whole group and project.

I also appreciate my supervisory committee members, Professors Mark Wener, Xiaohu Gao, and Daniel Ratner, for their support and feedback on my research. Their thoughtful guidance was critical throughout this process.

I would like to thank our collaborators for their work throughout the projects. Dr. Gonzalo Domingo and Lindsay Yokobe at PATH played critical roles in the Flu Project to provide us lateral flow strips and key information for signal quantification of gold nanoparticle-based assays. Dr. Janet Englund at Seattle Children's Hospital helped us to collect any of the real patient nasal swab samples to test our assay. Dr. Eva-Maria Strauch at the Baker lab supported measurement of the binding kinetics of antibodies and analyte that were used for assay development. Dr. Elain Fu generously provided us a preliminary mathematical model to apply to our influenza immunoassay to elucidate underlying mechanisms related to the reagent delivery

format. The ELITech group provided us lateral flow strips and reagents that were critical to develop the LFT-iSDA as our first study of immuno-NAAT on nitrocellulose.

I am also appreciative of all members of the Yager, Lutz, and Fu labs for their support and friendship. I had the pleasure of working on the projects with all members, particularly: Professors Elain Fu and Barry Lutz, Peter Kauffman (our communication in Japanese was special for me), Sujatha Kumar, Dr. Paula Ladd, Dr. Joshua Bishop, Dr. Erin Heiniger, Dr. Bhushan Toley, Dr. Xiaohong Zhang, Dr. Shichu Huang, Dr. Gina Fridley, Dr. Carly Holstein, Dr. Samantha Byrnes, Dr. Joshua Buser, Enos Kline, Steven Bennett, Tinny Liang, Caitlin Anderson, Kamal Shah, Dylan Guelig, Nuttada Panpradist, and Philip Lee. I would also like to thank Chelsea Musick for the operations of the administrative and financial aspects of the lab.

Research reported in this paper was supported by National Institute of Allergy and Infectious Diseases of the National Institutes of Health under award number 1R0-1AI096184, by the Defense Threat Reduction Agency under award number HDTRA1-16-C-0029, and by an award to KA from the Japan Student Services Organization. The content is solely the responsibility of the authors and does not necessarily represent the official views of the National Institutes of Health or the Defense Threat Reduction Agency.

Last but not least, I would like to thank to my friends and family for the many years of support. Especially, I would like to give the greatest appreciation to my parents and brother, who were there whenever I needed them.

DEDICATION

To my family. Thank you for being my biggest supporter.

1 INTRODUCTION

1.1 SIGNIFICANCE OF PROBLEM

Sandwich-immunoassay-based lateral flow tests (LFTs, also known as lateral flow immunoassays, LFIAs, and rapid diagnostic tests, RDTs) are currently used in low-resource point-of-care (POC) settings because of their characteristics including low-cost, rapid time to result, and being equipment-free.[1–3] In the context of influenza diagnosis, however, the performance of these tests has been limited because of the lack of sensitivity ranging from 50% to 70% compared to laboratory-based detection methods.[4] This relatively low sensitivity is due to limited development capabilities and budgets that are consequences of their low cost and primary use in low-resource settings, resulting in relatively low revenue generation.[5] Therefore, the sensitivity of LFTs should be improved for more accurate disease management while maintaining their cost and simplicity advantages.

1.2 PROPOSED SOLUTION

Given the poor performance of influenza LFTs, we aimed to improve the sensitivity of an influenza A nucleoprotein assay using two approaches: signal amplification by an enhanced optical absorbance-based detection method and nucleic acid amplification test (NAAT)-based method. We also investigated reagent delivery formats to achieved better sensitivity of the assay. A preliminary mathematical model was developed to predict assay performance and the assay's potential minimum limit of detection (LOD).

1.3 SUMMARY OF SPECIFIC AIMS

The proposed work has been divided into three specific aims. A summary of each aim is described below.

1.3.1 Specific Aim 1: Improve LOD by Signal Amplification Methods

We aim to improve LOD over commercially-available conventional gold nanoparticle-based assay by comparing existing methods: enzymatic creation and precipitation of visible dyes and increasing absorbance of gold nanoparticles. For the latter method, we used gold enhancement and silver enhancement solutions.

1.3.2 Specific Aim 2: Investigate Reagent Delivery Format

We aim to improve LOD of the lateral flow immunoassay by optimizing reagent delivery format. The premixed and sequential reagent delivery formats showed different LODs, which could be due to different binding kinetic constants of analyte and antibodies in the assay. In addition, for elucidating the underlying mechanism and predicting the behavior of the system, a preliminary model using experimental data was developed.

1.3.3 Specific Aim 3: Improve LOD through iSDA ("LFT-iSDA")

We aim to further improve the LOD of LFTs by a NAAT-based amplification method, isothermal strand displacement amplification (iSDA). Proof of concept of this "LFT-iSDA" was demonstrated on nitrocellulose membranes. To reduce nonspecific signals, which lead to false positives, we demonstrated washing and blocking strategies to minimize the occurrence of false positives in the LFT-iSDA assay. This is the first study of immuno-NAAT demonstrated on a

nitrocellulose membrane; the LFT-iSDA for influenza A nucleoprotein detection was ~10,000-fold more sensitive than the conventional LFT.

2 BACKGROUND

2.1 POINT-OF-CARE DIAGNOSTICS

2.1.1 Criteria for Point-of-Care Diagnostics

Point-of-care (POC) tests provide rapid diagnoses and are fundamental to disease management since appropriate treatments cannot be offered until the cause of diseases has been recognized. Recent studies described many definitions of POC tests. The most commonly used definition of a POC test has three key features, which differ from conventional laboratory tests.[6,7] First, POC tests do not require sophisticated laboratory infrastructures and well-trained staff to be utilized. Second, they are easy to use and interpret for the user. Third, they can provide a rapid diagnosis, commonly within 1 hour. Since POC tests need less sophisticated apparatus and skills compared to traditional laboratory tests, cost-effectiveness is another important key feature.[8] Especially in low-resource settings, lack of human resources and laboratory infrastructures could limit the accessibility of diagnostic tests because they are often too expensive for clinicians and patients.[6,8] To make therapeutic decisions in such settings, POC tests can play a critical role to provide key information with easier methods and fewer supplies.[9] POC tests are beneficial also in developed countries because they can decrease the time between sample collection and diagnosis, which is significant for disease management including treatment, isolation, and hospitalization.[10]

2.1.2 Current Point-of-Care Diagnostics

2.1.2.1 Nucleic acid amplification tests

Nucleic acid amplification tests (NAATs) have been used for the detection of one or more DNA or RNA sequences related to a pathogen.[11] Polymerase chain reaction (PCR)-based techniques and isothermal NAAT techniques are recently available as POC tests.[12] The use of PCR-based

techniques is limited in low-resource settings because they requires a certain apparatus and electrical power to achieve 30 to 40 cycles of heating to ~72°C. Assay time is usually between 20 and 100 min.[6] For POC tests, reverse transcription PCR (RT-PCR) is commonly used. Loop-mediated isothermal amplification (LAMP) is an alternative method that can be performed at a constant temperature of about 60°C. Since LAMP does not require a thermocycler, it makes NAATs more feasible for POC tests.[13] Higher sensitivity compared to immunochromatographic tests (ICTs) is one of the advantages of NAATs.

The GeneXpert from Cepheid, which uses a disposable cartridge with a permanent instrument for NAATs, would be the biggest success in global health diagnostics since it has significantly assisted the diagnosis of tuberculosis (TB).[14] While the GeneXpert has significantly improved the speed of TB diagnosis, the instrument is too expensive (e.g. a four-module Xpert instrument purchased by the Foundation for Innovative New Diagnostic for the use at the hospital located outside Abuja's metropolitan area in Nigeria was about 17k USD, plus $10 for every disposable cartridge) to be used in low-resource settings.[14,15] Therefore, the GeneXpert has been used in centralized laboratories within developing countries.[16]

The Xpert Flu system automates the detection of influenza A/B from nasopharyngeal swabs stored in universal transfer media (UTM), which was reported in ~70 minutes[17], and now in half that time. Compared to manual laboratory-based qRT-PCR as a reference method, influenza A sensitivity was reported as 97.3% for the Cepheid Xpert Flu A assay and 62.2-71.6% for rapid immunoassay-based tests.[18]

2.1.2.2 Lateral flow tests

Lateral flow tests (LFTs) or ICTs have been used for rapid detection of specific microorganism antigens as POC diagnostics for several decades.[19] LFTs consist of porous wicking materials, typically paper-like membranes, made of materials such as nitrocellulose. LFTs rely on capillary wicking to transport samples and buffers, making the use of an external pumping system unnecessary. Since LFTs are easy to use, inexpensive, disposable, and require no external equipment, they are recognized as well-suited devices for POC.[20] Infectious diseases such as HIV, malaria, and influenza are well known applications of LFTs as well as home pregnancy tests and drug abuse tests.[6,19] Due to their low cost and ease of use, LFTs have been used for hospitals, emergency rooms, and low-resource clinics in the developing countries. Despite their success, their low sensitivity is one of the disadvantages that drives the need for more accurate POC tests.[19]

2.2 Optical Methods in Paper-Based Device

2.2.1 Absorbance-Based Labels

Chromophoric optical labels have been commonly used in LFTs. Especially, inexpensive and highly stable gold nanoparticles are widely used as typical chromophores.[21] Since gold nanoparticles selectively absorb light at specific wavelengths, they are used to show red lines against the white background of the porous nitrocellulose membrane in LFTs.[22] While most commercially available assays utilize chromophoric labels, the large particle size of these labels could lead to aggregation and nonspecific binding to nitrocellulose membrane under extreme pH or salt concentrations.[23] Thus, one of the disadvantages of these labels is low sensitivity.[21]

2.2.2 Luminescent Labels

Luminescent labels, such as fluorescent, phosphorescent, and chemiluminescent labels, are alternative labels to improve the sensitivity of LFTs.[21,24] Luminescent labels can improve signal-to-noise ratio when the background intensity of the membrane at the wavelengths of interest is very low.[19] Fluorescent labels that have been used in LFTs include organic fluorophores, quantum dots, and lanthanide chelates. Organic fluorophores have an issue of photobleaching, which could result in reduced sensitivity.[24] Quantum dots have unique electrical and optical properties. They are water soluble, compatible with biomolecules, and have high photostability and absorption coefficients.[21,24] Lanthanide chelates also have unique properties, such as long fluorescence lifetimes and large Stokes shifts. However, the use of lanthanide chelates is limited due to their weaker luminescence and photobleaching.[21] Phosphorescent labels also have the potential to improve the signal-to-noise ratio because of their larger Stokes shifts than many fluorescent labels. However, they require a specific reader and few potential labels have been studied.[25] Chemiluminescent labels can be utilized with enzymes to produce chemiluminescence. One of the advantages of chemiluminescent labels is that no illumination source is required. However, since sensitivity depends on enzyme substrate combination and specialized strip reader in a dark environment is required, the use of chemiluminescent labels is also limited in LFTs.[24,26]

This dissertation does not particularly include the luminescent-based LFT detection methods, but an assay using quantum dots was investigated in my side project collaborating with Kamal Shah and recently reported.[27]

2.2.3 Sensitivity Enhancements

To improve the assay sensitivity in porous membranes, several approaches have been investigated, including signal amplification.[28] For signal detection, the most common colored particles for colorimetric visualization are gold nanoparticles because of their low cost, optical properties, compatibility with biomolecules, and easily-modified surface chemistry. Many methods enhancing the optical absorption by gold nanoparticles have been demonstrated to improve the assay sensitivity in LFTs, including silver and gold staining to increase the particle diameter[28] and thermal contrast detection[29]. Specifically for influenza virus detection, some detection methods have been explored not only in LFTs, but also in more sophisticated systems. These systems included enzyme-linked immunosorbent assays (ELISA) with horseradish peroxidase (HRP) as the enzyme and 3, 3', 5, 5'-tetramethylbenzidine (TMB) as a chromogenic substrate to detect equine influenza A (H3N8 and H7N7) nucleoprotein[30] and influenza A virus (H5N1)[31]. ELISA was also demonstrated for influenza A (H3N2) detection using magnetic nanoparticles combined with nanobodies (antigen-binding antibody fragments).[32] However, these ELISA methods require a microplate reader to read the signals and multiple assay procedures under well-controlled temperature, resulting in long sample processing times. Fluorescent immunochromatographic strip tests (FICTs) to detect avian influenza A nucleoprotein (H5N3, H7N1, H7N7, and H9N2)[33] and avian influenza virus[34] were also reported. However, to make these fluorescence-based detection methods practically available, more inexpensive and convenient portable system would be required to take advantage of LFTs.

Our lab demonstrated enzyme-based signal amplification to detect a malarial biomarker as a POC application and showed potential for long-term dry storage of the required reagents: the

HRP-conjugated-antibody label and its colorigenic substrate diaminobenzidine (DAB).[35] In this amplification system, HRP can catalyze the oxidation of DAB in the presence of H_2O_2. The oxidized DAB precipitates at the detection region, which amplifies the signal. To demonstrate an automated ELISA for detection of a malarial biomarker, our lab incorporated dry reagents into a two-dimensional paper network format (2DPN).[35]

2.3 Current Paper-Based Diagnostic Platforms

2.3.1 Microfluidic Paper Analytical Devices (μPADs)

Novel paper-based diagnostic platforms have recently gained strong attention. The recent emergence of such platforms began with the work of George Whitesides' group.[36,37] Flow paths in μPADs were made using photolithography or wax printing to create hydrophobic barriers on cellulose substrates.[36,38] Three-dimensional μPADs were also developed by stacking multiple layers of porous membranes using adhesive materials.[39] One of the successful applications of μPADs is the liver enzyme test, which is applicable for field-testing.[40] However, most μPADs require cellulose membranes, which would not be suited for the use of biological affinity reagents that is commonly used with nitrocellulose. Also, multistep chemical or enzymatic reactions have been limited in μPADs applications.

2.3.2 Two-Dimensional Paper Networks (2DPNs)

Our lab developed two-dimensional paper networks (2DPNs) as another platform for paper-based diagnostic device. 2DPNs utilize shaped paper with multiple inlets to "program" multiple assay procedures while requiring only a single user activation step.[41] Therefore, the use of sequential delivery of assay reagents (e.g. for signal amplification) using 2DPNs would lead to highly sensitive RDTs in a simple and low-cost POC format; this could be made available even

homes and small clinics and resource-limited settings. Recently, the Richards-Kortum group demonstrated a 2DPN to sequentially deliver six reagents utilizing a streptavidin-biotin detection system for malarial biomarker detection.[42]

2.4 Influenza Diagnostics

2.4.1 Disease Burden of Influenza

Influenza is the cause of seasonal epidemics and pandemics. In the United States, seasonal influenza virus infections in human cause >200,000 hospitalizations and >30,000 influenza-associated deaths annually.[43] The annual national economic burden of influenza-related illness is ~$87.1 billion, with direct medical costs of $10.4 billion.[44] Influenza pandemics are rare; there have been four cases in the last 100 years.[45] Recently, the 2009 Influenza A (H1N1) pandemic resulted in an estimated worldwide mortality of 284,400 deaths, 51% of which occurred in Southeast Asia and Africa.[46] Given the ongoing seasonal influenza burden and the threat of future pandemics, the ability to accurately diagnose influenza is extremely important not only for the primary-care setting in developed countries, but also for low-resource settings.

2.4.2 Current Influenza Diagnostics

Sandwich immunoassay-based LFTs are currently used as an appropriate approach for use in low-resource POC settings because of their characteristics including low-cost, rapid time to result, and being equipment-free.[3] In the context of influenza diagnosis, costs of LFTs are about $15 to $20 per assay, which is much less expensive than the cost of NAATs, about $40 to $150 or more.[47,48] They are simple to use and mostly utilize porous membranes, typically nitrocellulose in LFTs, giving results in 15 to 30 minutes. In general, positive results by LFTs are correlated well with actual infection of influenza virus.[48] However, the performance of these

tests has been limited because of the lack of sensitivity ranging from 50% to 70% compared to laboratory-based detection methods (e.g. NAATs), while specificity normally exceeds 90%.[4] Therefore, the sensitivity of LFTs should be improved for more accurate disease management even though the Centers for Disease Control and Prevention (CDC) and the World Health Organization (WHO) still consider them as useful tools for clinical decision-making and outbreak management, especially in case that the laboratory-based detection methods are not easily available.[4,47,49]

2.5 Computational Modeling of Paper Microfluidics

2.5.1 Modeling of Sandwich Immunoassay

Mathematical and computational models have been used to predict the performance of conventional microfluidic devices.[50] Previous reports have focused on the investigation of an in-solution analyte, which directly binds to its binding partner immobilized on surface. They investigated the effects of flow rate and binding constants in pressure-driven flow systems.[51] Lateral flow sandwich immunoassays have also been investigated with modeling to predict binding signal for different analyte and label concentrations with a single set of binding rate constants.[52] More recently, tools and methods, including computational modeling, have been developed to improve LFT development and optimization process. [5,53,54]

2.5.2 Modeling of Reagent Delivery Formats

To improve the assay performance, the 2DPN platform allows customization of the reagent delivery format. Recently, the Fu group investigated two types of reagent delivery formats in a sandwich immunoassay for malarial protein detection: a “premixed format”, which is similar to what occurs in conventional LFTs, and in a “sequential delivery” of reagents, which is a feature

that the 2DPN can provide.[55] They demonstrated a lower LOD with the sequential format compared the premixed format, attributing the advantage to the multivalent binding sites on the malarial protein and detection antibodies. Their mathematical model of the assay reproduced the experimental binding profiles (the intensity of the color from the leading to the trailing edge of the capture lines). The model has the potential to improve the sensitivity by customizing the reagent delivery format optimal for the number of binding sites available.

2.6 IMMUNO-NAAT TECHNOLOGIES

2.6.1 Principle of Immuno-NAAT

An important example of a method to improve immunoassay sensitivity is immuno-NAAT, which was reported as early as 1992 as an approach that combines the advantages of immunoassays and NAAT-based method, PCR.[56–58] Typically, immuno-PCR uses a detection antibody conjugated to a DNA template that can be amplified by PCR. Reported immuno-PCR assays can be ~10-10^8 times more sensitive than traditional ELISAs, depending on the target protein.[57,58] However, PCR methods require distinct incubation temperatures for each of the cyclic denaturation, annealing, and elongation steps. These incubation temperatures are generally provided by a thermal cycler instrument; this requirement limits the use of immuno-PCR in low-resource settings as a POC diagnostic method.

2.6.2 Current Immuno-NAAT Technologies

One example of the current immuno-NAAT method is immuno-loop-mediated isothermal amplification (immuno-LAMP); although it required immobilization of the protein target on magnetic beads, it was reported to have 10^3 to 10^6-fold better LOD than ELISA.[59,60] Another example is immuno-rolling circle amplification (immuno-RCA), which uses a circular DNA

probe and yields randomly coiled DNA amplicons.[61] Immuno-RCA was demonstrated to detect a cell-surface protein in microfluidic devices and showed at least 10^3-fold amplification compared to conventional direct immunostaining procedure.[62] However, to date these immuno-PCR, immuno-LAMP and immuno-RCA approaches have required microarray-based equipment and multistep procedures, and are not inexpensive, rapid, or simple to use. Therefore, a different implementation approach is required to improve the sensitivity of immunoassays for a POC diagnostic platform.

2.7 Isothermal Strand Displacement Amplification (iSDA)

2.7.1 Principle of iSDA

In collaboration with the ELITech Group, our lab recently demonstrated isothermal strand displacement amplification (iSDA) of DNA targets using porous materials as part of a NAAT-based POC diagnostic platform.[63,64] The iSDA reaction is performed by two enzymes: a nicking enzyme and a DNA polymerase. The nicking enzyme generates a single-stranded nick in the double stranded DNA sequence. DNA polymerase has strong 5'→3' strand displacement activity but lacks 5'→3' exonuclease activity (i.e. proofreading). Two pairs of primers are also used in the iSDA reaction: a pair of flapped extension primers and a pair of bumper primers. The flap portion of extension primers is not complementary to the target sequence and can be recognized by the nicking enzyme (i.e. nicking site). The nicking enzyme acts on nicking sites to produce nicked products, which can be extended and displaced by the polymerase to produce single strands. These single strands are then amplified by the primers and enzymes in the exponential phase. This iSDA reaction is a truly isothermal amplification and does not need DNA

denaturation for initiation of the reaction, which meets the criteria of an ideal POC platform described above.

2.7.2 Current iSDA Applications

The iSDA reaction has been shown to be capable of detecting 10 copies of a target methicillin-resistant *Staphylococcus aureus* (MRSA) sequence (NO.-inducible L-lactate dehydrogenase, *ldh1*) in a clean sample[63], 50 target (*ldh1*) copies in the presence of a high concentration of genomic DNA and mucins[63], and ~5 × 10^3 target (*ldh1* and *mecA*, another sequence which confers methicillin resistance in *S. aureus*) copies in porous material networks that automated a sample-to-result NAAT for nasal swab specimens[64]. We believe that this paper-based iSDA can be the basis of an inexpensive and simple POC diagnostic platform.

3 SPECIFIC AIM 1: IMPROVE LOD BY SIGNAL AMPLIFICATION METHODS

3.1 MOTIVATION AND GOALS

The goal of the Specific Aim 1 was to develop a sensitive paper-based diagnostic for the detection of influenza A nucleoprotein using two signal amplification methods: (1) increasing absorbance of Au nanoparticles (e.g. gold enhancement (AuE) and silver enhancement (AgE)) and (2) enzymatic creation and precipitation of visible dyes (e.g. HRP/DAB assay). The performance goal was higher analytical sensitivity and reproducibility at least comparable to current FDA-approved influenza LFTs. Mitamura and co-workers have shown the benefits of AgE for the detection of influenza virus.[65] Compared to the conventional assay kit, the LODs of their system were 8 times lower for influenza A viruses. Here, we compared these chemical amplification-based tests to develop a sensitive LFT for influenza nucleoprotein detection.

3.2 GOAL 1: AMPLIFY SIGNAL BY INCREASING ABSORBANCE OF AU NANOPARTICLES

3.2.1 Introduction

In this section, we performed work that was intended to improve the LOD of an available influenza A nucleoprotein immunoassay by increasing the optical absorbance of gold nanoparticle labels after the assembly of the complete immunoassay stack. To improve the LOD of this influenza nucleoprotein assay, we implemented AgE as had been done in previous work.[65] We collaborated with PATH (Seattle, WA) and they provided LFT strips that were optimized for gold nanoparticle-based sandwich immunoassay. We also investigated AuE since AgE resulted in high background intensity, which reduced the assay sensitivity.

3.2.2 Methods

Backed nitrocellulose membranes were used as paper-based substrates in LFT. Recombinant nucleoprotein of influenza A (Brisbane/10/2007/H3N2, International Reagent Resource (IRR)) was used as a sample analyte. Monoclonal mouse anti-influenza A nucleoprotein IgGs (InA108 and InA245, Hytest, Turku, Finland) were used as capture and detection antibodies. The detection antibody was biotinylated, and streptavidin colloidal gold conjugate was used as an optical assay label (Figure 3.1). Each reagent was applied sequentially using 96-well plate. Washing buffer (1% BSA in PBST) was applied in the last assay step to rinse away gold nanoparticles. AgE and AuE solutions were then used for chemical signal amplifications. The principle of AgE and AuE is also described in Figure 3.1.

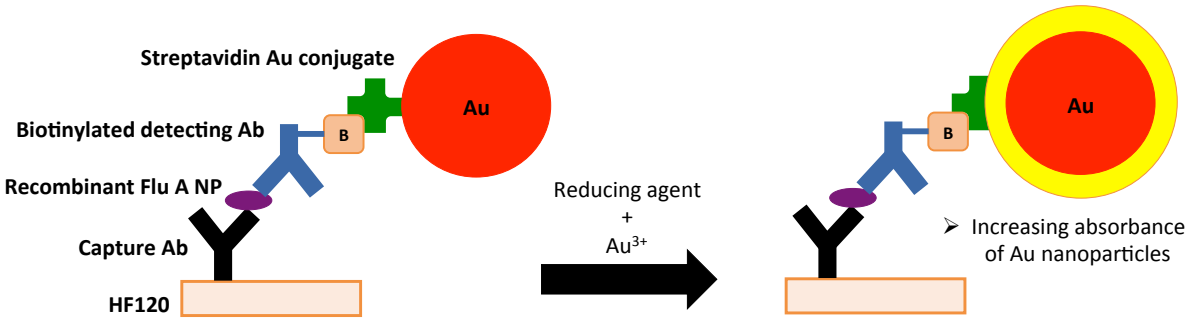

Figure 3.1. Schematic of AuE/AgE assay. A metallic assay label catalyzes the reduction of a gold or silver salt by a reducing agent, resulting in the deposition of metallic gold/silver on the surface of the label. The growth in particle size increases the absorbance, which thus increases the optical signal generated per nanoparticle.

3.2.3 Results and Discussion

3.2.3.1 Light sensitivity of AgE solution

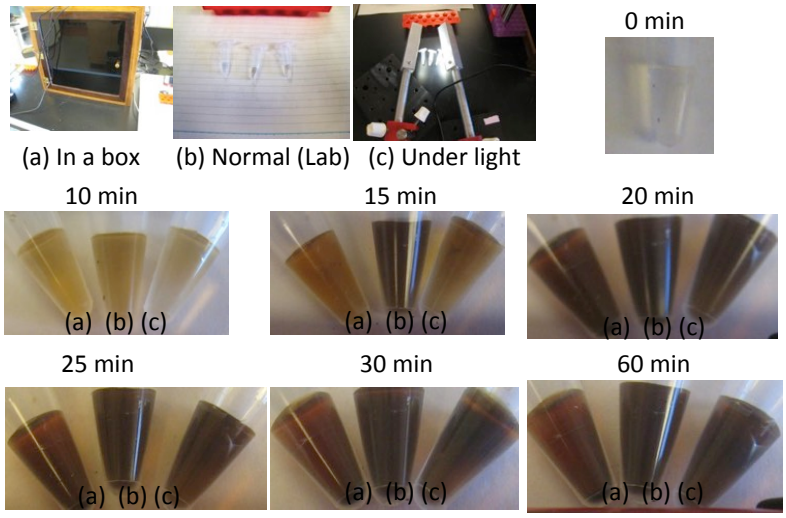

Figure 3.2. Light sensitivity of the AgE solution (SE100, Sigma, St. Louis, MO). The mixture of AgE solution was kept (a) in a box, (b) under normal condition in lab, and (c) under extra light for 60 min.

To evaluate light sensitivity of the AgE solution (the mixture of Solution A (silver salt) and Solution B (initiator), provided by Sigma), the mixture in each tube was kept in different illumination conditions (Figure 3.2, a: in a box, b: normal condition in lab, c: under extra light)

for 60 min. As shown in Figure 3.2, the color of all solutions became dark black within 20 min. This demonstrated that the mixture of AgE solution was highly sensitive to the light even in a dark environment. This issue should be addressed to make the AgE feasible for POC LFT.

3.2.3.2 Preliminary test using mouse IgG and Au-goat-anti (α)-mouse IgG

To evaluate the performance of AgE solution, Mouse-α-hemagglutinin (HA) antibody (IRR, #FR-505, CA09/Ab2) was spotted by hand on nitrocellulose membrane (HF135, Millipore, Billerica, MA) and Au-Goat-α-Mouse antibody (Arista Biologicals, Inc., Allentown, PA) was used as a secondary antibody (Figure 3.3).

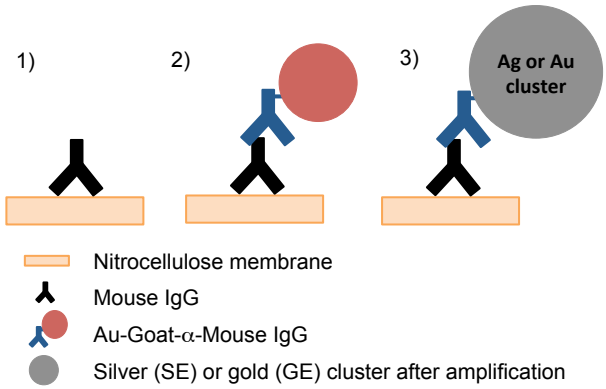

Figure 3.3. Schematic diagram of the expected assay stack for AgE and AuE. 1) Spotted mouse IgG, lateral flow of 2) Au-goat-a-mouse IgG and 3) AgE/AuE solution are shown.

As shown in Figure 3.3, Mouse-α-HA antibody was spotted by hand on each membrane. Each leg of a nitrocellulose membrane device was used for signal amplification under varied conditions (Figure 3.4). Figure 3.4a shows experimental conditions for each leg (leg a, b, c, and d). A cellulose wicking pad and a 96-well plate were used to run each step (Figure 3.4b). As a result, leg a and b did not show signals because BSA was not used for real-time blocking (Figure 3.4c). Compared to leg d, AgE on leg c showed darker signal. However, the background intensity was significantly high. Additionally, signal was decreased during lateral flow of AgE solutions

(recorded between 16 min 45 s and 20 min 13 s, shown in Figure 3.4c). After the decrease of signal, silver clusters were formed around the gold particles and thus color turned from red to black. Therefore, the signal reduction during the lateral flow of AgE solutions should be avoided to obtain more enhanced signals. In further study, solution A and B of the Sigma AgE kit should be applied separately to explore the cause of the decrease of signal.

(a)

	(a) (Control)	(b) (Control)	(c)	(d) (Control)
Step 1	Au-Goat-a-Mouse (PBS only)	Au-Goat-a-Mouse (PBS only)	Au-Goat-a-Mouse (PBS+1% BSA)	Au-Goat-a-Mouse (PBS+1% BSA)
Step 2	Wash (PBS only)	Wash (PBS only)	Wash (PBS+1% BSA)	Wash (PBS+1% BSA)
Step 3	Silver enhancer	PBS only	Silver enhancer	PBS+1% BSA
Step 4	Wash (PBS only)	Wash (PBS only)	Wash (PBS+1% BSA)	Wash (PBS+1% BSA)

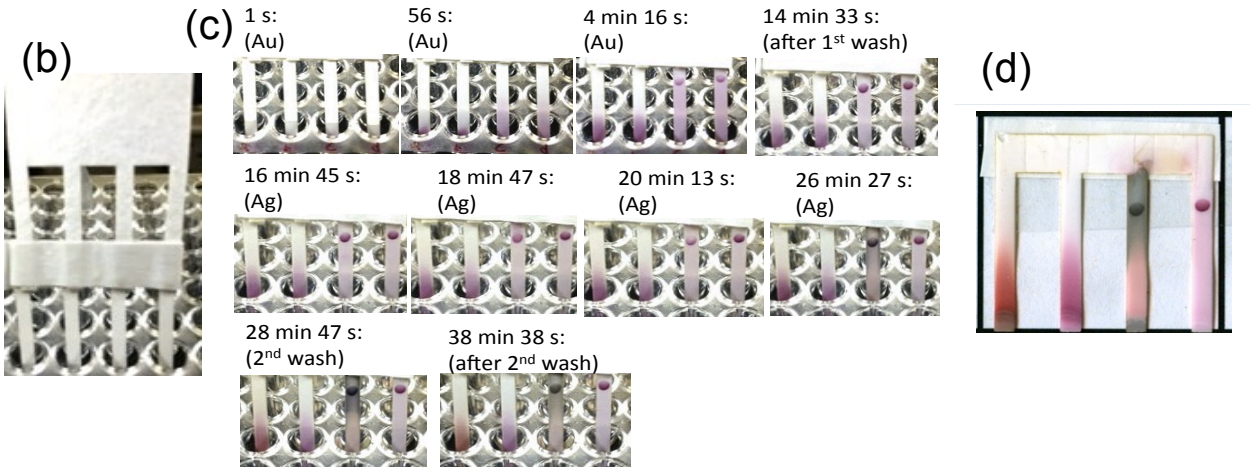

Figure 3.4. Signal amplification using silver enhancer solution. (a) Assay procedures applied for each leg, (b) photo of a 4-leg nitrocellulose device with a 4-leg cellulose wicking pad inserted in a 96 well plate, (c) image sequence of each assay step, and (d) 4-leg device scanned after running assay are shown.

3.2.3.3 Assessment of blocking reagents

Since the background intensity was high, membranes blocked with BSA or casein were prepared. Also, PBST (phosphate-buffered saline + 0.05% Tween 20) was compared with PBS to test Tween 20 as a blocking agent. Figure 3.5a shows assay procedures applied for each leg of the

device. Mouse-α-HA antibody was spotted using a piezo-driven spotter (sciFLEXARRAYER S3, Scienion AG, Berlin, Germany) on each leg of the device (Figure 3.5b). Each leg was used for signal amplification under varied conditions. Blocked membranes showed lower background intensity than unblocked membrane (Figure 3.5c). However, the total assay time was longer with blocked membranes (unblocked: 30 min, BSA-blocked: 40 min, and casein-blocked: 55 min) because the flow rates of the membranes changed. The best result in Figure 3.5 was the assay with 1% BSA in PBST using unblocked membrane because of the lower background intensity and shorter assay time. Different types of nitrocellulose membrane and AgE solution were evaluated in the next section.

(a)

	(a)	(b) (Control)	(c)	(d) (Control)
Step 1	Au-Goat-a-Mouse (PBS+1%BSA)	Au-Goat-a-Mouse (PBS+1%BSA)	Au-Goat-a-Mouse (PBST+1%BSA)	Au-Goat-a-Mouse (PBST+1%BSA)
Step 2	Wash (PBS+1% BSA)	Wash (PBS+1% BSA)	Wash (PBST+1% BSA)	Wash (PBST+1% BSA)
Step 3	Silver enhancer	Wash (PBS+1% BSA)	Silver enhancer	Wash (PBST+1% BSA)
Step 4	Wash (PBS+1% BSA)	Wash (PBS+1% BSA)	Wash (PBST+1% BSA)	Wash (PBST+1% BSA)

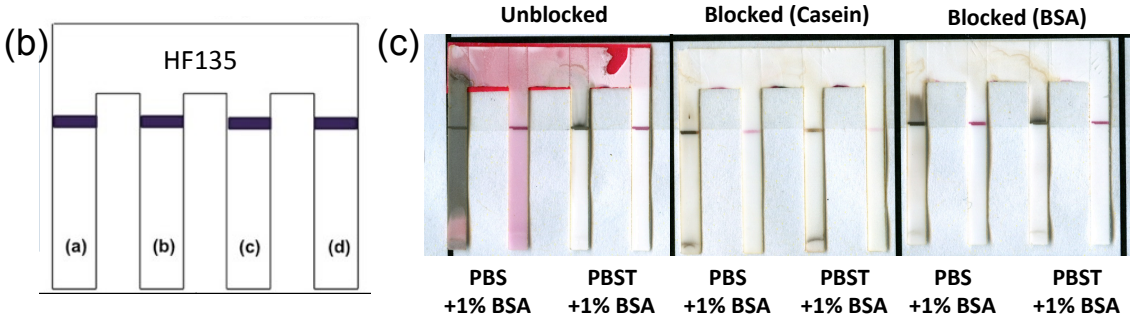

Figure 3.5. Assessment of blocking reagents. (a) Assay procedures applied for each leg are shown. (b) Mouse-α-HA antibodies were spotted as a test line on each leg of a 4-leg nitrocellulose membrane (Millipore HF135). (c) Scanned images of each membrane after running assay are shown.

3.2.3.4 Assessment of nitrocellulose membranes and AgE reagents

The experimental goals for the work reported in this section were to reduce nonspecific signals and background by comparing (1) different types of nitrocellulose membrane, (2) different AgE solutions, and (3) different washing solutions used before and after applying AgE (Figure 3.6a). The reason to use DI water as a washing solution was to remove any salts that increase autonucleation and background intensity. Also, BBI AgE solution (BBI solutions, UK) was used because its lower light sensitivity compared to Sigma AgE solution (data not shown). Mouse-α-HA antibody (1 mg/mL) was spotted on each leg of the device. Five assay steps were employed to perform AgE (Figure 3.6a) and signals were scanned using an office scanner (Perfection V700 Photo Scanner, Epson, Nagano, Japan) (Figure 3.6b).

(a)

	(a)	(b)	(c)	(d)
Step 1	Au-Goat-a-Mouse (PBST+1%BSA)	Au-Goat-a-Mouse (PBST+1%BSA)	Au-Goat-a-Mouse (PBST+1%BSA)	Au-Goat-a-Mouse (PBST+1%BSA)
Step 2	PBST+1% BSA	PBST+1% BSA	PBST+1% BSA	PBST+1% BSA
Step 3	DI water	PBST+1% BSA	DI water	PBST+1% BSA
Step 4	Silver enhancer (Sigma)	Silver enhancer (Sigma)	Silver enhancer (BBI)	Silver enhancer (BBI)
Step 5	DI water	PBST+1% BSA	DI water	PBST+1% BSA

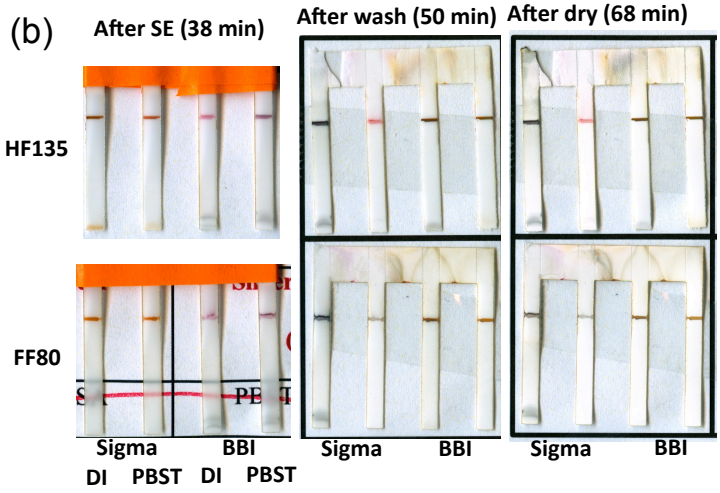

Figure 3.6. Assessment of nitrocellulose membranes and AgE reagents. (a) Assay procedures applied for each leg and (b) scanned images of each membrane are shown.

The total assay time (50 min) was longer than the ideal assay time for POC diagnostics (~20 min). Although the assay time can be shortened by reducing the volume of each solution, the balance between total assay time and assay sensitivity should be considered. As shown in Figure 3.6b, AgE amplified signals in most cases. The least enhanced signal was detected at the second leg of HF135 where Sigma AgE solution and PBST were applied. This could be due to the effect of PBST (phosphate-buffered saline + 0.05% Tween 20); PBST could interfere with the interaction between Au and AgE solution, and/or PBST could rinse away a certain amount of Au-antibody conjugate from the detection region. Compared to Sigma AgE solution, higher signals were detected by BBI AgE solution (discussed in the next section). The third leg of HF135, where BBI AgE solution and DI water were applied, showed the highest signal-to-background ratio. In the next section, this condition was tested with the full assay stack using recombinant nucleoprotein (NP) and its antibodies.

3.2.3.5 Signal quantification

Figure 3.7 shows results of colorimetric analysis of AgE amplified signals. As shown in Figure 3.7a, each leg of the device was used to compare different washing solutions and AgE solutions. DI water was used as a washing solution before applying silver enhancement solution to remove any salts that increase autonucleation and background intensity. As shown in Figure 3.7c, FF80HP (GE Healthcare Life Sciences, Marlborough, MA) showed lower signals compared to HF135. One of the reasons for the lower signals could be the flow rate of the membrane (discussed in the section 3.2.3.6~3.2.3.7 with Figure 3.8~3.10). In Figure 3.7b, Sigma AgE solution resulted in test lines broader than test lines enhanced by BBI AgE solution. This could be due to the pH of the Sigma solution (discussed in the section 3.2.3.8 with Figure 3.11). Also, the spotting condition of capture antibody would affect the intensity of amplified signal

(discussed in the section 3.2.3.9 with Figure 3.12). In terms of background intensity, DI water did not rinse well for Sigma AgE solution while it worked to reduce background intensity for BBI AgE solution. Higher signal-to-background ratio was observed by the assay using BBI AgE solution, HF135, and DI water.

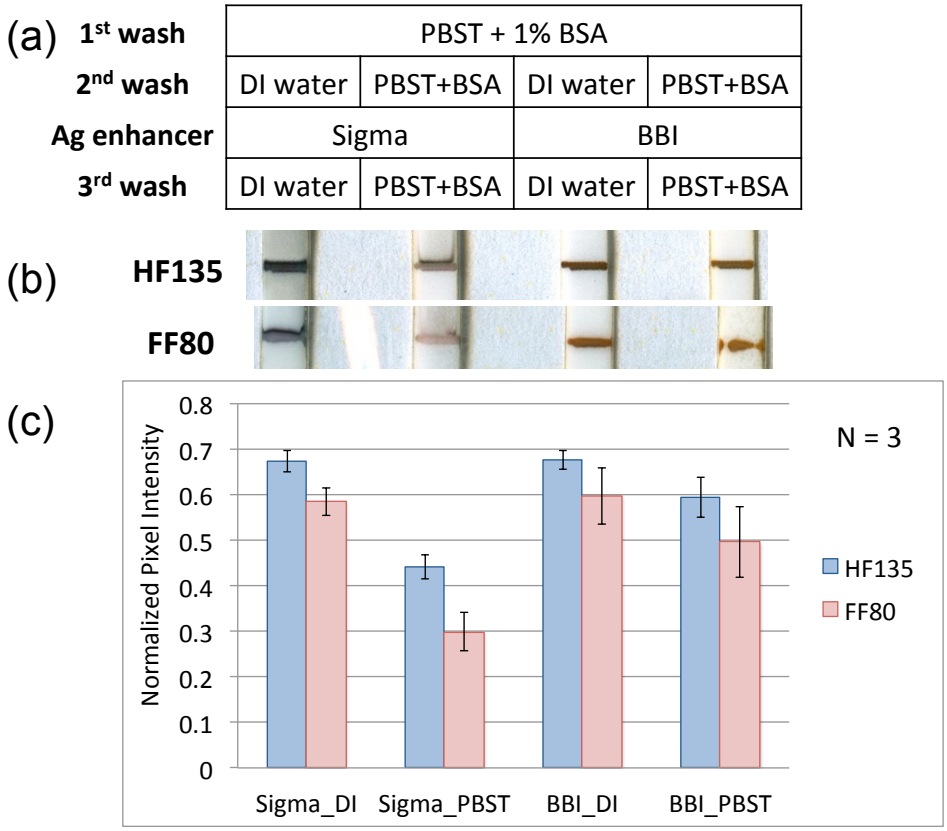

Figure 3.7. Signal quantification of amplified signals. (a) Assay procedures applied for each leg, (b) scanned images of amplified signals, and (c) pixel intensity of the detection region normalized with corresponding background intensity are shown (n=3).

3.2.3.6 Real-time signal assessment

Figure 3.8 shows image sequences taken during assays with a cell-phone camera. As shown in the top of Figure 3.8, the flow rate (measured by each company) of FF80HP is faster than HF135. Faster flow rate could result in less reaction time between antibodies and silver enhancement solution, leading to lower signal intensity. This can be a reason of lower signal

intensity with FF80HP compared to HF135 before silver enhancement (blue dashed box in Figure 3.8). Flow rate of each membrane was measured using weight scale (discussed in the following section). Test lines were broadened or becoming less intense by Sigma AgE solution (green dashed boxes in Figure 3.8). This could be due to the low pH of Sigma solution (shown in Figure 3.11) since low pH could have negative impact on the binding reaction between capture and detection antibodies.

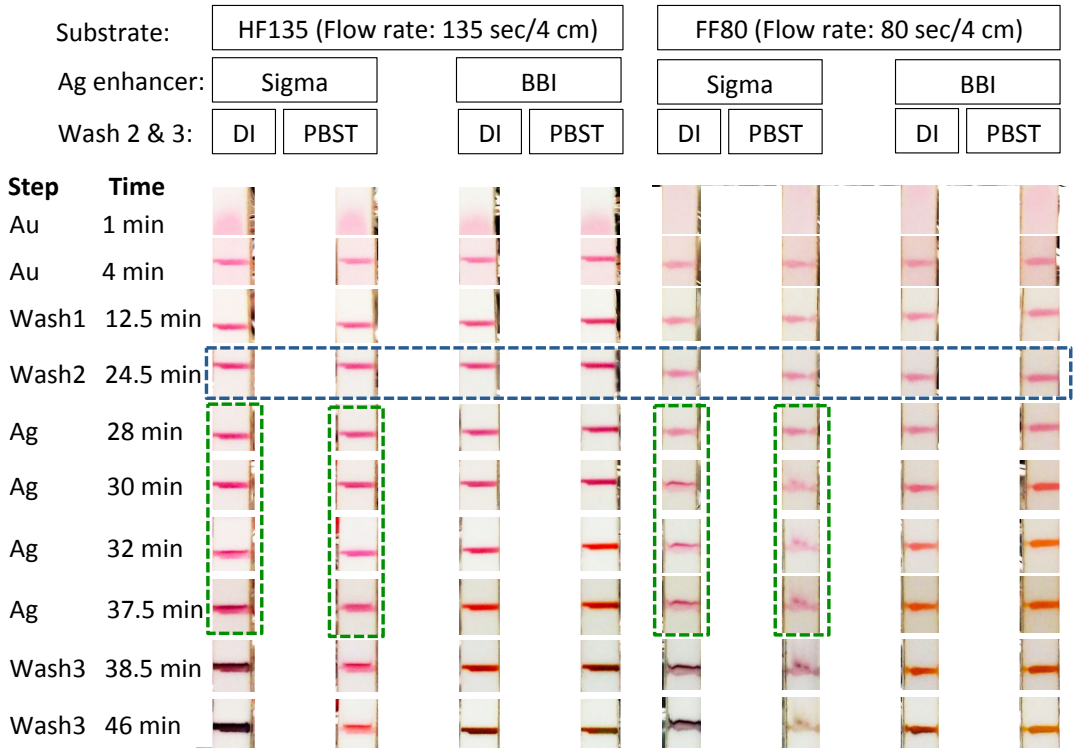

Figure 3.8. Image sequence during assay using HF135 (left 4 legs) and FF80HP (right 4 legs). Each leg was used with different AgE solutions and washing solutions. Each row shows pictures taken by cell-phone camera at different assay steps (shown on the left of figure). Blue dashed box shows the difference of signal intensity before silver enhancement. Green dashed boxes show the test lines that were broadened or becoming less intense caused by Sigma AgE solution. This effect could be due to the low pH of Sigma solution (shown in Figure 3.11).

3.2.3.7 Flow rate measurement

To investigate the effect of the flow rate on signal intensity, the flow rate of each membrane was quantified by measuring their wicking rates using PBS (Figure 3.9 and 3.10). Figure 3.9 shows

experimental settings. A cellulose absorbent pad was attached to the forked nitrocellulose membrane using adhesive tape. At first, the evaporation rate of PBS was quantified (Figure 3.10a, blue line). The wicking rate of each membrane was then measured (Figure 3.10a, green and red line). The evaporation rate was then subtracted from the wicking rate to calculate flow rate (shown in Figure 3.10b).

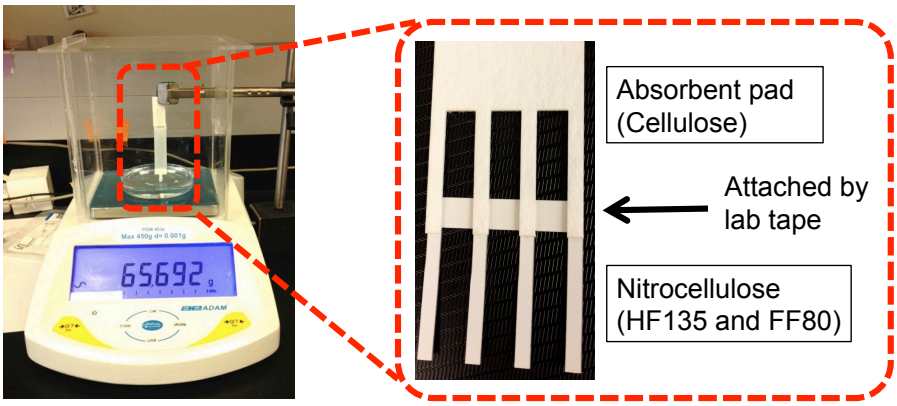

Figure 3.9. Flow rate measurement method. Wicking rate of membrane was quantified using scale connected to computer software. Sample solution was PBS. Cellulose absorbent pad was attached on nitrocellulose by adhesive lab tape. Flow rate before and after reaching absorbent pad was measured.

(a)

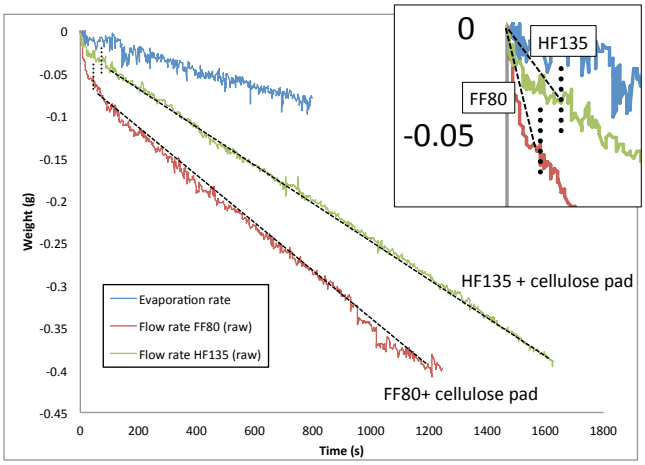

(b)

Measured flow rate (n = 1)	[mg/s]
Flow rate FF80	1.125
Flow rate HF135	0.392
Flow rate FF80 + cellulose pad	0.177
Flow rate HF135 + cellulose pad	0.124

(c)

Ratio of flow rate (n = 1)	[mg/s]	[cm/s]
FF80 / HF135 (by company)		1.688
FF80 / HF135 (by experiment)		1.667
FF80 / HF135	2.868	
FF80+pad / HF135+pad	1.429	

Figure 3.10. Flow rate measurement. (a) Raw data of wicking rate of membrane and evaporation rate of PBS, (b) calculated flow rate of membrane, and (c) ratio of flow rate (FF80/HF135) are shown.

As shown in Figure 3.10a, the flow rate changed after sample solution reached absorbent pad (indicated as round dashed line). Therefore, flow rates before and after sample reached absorbent pad were calculated for each nitrocellulose membrane. Figure 3.10b shows calculated flow rates and Figure 3.10c illustrates ratio of calculated flow rates in mg/s and cm/s. Experimentally measured ratio in cm/s was close to the value measured by each company, indicating that flow rate of FF80HP was faster than that of HF135. Calculated ratio in mg/s also showed faster flow rate with FF80HP. After sample reached absorbent pad, flow rate of FF80HP was still faster than that of HF135. As a conclusion, flow rate of FF80HP was faster than that of HF135 both before and after sample reached absorbent pad; FF80HP could have shorter time for interaction between antibodies, gold conjugates, and silver enhancement solution, resulting in lower signal intensity by FF80HP compared to HF135. The flow rate measurement should be replicated to evaluate reproducibility of the measurement.

3.2.3.8 pH of AgE solution

As shown in Figure 3.8, Sigma AgE solution slightly decreased signal intensity during assay and then amplified the signal. To investigate this effect, pH of each silver enhancement solution was measured (Figure 3.11). pH of BBI AgE solution was approximately 7 while pH of Sigma AgE solution was 2.3. Lower pH environment could affect the immobilization of capture antibodies on membrane and the binding reaction between capture and detection antibodies. Therefore, this can cause lower signal intensity and broadened width of test line by Sigma AgE solution. Thus, BBI AgE solution was selected for further studies.

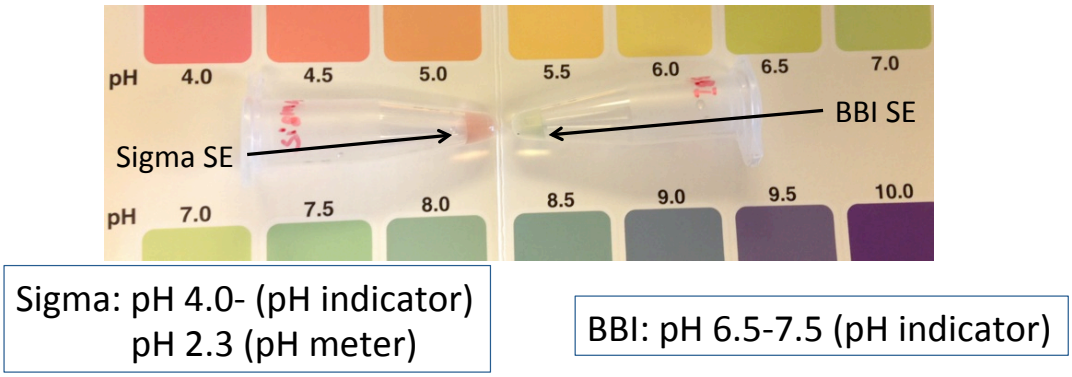

Figure 3.11. pH of AgE solutions. Sigma AgE solution showed pH 2.3-4.0. BBI AgE solution showed pH 6.5-7.5. Low pH of Sigma AgE solution could affect signal intensity.

3.2.3.9 Protein staining to investigate spotting condition for capture antibody immobilization

Lower signal intensity with FF80HP compared to HF135 can be also due to spotting conditions of capture antibodies. To investigate the distribution of spotted antibodies, Ponceau S (P7170, Sigma) was used to stain spotted antibodies (Figure 3.12). Uniformly-distributed lines were reproduced at each leg of HF135. On the other hand, ununiformly-distributed antibodies were observed on FF80HP. This is due to the spotting settings (e.g. droplet size, number of droplets in each spot, gap between spots, etc.) that were optimized for HF135. Therefore, spotting settings should be optimized for FF80HP to perform experiments comparable to different membranes.

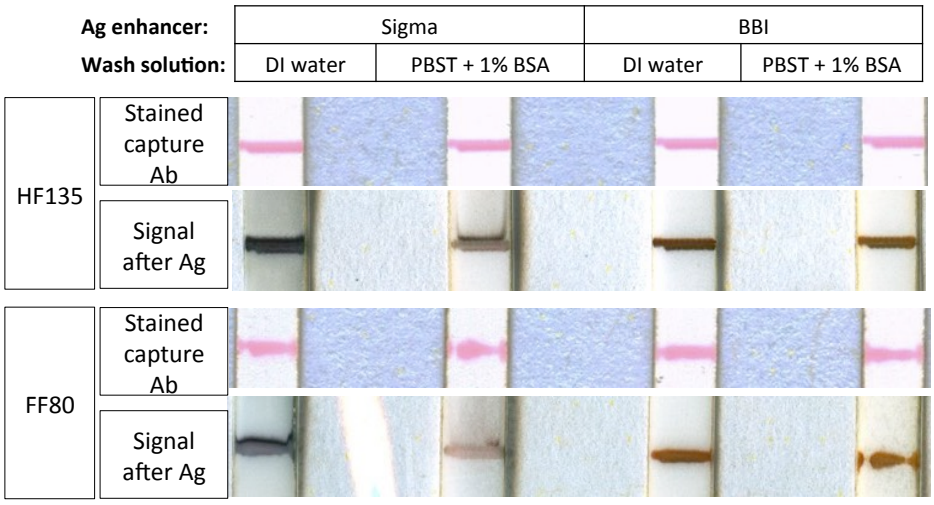

Figure 3.12. Stained capture antibodies and enhanced signals by AgE solution.

3.2.3.10 LOD assessment of Au-goat-α-mouse IgG

To investigate the performance of AgE solution, different concentrations of gold conjugate were applied, and amplified/unamplified signals were compared (Figure 3.13). LOD of gold conjugates was ~0.5 μg/mL without signal amplification. On the other hand, LOD after silver enhancement was ~ 0.05 μg/mL, showing 10-fold improvement.

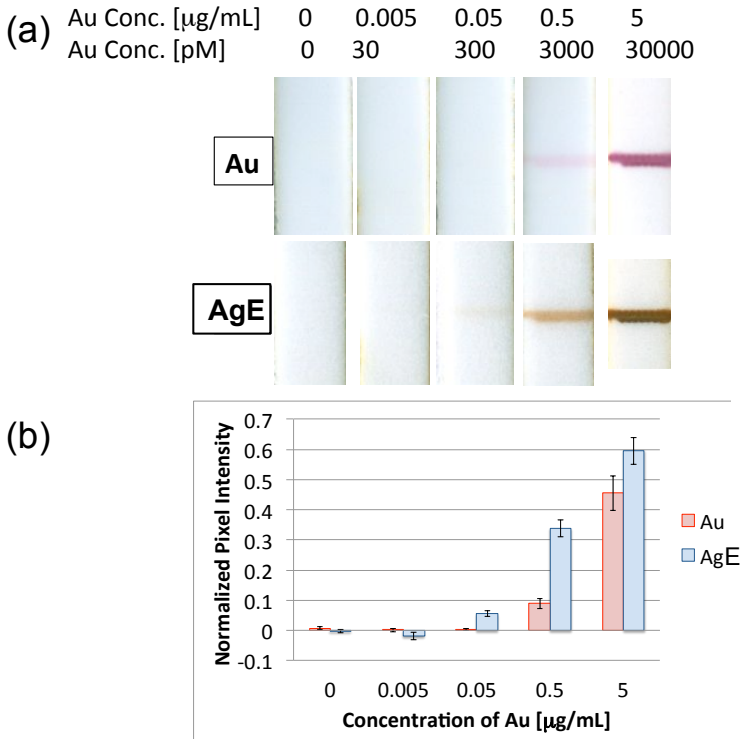

Figure 3.13. LOD of gold conjugate after silver enhancement (n=3). (a) Scanned images of amplified and unamplified signals and (b) normalized pixel intensities are shown. Mouse-α-HA IgG was spotted at 1 mg/mL on HF135. Au-Goat-α-Mouse IgG (20 μL) and washing buffer (20 μL of PBST + 1% BSA) were sequentially applied. BBI AgE solution (20 μL) was then applied for signal amplification.

3.2.3.11 Summary of AgE

Figure 3.14 shows a summary of AgE assessment: (1) BBI AgE solution was selected as signal amplification reagent, (2) HF135 was selected as porous membrane, (3) DI water was selected as wash solution before applying AgE reagent, and (4) Tween-20 (0.05% (v/v)) was selected as blocking agent to obtain high signal-to-background ratio. Pre-blocking of membrane was not

necessary because (1) Tween-20 in running buffer can reduce background intensity and (2) pre-blocking by BSA or Casein resulted in longer assay time, which is not ideal for POC test.

(a)

Parameter	Option 1	Option 2	Option 3
Silver enhancement product	**BBI**	Sigma	-
Substrate	**Millipore HF135**	GE FF80	-
Wash solution (before silver enhancement)	**DI water (to remove any salts)**	PBST	-
Use of surfactant	**Tween-20**	No Tween-20	-
Pre-blocking of membrane	**No blocking**	With BSA	With Casein

(b)

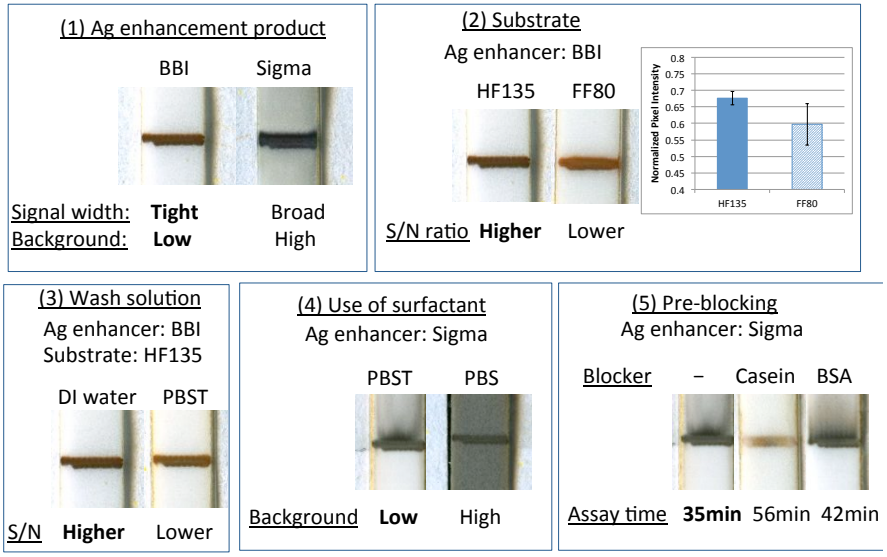

Figure 3.14. Summary of AgE assessment. (a) Options of each parameter for AgE (first choices are shown as bold) and (b) comparisons of each parameter for AgE are shown.

3.2.3.12 Assessment of AgE and gold enhancement (AuE) using simple assay stack

To evaluate performance of AgE and AuE, mouse-α-HA IgG (1 mg/mL) was spotted by the piezo-driven spotter on nitrocellulose membrane (HF 135) and Au-Goat-α-Mouse antibody was used as label (Figure 3.15a). Figure 3.15 shows experimental conditions and amplified or unamplified signals. Goat-α-mouse IgG without Au nanoparticles was used as a competitor of the Au conjugate to make the total concentration of IgG constant. As shown in Figure 3.15b and 3.15c, signal intensities amplified by AgE and AuE were higher than unamplified signals. Also,

negative controls (blank samples) resulted in very low false positive in each case, indicating that spotted capture antibody and/or the competitor antibody were not main cause of nonspecific signals. Figure 3.15c shows the normalized pixel intensity of amplified and unamplified signals. LODs by AgE (1.8×10^{-2} μg/mL) and AuE (3.8×10^{-2} μg/mL) were 3.6 times and 1.7 times better compared to unamplified assays (6.5×10^{-2} μg/mL), respectively.

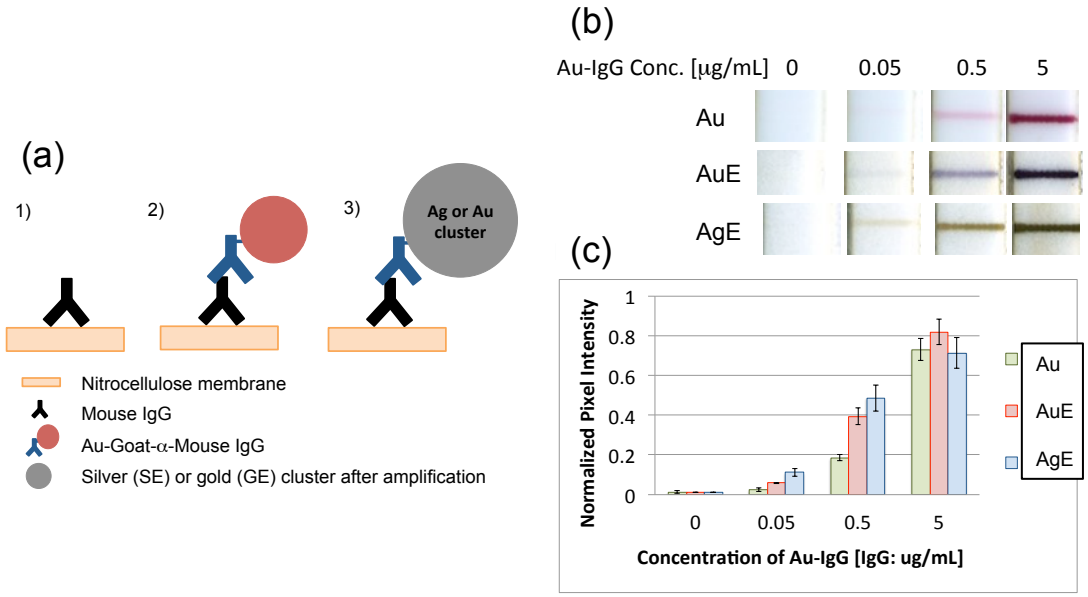

Figure 3.15. Assessment of AgE and AuE using simple assay stack. (a) Schematic of the expected assay stack for AgE and AuE is shown. 1) Spotted mouse IgG, 2) Au-goat-α-mouse IgG bound to the immobilized mouse IgG, and 3) Ag or Au cluster after AgE or AuE are illustrated. (b) Scanned images of amplified and unamplified signals using a range of concentrations of Au conjugate are shown. (c) The raw pixel intensity of the test region was corrected using the pixel intensity of a corresponding background region and inverted and scaled from 0 (white) to 1 (dark) (n=3).

3.2.3.13 AgE and AuE using full influenza A nucleoprotein assay stack

Figure 3.16 shows scanned images and quantified signals of amplified and unamplified influenza A nucleoprotein (NP) assay. As shown in Figure 3.16b, Amplified assays showed statistically significant higher signal intensity compared to unamplified assays. Nonspecific signal was relatively low, but it should be reduced to further improve the assay sensitivity.

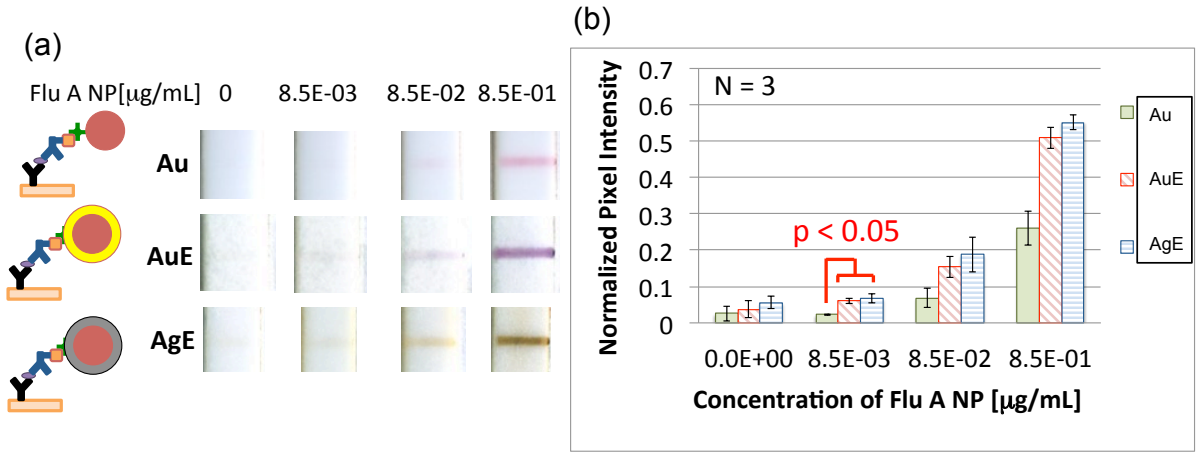

Figure 3.16. Amplified and unamplified signals using a range of concentrations of influenza A nucleoprotein. (a) Scanned images and (b) normalized pixel intensities of detection region (n=3) are shown.

3.2.3.14 AgE and AuE using full assay stack with virus

Figure 3.17 shows results of influenza A virus assay using strips provided by PATH. Amplified signals using 5×10^5 IU/mL (IU/mL=$TCID_{50}$/mL) virus was higher than unamplified signals. Nonspecific signals indicated the nonspecific binding of gold conjugates at and near the detection region. AuE showed lower LOD (~2×10^5 IU/mL) compared to AgE (~4×10^5 IU/mL) and unamplified assays (~6×10^5 IU/mL) because AuE showed low nonspecific signals.

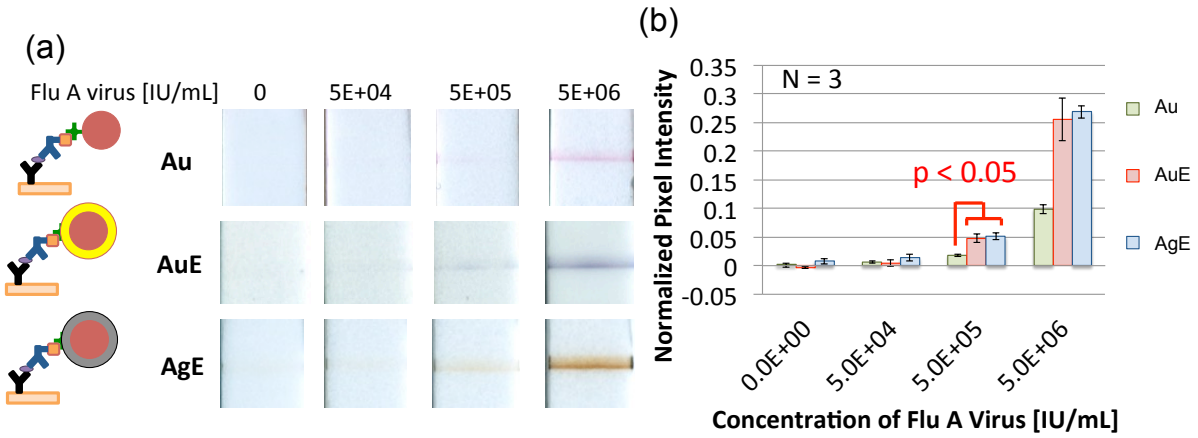

Figure 3.17. Assessment of AgE and AuE for influenza A virus (California/7/2009/H1N1) assay (IU/mL=$TCID_{50}$/mL). (a) Scanned images and (b) quantified signal intensities of amplified and unamplified signals are shown (n=3).

3.2.4 Conclusions

This work represents an attempt to develop a sensitive LFT platform using chemical amplification-based assays for influenza A NP detection. The best result using AuE showed approximately 3-fold better LOD (~2 × 10^5 $TCID_{50}$/mL) compared to unamplified gold nanoparticle-based assay. However, since the lowest clinically relevant concentrations of nucleoprotein and virus are much lower (described in the next section), LOD should be improved further. Thus, an alternative amplification method using enzyme and its colorimetric substrate was studied in the next section.

3.3 Goal 2: Amplify Signal by Enzymatic Creation and Precipitation of Visible Dyes

3.3.1 Introduction

Our lab previously demonstrated enzyme-based signal amplification to detect a malarial biomarker as a POC application and showed potential for long-term dry storage of the required reagents: the horseradish peroxidase (HRP)-conjugated-antibody label and its colorigenic substrate diaminobenzidine (DAB).[35] To demonstrate an automated paper-based ELISA for detection of a malarial biomarker, our lab has incorporated dry reagents into a two-dimensional paper network (2DPN) format.[35] Sequential assay reagent delivery for signal amplification using 2DPNs would lead to highly sensitive RDTs in a simple and low-cost POC format.

In this study, we sought to develop a highly sensitive sandwich immunoassay RDT for influenza A NP using two types of assay stacks with HRP and DAB. We experimentally explored assay

performance for each assay stack. We also investigated a dry reagent platform for a POC RDT application and the sensitivity was compared to the commercial kit.

3.3.2 Methods

3.3.2.1 Lateral flow strip fabrication

Lateral flow strips were fabricated at PATH by the following procedure using an Imagene IsoFlow™ Reagent Dispenser (Hanover, NH, USA). Nitrocellulose membranes (Millipore Hi-Flow 120, 4 mil backed, Billerica, MA, USA) were cut to a sheet (25 mm × 200 mm). Anti-influenza A NP monoclonal antibodies (1.0 mg/mL, InA108, Hytest, Turku, Finland) were striped in the capture region (11.5 mm from top of the nitrocellulose strips). Anti-mouse IgG (0.4 mg/mL, Jackson ImmunoResearch AffiniPure Goat Anti-Mouse IgG, West Grove, PA, USA) was striped in the control region (7.5 mm from top of the nitrocellulose). The dispense rate and speed were 0.08 μL/mm and 50 mm/s, respectively. Striped nitrocellulose membranes were dried in a forced air incubator at 37 °C for 2 hours in a desiccated container. The dried nitrocellulose membranes and the wicking pads (Grade 243, 32 mm × 200 mm, Ahlstrom, Helsinki, Finland) were assembled by overlapping 2 mm and attached onto adhesive laminate backing cards (GL-57623, 55 mm × 200 mm, Lohmann, Orange, VA, USA). The assembled membranes were cut to 5 mm-wide strips and stored in sealed pouches (VLBFNX00-1, large Mylar plate pouches, ZipSeal, Impak, Los Angeles, CA, USA) with 0.5 gram desiccant packs (38MC33, Impak) at room temperature.

3.3.2.2 Sandwich immunoassay with enzymatic signal amplification

LFTs were performed by sequentially applying reagent solutions using a 96-well plate until the fluid was drawn from each well (i.e. “dipstick” format using wet reagents). The assay running buffer consisted of 1% (w/v) BSA (A-3249, bovine serum albumin fraction V, Sigma, St. Louis,

MO, USA) in PBST (P3563, 10 mM PBS and 0.05% Tween 20, Sigma). The assay lysis buffer consisted of 5% (v/v) Triton X-100 (T-9284, Sigma) in the running buffer. The lateral flow assay consisted of the following four reagents: (1) 20 μL of recombinant influenza A NP containing a histidine tag (FR-480, Brisbane/10/2007 (H3N2), International Reagent Resource (IRR), Influenza Division, WHO Collaborating Center for Surveillance, Epidemiology and Control of Influenza, Centers for Disease Control and Prevention, Atlanta, GA, USA) or influenza A virus (A/California/07/2009, Virapur, San Diego, CA, USA) diluted into the lysis buffer; (2) 40 μL of HRP-conjugated detection antibody (HRP-IgG, 10 μg/mL, 3IN5C InA245, HyTest, Turku, Finland) or the mixture of 20 μL of biotinylated detection antibody (biotin-IgG, 2 μg/mL, 3IN5B InA245, HyTest) and 40 μL of Pierce streptavidin poly-HRP (0.5 μg/mL, 21140, Thermo Fisher Scientific, Waltham, MA, USA), each in the running buffer; (3) 20 μL of the running buffer as washing solution; and (4) 20 μL of DAB (50 μg/mL in PBST, D5905, Sigma) with 0.0125% (w/v) sodium percarbonate as a source of H_2O_2 (predicted H_2O_2 concentration is ~0.01% (w/v)). Fitzgerald streptavidin poly-HRP80 (65R-S118, Fitzgerald, Acton, MA, USA) was compared with Pierce streptavidin poly-HRP.

3.3.2.3 Image acquisition and data analysis

Image data (600 dpi) was acquired using a high-resolution flatbed scanner (Perfection V700 Photo Scanner, Epson, Nagano, Japan). A custom MATLAB (MathWorks, Natick, MA, USA) script was used to identify and quantify the mean and standard deviation of the signal intensity of the capture region on each strip. In brief, each signal was quantified by the following procedure. The capture region was selected by drawing a box around the region with some background downstream and upstream. Blue in RGB color channel was used to quantify signals because it is the most sensitive channel to quantify brown color of oxidized DAB. Average intensities across

row pixels were then plotted with curve fit to normalize with background. Average intensities that are higher than 3 standard deviations of background were then integrated. For LOD analysis, a previously-developed script was then used to fit a four-parameter logistic curve to the signal intensities for each paper, to quantify limits of detection with 95% confidence intervals, and to calculate t-statistics.[66] For the optimization of each reagent concentration, intensity of specific signal was subtracted by intensity of nonspecific signal.

3.3.2.4 Dry reagent storage of HRP and biotin-IgG

Dry storage pads were made from glass fiber membrane (GF8950, Ahlstrom, Helsinki, Finland). Glass fiber membrane pads (5 mm × 10 mm, ~20 μL fluid capacity) were blocked by soaking in the running buffer for 1 hour. The pads were then dried in a desiccated oven at 37 °C for 2 hours, then transferred to a desiccator for storage until use.

To make dry storage pads for the detection antibody-HRP conjugate, streptavidin poly-HRP (2 μg/mL) and biotin-IgG (4 μg/mL) were mixed with a preservation mixture (0.01 M $FeSO_4$-EDTA (Sigma F8048 and Fluka Analytical 03690), 4% (w/v) trehalose (T5251, Sigma), and 0.1% BSA in PBS) based on the previous work from the Yager lab.[35] A 20 μL sample of the detection antibody-HRP conjugate in the preservation mixture was added to each blocked pad. The pads were dried at 30°C under vacuum (Genevac Inc., Gardiner, NY, USA) for 1.5 hours. The dried pads were stored in a moisture-proof pouch (Ted Pella, Redding, CA, USA) with a 1 gram of blue-indicating silica gel (Delta Adsorbents, Roselle, IL, USA) at room temperature.

3.3.2.5 Prototype of POC assay device with dry storage pads

A prototype of a POC assay device was fabricated that coupled the wet lateral flow assay to the dry antibody-HRP pad. Materials were cut to desired shapes and sizes using a CO_2 laser

(Universal Laser Systems, Scottsdale, AZ, USA). Glass fiber membranes (GF8950, Ahlstrom, Helsinki, Finland) were cut to 5 mm × 10 mm as the dry storage pads. Cellulose pads (CFSP223, Millipore, Billerica, MA, USA) were cut to 7 mm × 12 mm as wicking pads. Nitrocellulose membranes were cut to 5 mm × 18 mm. Five-mm-wide Glass fiber membranes were also cut into 12 mm, 22 mm and 52 mm lengths as sample-delivery regions. A 5 mm × 12 mm glass fiber membrane was used to apply 50 μL of influenza virus sample in lysis buffer to rehydrate the HRP dry storage pad. A 5 mm × 22 mm glass fiber membrane was used to apply 35 μL of running buffer as washing solution. A 5 mm × 52 mm glass fiber membrane was used to apply 240 μL of DAB solution.

The assays using dry antibody-HRP conjugate pad were run by the following protocol: (1) the wicking pads, nitrocellulose membranes, antibody-HRP conjugate pads, and 12 mm-long glass fiber sample application zones were assembled and attached onto the adhesive laminate backing cards; (2) influenza virus samples in lysis buffer were added to the glass fiber pads to rehydrate the antibody-HRP conjugate pads; (3) 22-mm-long glass fiber pads were attached to the ends of the strips and aliquots of running buffer were added as washing solutions; and (4) 52-mm-long glass fiber pads were attached to the end of the strips and DAB solution was added. Each membrane was assembled by overlapping 2 mm. Each step took 10~20 min and total assay time was ~40 min.

3.3.3 Results and Discussion

3.3.3.1 Assessment of HRP-IgG

Since nonspecific signals have been an issue with the assay stacks using biotinylated detection antibody and streptavidin gold conjugate, enzymatic creation and precipitation of visible dyes

were tested as another signal amplification approach (Figure 3.18). Detection Ab was conjugated to HRP as an enzyme and DAB was used as a substrate.

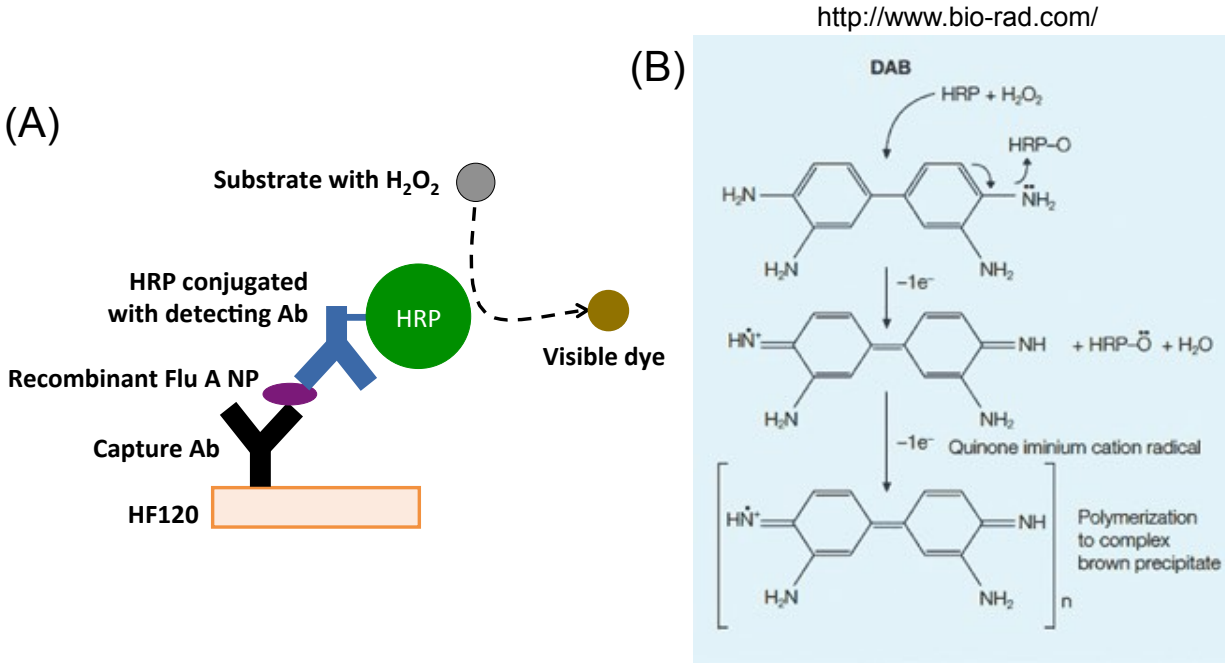

Figure 3.18. Chemistry of HRP/DAB reaction. (A) Expected assay stacks for enzymatic creation and precipitation of visible dyes. HRP is conjugated to detection antibody (Ab). DAB is used as a substrate. (B) Detailed chemistry of HRP/DAB/H_2O_2 reaction (http://www.bio-rad.com/ and Tsang VC et al. (1985), Enzyme-linked immunoelectrotransfer blot (EITB), In Enzyme-Mediated Immunoassay, T.T. Ngo and H.M. Lenhoff, eds. (New York: Plenum Press), pp 389–414.).

Figure 3.19 shows results of signal amplification with HRP conjugate and DAB. A range of concentration of HRP conjugate (0-10 μg/mL in PBS) and DAB (61-244 μg/mL in PBST) were tested for influenza A recombinant NP (0 and 85 ng/mL) assay. With 85 ng/mL of NP (Figure 3.19a and 3.19b), 5 μg/mL for HRP conjugate and 244 μg/mL for DAB showed the best signal-to-background ratio. Moreover, the most important result was that nonspecific signals were relatively low after signal amplification (Figure 3.19c and 3.19d). This shows a potential of HRP amplification to achieve better LOD compared to the assay stacks with gold conjugate.

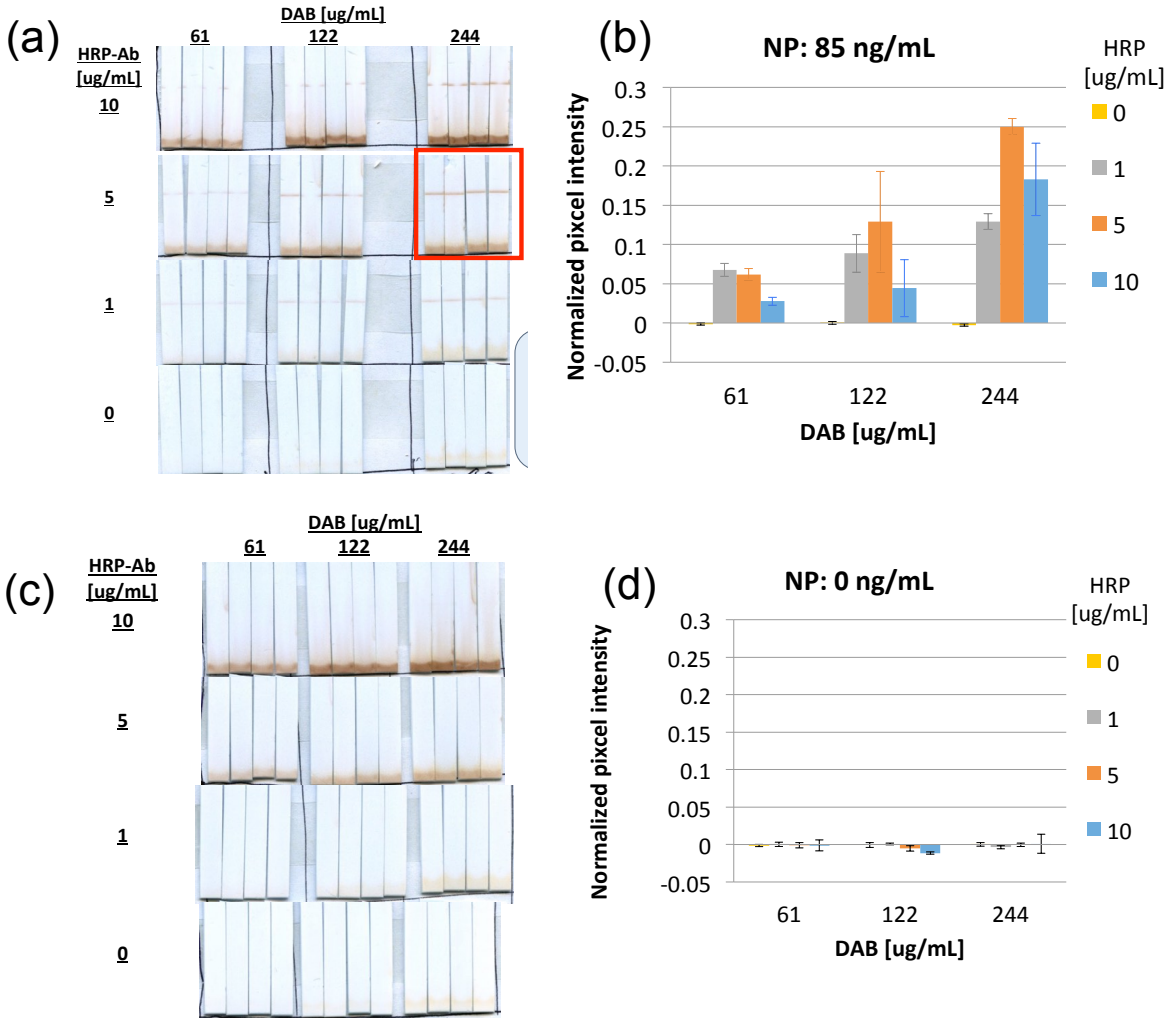

Figure 3.19. Signals from different concentrations of HRP conjugate and DAB. (a) Scanned image of positive influenza A NP (85 ng/mL) assay and (b) quantified signal intensities are shown (n=4). (c) Scanned image of negative influenza A NP (0 ng/mL) assay and (d) quantified signal intensities are shown. HF120, cellulose pad, and backing card are used. Recombinant influenza A NP (0 and 85 ng/mL in lysis buffer), HRP conjugate (0-10 µg/mL in PBS), DAB (61-244 µg/mL in PBST) with sodium percarbonate (0.025 w/v%) as a source of H_2O_2, and running buffer as washing solution were applied sequentially. Lysis buffer consists of 10 mM PBS, 0.05% Tween 20, 1% (w/v) BSA, and 5% (v/v) Triton X-100. Running buffer consists of 10 mM PBS, 0.05% Tween 20, and 1% (w/v) BSA.

3.3.3.2 Assessment of washing method for the assay using HRP-IgG

Since background intensity was a problem, several combinations of washing steps were tested (Figure 3.20). Combinations of washing step 1 (after applying NP sample), 2 (after applying HRP conjugate) and 3 (after applying mixture of DAB and H_2O_2) were investigated. Running

buffer was used as washing solution. Since DAB becomes dark in the presence of HRP and H_2O_2, the washing step 2 was expected as the most important to reduce background. In addition, since DAB precipitates would not be rinsed well, the washing step 3 was expected as unnecessary. Therefore, the combination 2 and 4 in Figure 3.20 were expected as efficient washing steps.

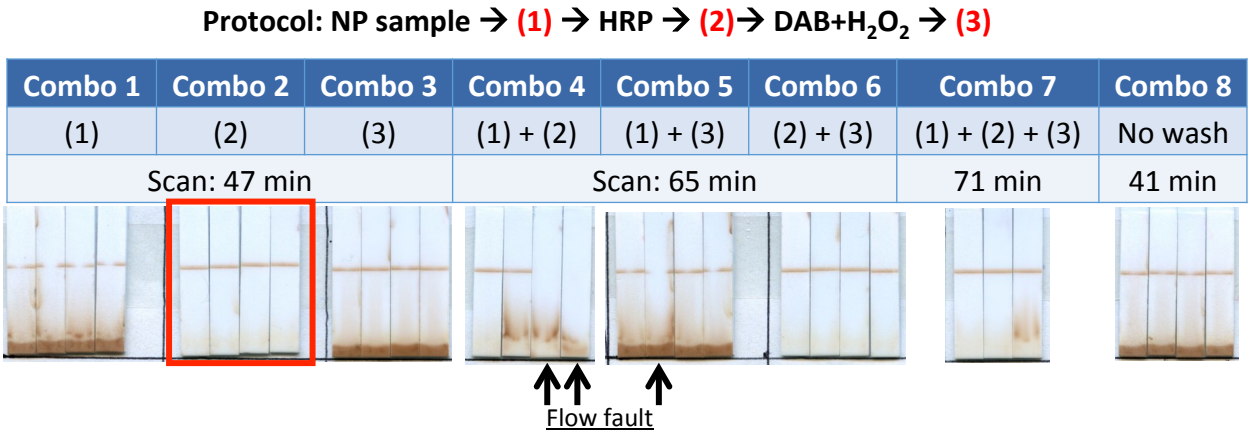

Figure 3.20. Optimization of the washing step. Combinations of washing step 1 (after applying NP sample), 2 (after applying HRP conjugate) and 3 (after applying mixture of DAB and H_2O_2) were investigated. Running buffer was used as washing solution. HF120, cellulose pad, and backing card are used. Recombinant influenza A NP (85 ng/mL in lysis buffer), HRP conjugate (5 µg/mL in PBS), and DAB (244 µg/mL in PBST) with sodium percarbonate (0.025 w/v%) as a source of H_2O_2 were applied sequentially. Lysis buffer consists of 10 mM PBS, 0.05% Tween 20, 1% (w/v) BSA, and 5% (v/v) Triton X-100. Running buffer consists of 10 mM PBS, 0.05% Tween 20, and 1% (w/v) BSA.

As a result, the combination 2 (only washing step 2), the combination 4 (both washing step 1 and 2), the combination 6 (both washing step 2 and 3), and the combination 7 (washing step 1, 2 and 3) showed less background intensity compared to other combinations as expected. To balance total assay time and background intensity, the combination 2 (only washing step 2) was the most promising. Therefore, the combination 2 was employed in the following experiments.

3.3.3.3 Assessment of H_2O_2 concentration

Since concentration of H_2O_2 is also important factor to achieve effective enzymatic reaction by HRP and DAB, a range of concentration of sodium percarbonate (0.00625-0.8 w/v%) was tested for influenza A NP (85 ng/mL) assay (Figure 3.21). Increasing H_2O_2 concentration resulted in decreasing signal intensities. This could be due to low pH condition by high H_2O_2 concentration compared to optimum pH range for HRP (pH 6.0-7.5). Both 0.0125 and 0.025 w/v% of sodium percarbonate were tested in the following LOD analysis.

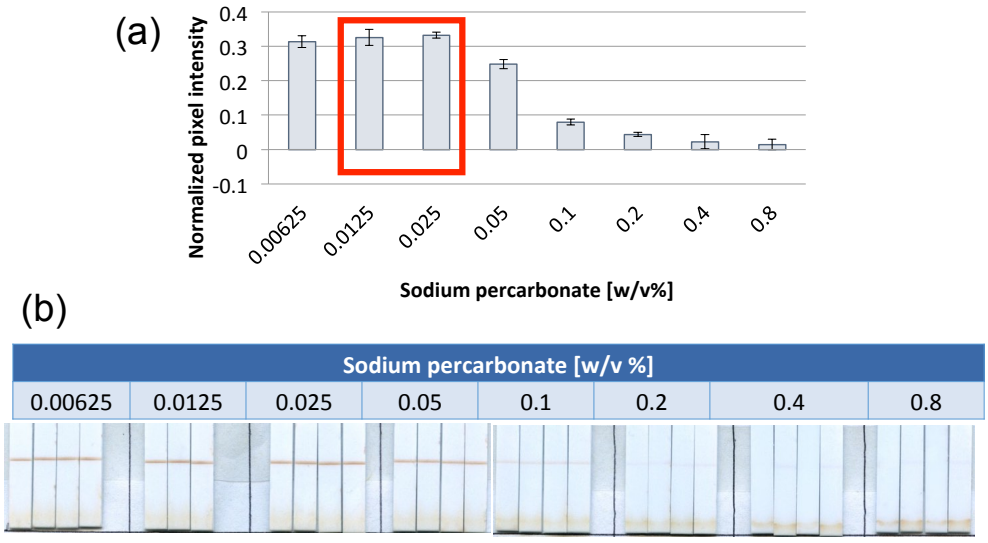

Figure 3.21. Effect of H_2O_2 concentration on HRP amplification with DAB. (a) Signal intensities over a range of sodium percarbonate concentration (0.00625-0.8 w/v%) and (b) scanned image of the strips are shown (n=3~4). HF120, cellulose pad, and backing card are used. Recombinant influenza A NP (85 ng/mL in lysis buffer), HRP conjugate (5 µg/mL in PBS), DAB (244 µg/mL in PBST) with sodium percarbonate as a source of H_2O_2, and running buffer as washing solution were applied sequentially. Lysis buffer consists of 10 mM PBS, 0.05% Tween 20, 1% (w/v) BSA, and 5% (v/v) Triton X-100. Running buffer consists of 10 mM PBS, 0.05% Tween 20, and 1% (w/v) BSA.

3.3.3.4 LOD analysis of recombinant NP using HRP-IgG

Based on the improved conditions for HRP conjugate, DAB, sodium percarbonate, and washing step, LOD was measured with a range of influenza A NP concentration (Figure 3.22). Measured LOD ($Mean_{blank}$ + 3 $standard\ deviation_{blank}$) of NP was 1.8-4.2 ng/mL, which is within our target

LOD (0.29-2.9 ng/mL, and is 10~100-fold lower than commercial test kits[67]). However, since each factor was optimized using 85 ng/mL of influenza A NP, signal intensities at lower NP concentrations were higher than the lowest target LOD (0.29 ng/mL). Therefore, optimization of each factor was performed using lower NP concentration (8.5 ng/mL). Also, this was in absolutely ideal circumstances—no human samples, used a recombinant analyte, and was enabled using all manual steps in a 96-well plate. Thus, it is important to test real human sample to evaluate this HRP/DAB assay.

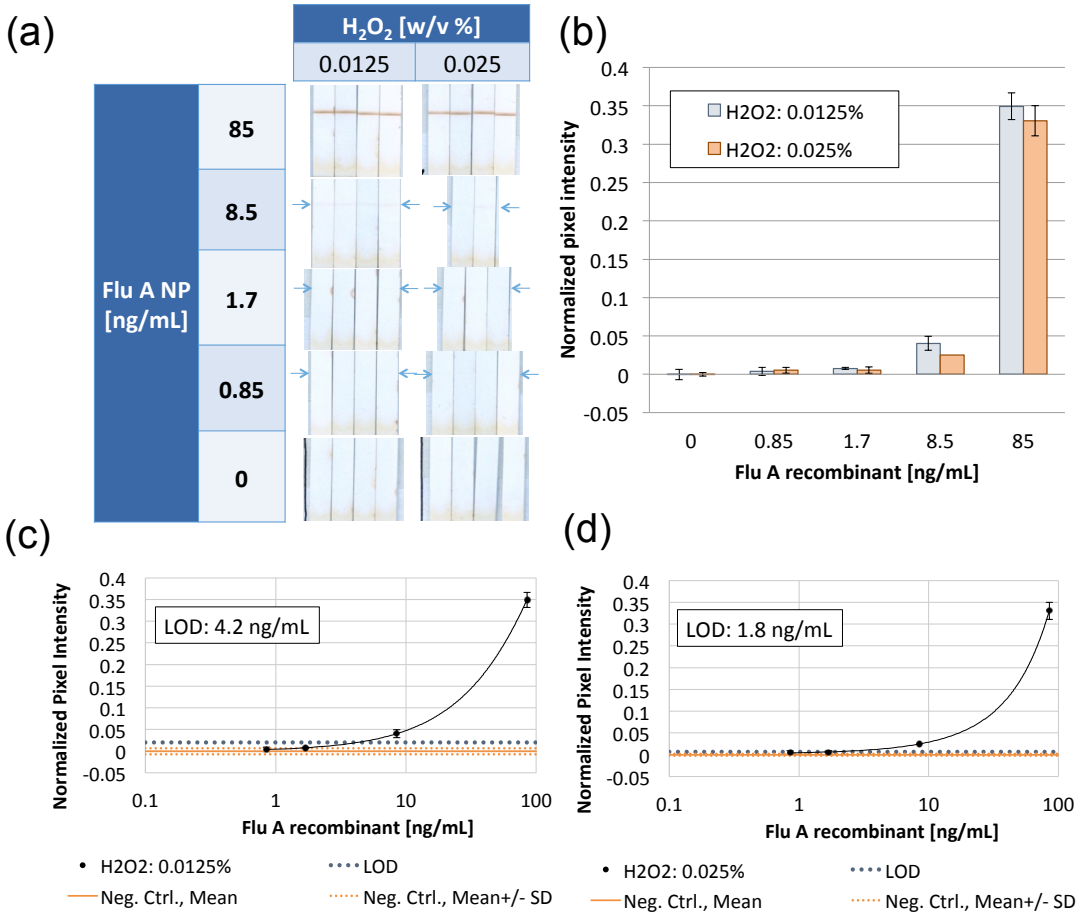

Figure 3.22. LOD analysis with optimized conditions for HRP conjugate, DAB, sodium percarbonate and washing step. (a) Scanned images of influenza A NP assay, (b) quantified signal intensities, and LOD measurements ($Mean_{blank}$ + 3 $standard\ deviation_{blank}$) using (c) 0.0125 and (d) 0.025 w/v% of sodium percarbonate are shown (n=2~4). HRP conjugate (5 µg/mL in PBS) and DAB (244 µg/mL in PBST) with sodium percarbonate as a source of H_2O_2 were applied.

3.3.3.5 Optimization of reagent concentrations using HRP-IgG

The goal of the following experiments was to re-optimize HRP and DAB concentrations with 8.5 ng/mL of recombinant influenza A NP. A range of concentration of HRP conjugate (1~15 μg/mL in PBS) and DAB (61~976 μg/mL in PBST) were tested for influenza A recombinant NP (8.5 ng/mL) assay (Figure 3.23). With 488~976 μg/mL of DAB, high background was observed and almost no signals were detected. A 1 μg/mL of HRP conjugate also showed almost no signals. Therefore, those conditions were eliminated for the following experiments for the optimization. Since signal intensities were increased with higher concentration of HRP conjugate, wider range of HRP concentrations (5~20 μg/mL) was tested for the following experiment. In addition, negative control (0 ng/mL of NP) was tested to investigate nonspecific signal (Figure 3.24).

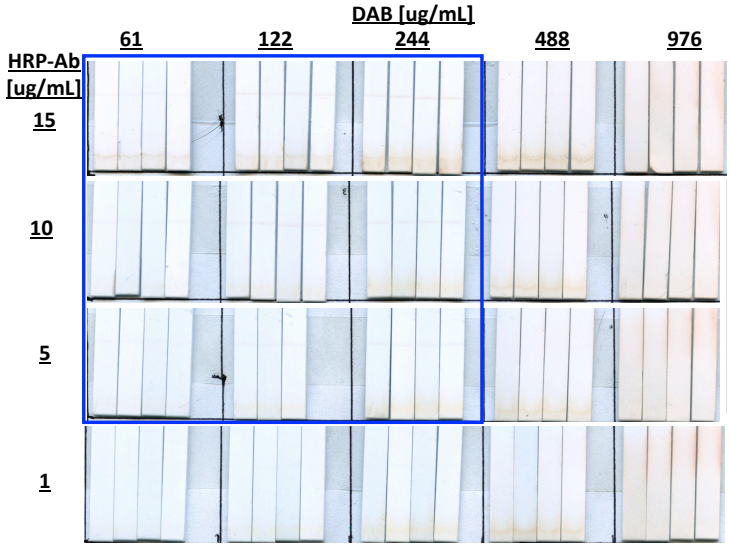

Figure 3.23. Specific signals by different concentrations of HRP conjugate and DAB. Recombinant NP (20 μL of 8.5 ng/mL in lysis buffer), HRP conjugate (40 μL of 1~15 μg/mL in PBS), running buffer as washing solution (20 μL), and DAB (20 μL of 61~976 μg/mL in PBST) with sodium percarbonate (0.025 w/v%) as a source of H_2O_2 were applied sequentially (n=4).

Figure 3.24 shows results of the re-optimization with a range of HRP and DAB concentrations. With 0 ng/mL of recombinant NP, 5 conditions (3 conditions with 20 μg/mL of HRP and 2

conditions with 15 μg/mL of HRP) showed relatively high background intensity (Figure 3.24a and 3.24b). Therefore, those 5 conditions were eliminated and remained 7 conditions (indicated as blue boxes in Figure 3.24a and 3.24b) were selected as better candidates. With 8.5 ng/mL of NP, 10 μg/mL of HRP and 122 μg/mL of DAB showed the best signal-to-background ratio (Figure 3.24c and 3.24d, indicated as blue box and arrow). Therefore, this condition was selected as the improved condition.

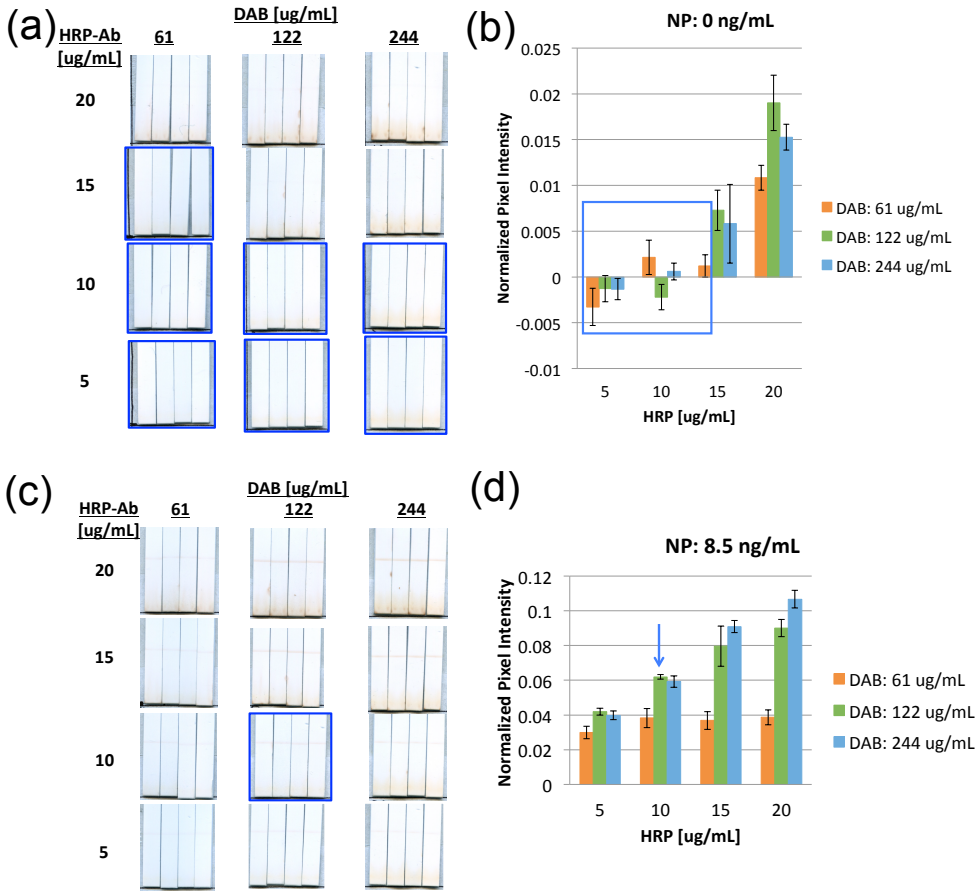

Figure 3.24. Signals from different concentrations of HRP conjugate and DAB. Scanned images of influenza A NP assay ((a) 0 and (c) 8.5 ng/mL of NP) and quantified signal intensities ((b) 0 and (d) 8.5 ng/mL of NP) are shown (n=4). HRP conjugate (40 μL of 5~20 μg/mL in PBS) and DAB (20 μL of 61~244 μg/mL in PBST) with sodium percarbonate (0.025 w/v%) were applied.

3.3.3.6 LOD analysis with improved reagent concentrations using recombinant NP

Figure 3.25 shows LOD analysis with re-optimized conditions (10 μg/mL of HRP and 122 μg/mL of DAB) with a range of NP and sodium percarbonate concentrations. Figure 3.25a shows nonspecific signals, but their intensities were lower than the nonspecific signal intensity in the assay with gold conjugate. Figure 3.25b shows quantified signal intensities for LOD analysis. LOD by the improved condition was better than the previous LOD. The calculated LODs were 0.28 and 0.74 ng/mL with 0.0125 and 0.025 w/v% of sodium percarbonate (Figure 3.25c and 3.25d), respectively, which are approximately 10-fold better than the previous LOD (1.8~4.2 ng/mL) and the LOD of commercial kits (1~10 ng/mL).

3.3.3.7 LOD analysis with improved reagent concentrations using virus

The goal of the following experiments was to analyze LOD with lysed virus and compare with the LOD of a commercial kit (Directigen EZ Flu A+B, BD, Franklin Lakes, NJ USA). For this experiment, a range of concentration of influenza A virus (Virapur, from 0 to 5×10^6 IU/mL, IU/mL=$TCID_{50}$/mL) and sodium percarbonate (0.0125 and 0.025 w/v%) were tested with the improved HRP/DAB concentration (Figure 3.26). Lower concentration of sodium percarbonate resulted in better signal intensities, which would be due to the effect described in the section 3.3.3.3. Also, HRP/DAB amplification resulted in better signal intensities compared to results provided by PATH using gold conjugate as label. Each LOD was calculated with standard method (i.e. mean + 3 standard deviations of blank sample) and calculated LODs were 4.6×10^3, 1.4×10^4, and 1.4×10^5 $TCID_{50}$/mL for the assay using 0.0125 and 0.025 % of sodium percarbonate, and the assay using gold conjugate performed by PATH, respectively. Therefore, ~10-fold improvement was achieved by HRP amplification compared to the assay using gold conjugate at PATH.

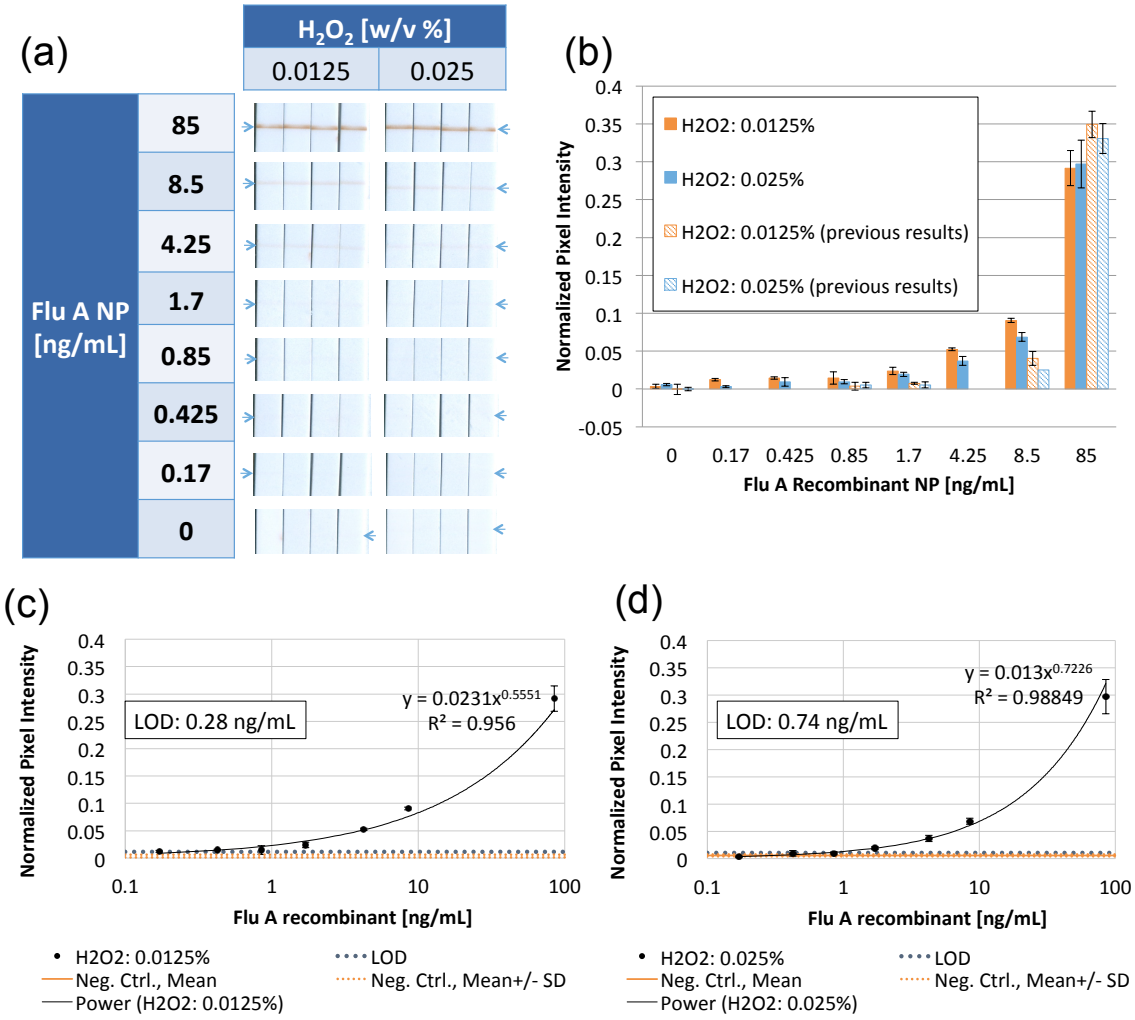

Figure 3.25. LOD analysis with re-optimized conditions for HRP conjugate and DAB. (a) Scanned images of NP assay, (b) quantified signal intensities, and LOD measurements ($Mean_{blank}$ + 3 $standard\ deviation_{blank}$) with (c) 0.0125% and (d) 0.025% of sodium percarbonate are shown (n=4).

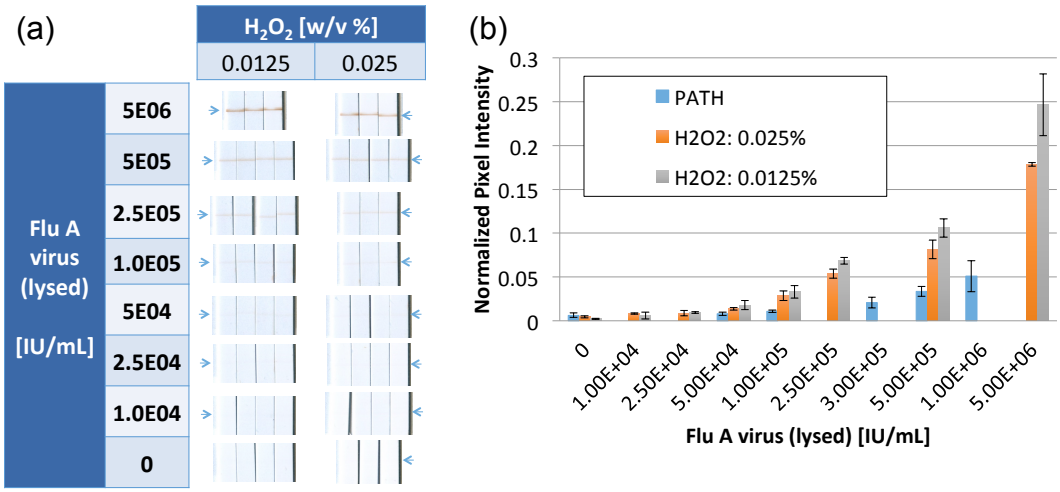

Figure 3.26. LOD analysis of influenza A virus assay. (a) Scanned images of the assay and (b) normalized pixel intensities including the data provided by PATH using gold conjugate label are shown (n=3~4). HF120, cellulose pad, and backing card are used. Capture antibody was striped on the membrane at PATH. Influenza A virus (20 µL in lysis buffer), HRP conjugate (40 µL of 10 µg/mL in PBS), running buffer as washing solution (20 µL), and DAB (20 µL of 122 µg/mL in PBST) with sodium percarbonate (0.0125 and 0.025 w/v%) as a source of H_2O_2 were applied sequentially. Lysis buffer consists of 10 mM PBS, 0.05% Tween 20, 1% (w/v) BSA, and 5% (v/v) Triton X-100. Running buffer consists of 10 mM PBS, 0.05% Tween 20, and 1% (w/v) BSA.

3.3.3.8 LOD comparison with a commercially available kit

LOD was also compared with the LOD of a commercially-available kit from BD (Figure 3.27). The lowest detectable virus concentration by BD kit was 5.0×10^4 $TCID_{50}$/mL. For HRP/DAB assay, LOD calculated by the standard method (i.e. mean + 3 standard deviations of blank sample) was 1.1×10^4 $TCID_{50}$/mL. Therefore, approximately 5-fold lower LOD was achieved by HRP amplification compared to the LOD of BD kit.

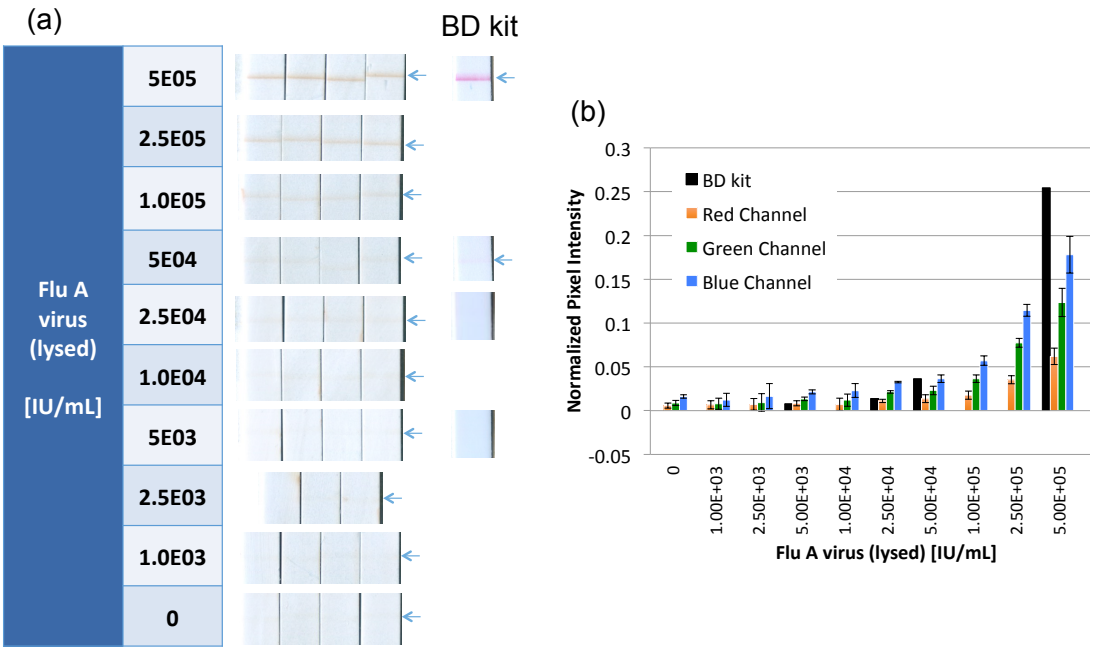

Figure 3.27. LOD analysis using influenza A virus. (a) Scanned images of detected signals and (b) normalized pixel intensities with different color channels (red, green and blue channels for HRP/DAB amplification (n=3~4) and green channel for BD kit (n=1)). HF120, cellulose pad, and backing card are used. Capture antibody was striped (1 mg/mL) on the membrane at PATH. Influenza A virus in lysis buffer (20 µL), HRP conjugate (40 µL of 10 µg/mL in PBS), running buffer (20 µL) as washing solution, and DAB (20 µL of 122 µg/mL in PBST) with sodium percarbonate (0.0125 w/v%) as a source of H_2O_2 were applied sequentially. Lysis buffer consists of 10 mM PBS, 0.05% Tween 20, 1% (w/v) BSA, and 5% (v/v) Triton X-100. Running buffer consists of 10 mM PBS, 0.05% Tween 20, and 1% (w/v) BSA.

3.3.3.9 Comparison of signal quantification methods

The goal of the following experiments was to test different LOD analysis methods with the same data set. For the detection of signal intensities, two approaches were tested: Integral Intensity and Local Background Correction methods. For the Integral Intensity method, the following protocols were employed: (1) scan signals, (2) draw a box around signals to plot test line profile, (3) normalize by removing background, and (4) calculate integrate intensities over range that is more than 3 standard deviations of background (Figure 3.28). This method works especially for the analysis of low signal intensities. For Local Background Correction method, the following protocols were demonstrated: (1) draw a box around signals to calculate the average intensity in

the box, and (2) the raw pixel intensity is corrected using the pixel intensity of corresponding background region to invert and scale from 0 (white) to 1 (dark) (Figure 3.29).

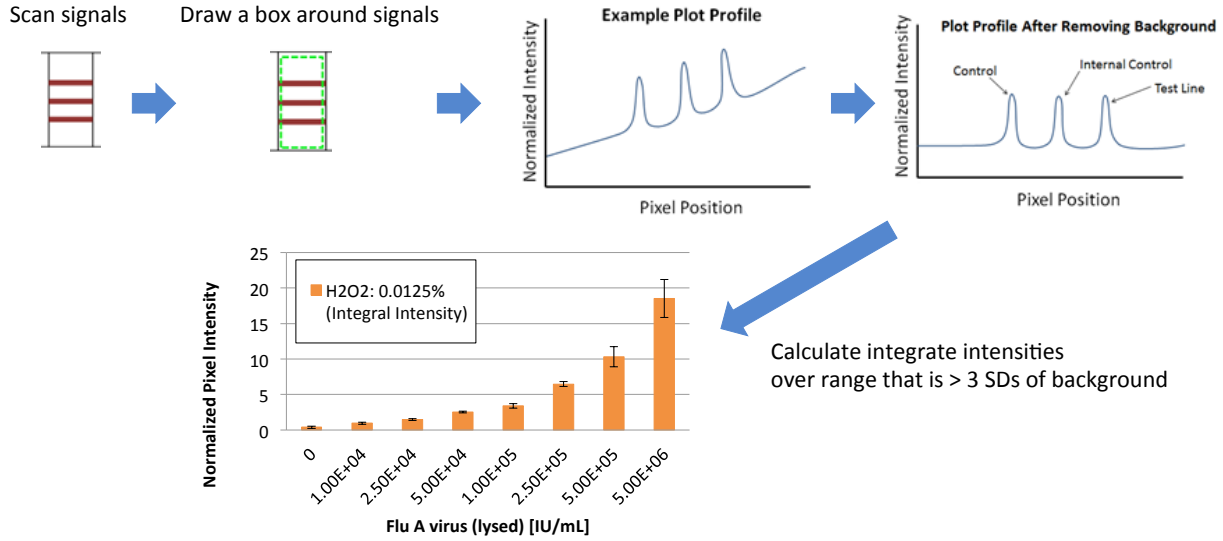

Figure 3.28. Procedure for Integral Intensity method. (1) Scan signals, (2) draw a box around signals to plot test line profile, (3) normalize by removing background, and (4) calculate integrate intensities over range that is more than 3 standard deviations of background.

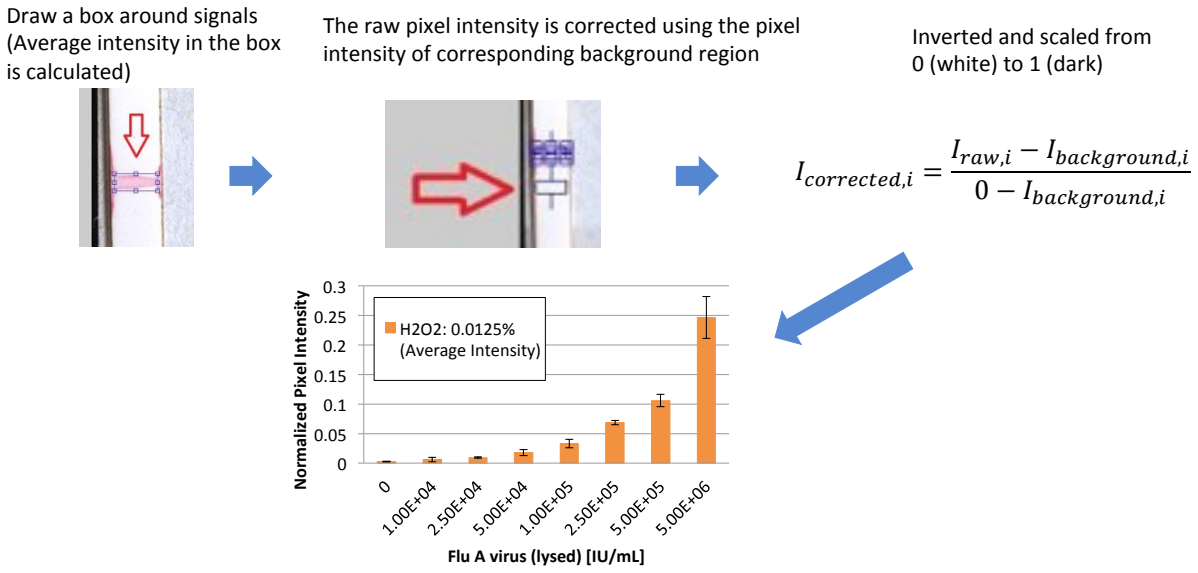

Figure 3.29. Procedure for Local Background Correction method. (1) Draw a box around signals to calculate the average intensity in the box, and (2) the raw pixel intensity is corrected using the pixel intensity of corresponding background region to invert and scale from 0 (white) to 1 (dark).

A range of concentration of influenza A virus (Virapur, from 0 to 5 × 10^6 $TCID_{50}$/mL) was tested and analyzed with the two image analysis approaches (Figure 3.30). Since background intensity was relatively low with HRP/DAB amplification, Integral Intensity method would be easier way to detect low signal intensities (Figure 3.30a and 3.30b). Local Background Correction method resulted in similar signal intensities (Figure 3.30c), but drawing a box around a signal with a low intensity would cause some artifacts. Therefore, Integral Intensity method would be more feasible approach compared to Local Background Correction method.

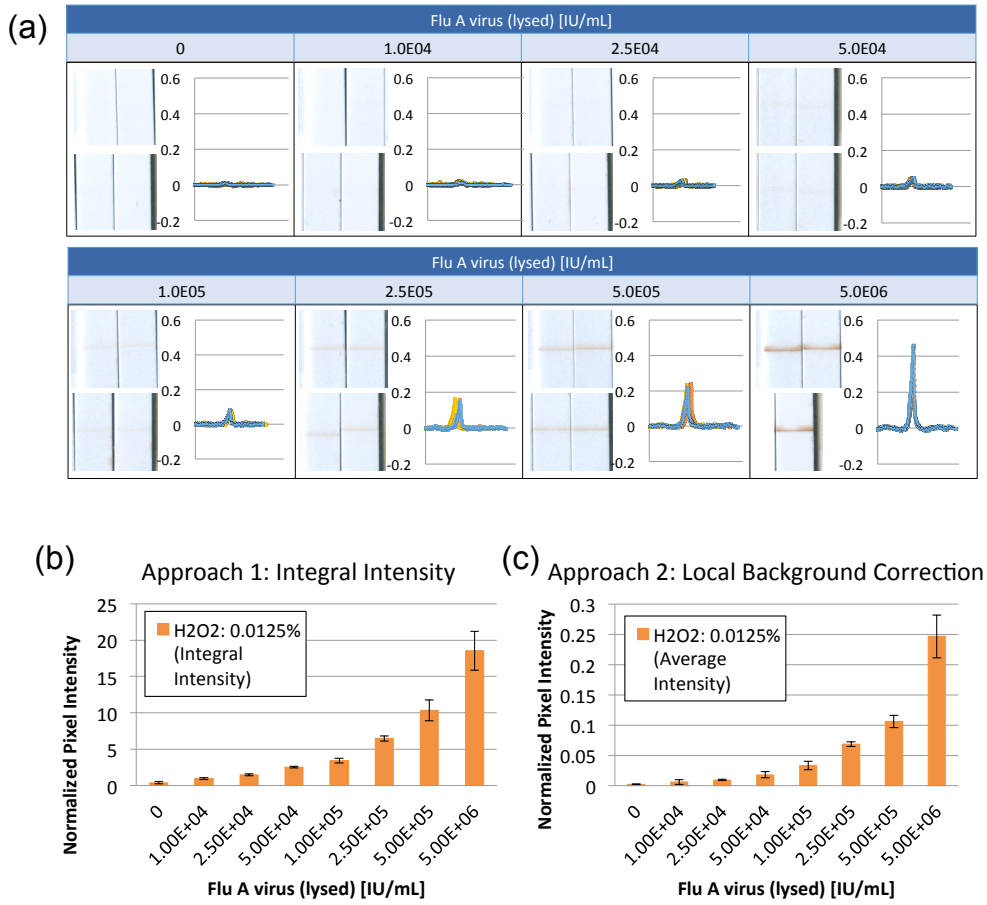

Figure 3.30. Assessment of image analysis methods using influenza A virus (California/7/2009 (H1N1), IU/mL=$TCID_{50}$/mL). (a) Scanned images and test line profiles, (b) integral intensities, and (c) normalized pixel intensities with local background correction are shown (n=4). Virus (20 µL in lysis buffer), HRP conjugate (40 µL of 10 µg/mL in PBS), running buffer as washing solution (20 µL), and DAB (20 µL of 122 µg/mL in PBST) with sodium percarbonate (0.0125 w/v%) as a source of H_2O_2 were applied sequentially.

3.3.3.10 Drydown and rehydration of HRP-IgG using glass fiber

Since conjugate pad is required to develop LFT, drydown and rehydration of HRP conjugate on glass fiber were tested. Protocol of drydown and rehydration is shown in Figure 3.31. HRP conjugate was mixed with trehalose and BSA in PBS. This solution was added on glass fiber (Ahlstrom 8950). Drydown was tested using two approaches: vacuum drying and lyophilization. The glass fiber was then attached on nitrocellulose and NP sample was applied on glass fiber. After 20 min, nitrocellulose was removed from the glass fiber and each reagent (washing buffer, DAB solution, and chase buffer) was applied using 96-well plate. As shown in Figure 3.32, signal intensities using the dry conjugate pad were lower than signals by the dipstick format using wet reagents. This could be due to (1) decreasing of stability of enzyme in the process of drydown and/or (2) inefficient rehydration. To address the issue of enzymatic stability, $FeSO_4$, which was used for the malarial assay[35], was tested for drydown. Also, blocking of glass fiber using BSA and Tween 20 were tested.

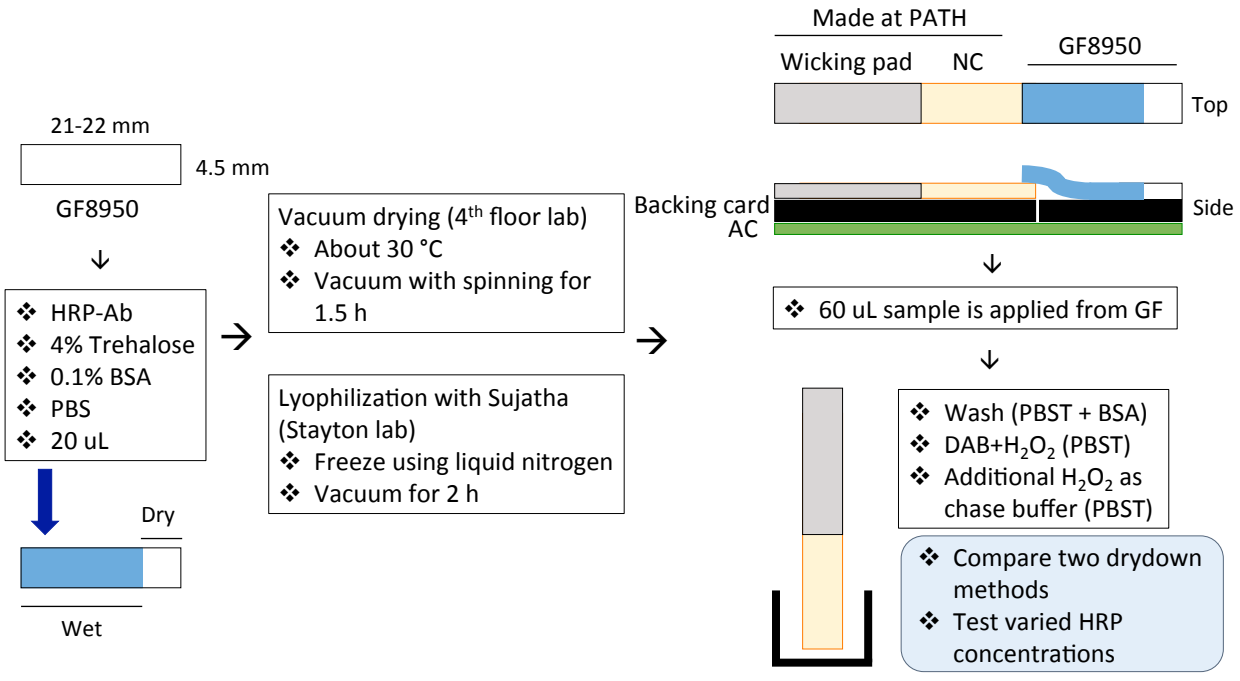

Figure 3.31. Protocol for drydown and rehydration of HRP on glass fiber.

NP (ng/mL)	85								850								8.5	85	850
Drydown	Lyophilization				Vacuum drying				Lyophilization				Vacuum drying				Wet (Dipstick)		
HRP (ug/mL)	3.3	6.7	13	40	3.3	6.7	13	40	3.3	6.7	13	40	3.3	6.7	13	40	6.7		

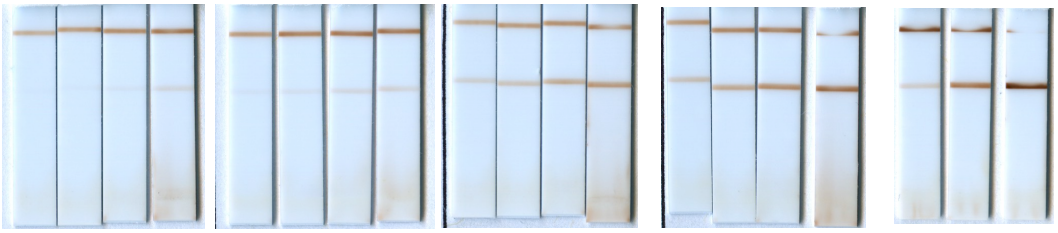

Figure 3.32. Results of drydown and rehydration. Blue table shows results by drydown and rehydration. Red table shows results by dipstick format using wet reagents. HF120, cellulose pad, and backing card are used. Capture antibody for influenza A assay was striped on the membrane at PATH. Virus (20 µL in lysis buffer), HRP conjugate (40 µL of 10 µg/mL in PBS), running buffer as washing solution (20 µL), DAB (20 µL of 122 µg/mL in PBST) with sodium percarbonate (0.0125 w/v%) as a source of H_2O_2, and chase buffer were applied sequentially. Lysis buffer consists of 10 mM PBS, 0.05% Tween 20, 1% (w/v) BSA, and 5% (v/v) Triton X-100. Running buffer consists of 10 mM PBS, 0.05% Tween 20, and 1% (w/v) BSA.

3.3.3.11 Assessment of glass fiber as conjugate pad

The goal of the following experiments was to test different types of glass fiber and varied concentrations of HRP conjugate as an assessment of conjugate pad. As shown in Figure 3.33, pre-blocked Ahlstrom 8964 and 8950 showed better signals. STD17 (GE Healthcare Life Sciences, Pittsburgh, PA, USA) did not show significant improvement by blocking. Since STD17 showed better signal intensities with both unblocked and blocked conditions compared to other glass fiber types, STD17 was used for further optimization of HRP conjugate drydown.

(a)

Glass fiber	Ahlstrom 8964			Ahlstrom 8950			STD17			Dipstick					
HRP [ug/mL]	13.3 (with $FeSO_4$ & Trehalose)									6.7			6.7 ($FeSO_4$ & Trehalose)		
Pre-blocking	No			Yes			No			Yes			No			Yes			No glass fiber					
NP (ng/mL)	0	8.5	85	0	8.5	85	0	8.5	85	0	8.5	85	0	8.5	85	0	8.5	85	0	8.5	85	0	8.5	85

(b)

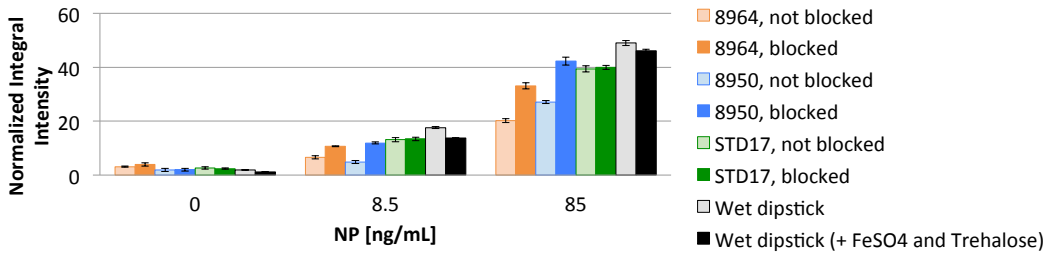

Figure 3.33. Assessment of conjugate pad. (a) Scanned images of signals are shown. Blue table shows results by conjugate pad. Red table shows results by dipstick format. (b) Normalized signal intensities with each condition are shown (n=4). HRP was mixed with 10 mM $FeSO_4$, 4% trehalose, and 0.1% BSA in PBS. 20 µL of the mixed solution was used for drydown on a glass fiber pad (21.5 × 4.5 mm). For pre-blocking of glass fiber pad, a solution of 1% BSA and 0.05% Tween 20 in PBS was used. Glass fiber pads were soaked in the pre-blocking solution, shaken for 1h, and dried in 37°C overnight. Premixed sample of NP (20 µL in lysis buffer) and HRP conjugate (40 µL of 10 µg/mL in PBS), running buffer as washing solution (20 µL), DAB (20 µL of 122 µg/mL in PBST) with sodium percarbonate (0.0125 w/v%) as a source of H_2O_2, and chase buffer were applied sequentially. Lysis buffer consists of 10 mM PBS, 0.05% Tween 20, 1% (w/v) BSA, and 5% (v/v) Triton X-100. Running buffer consists of 10 mM PBS, 0.05% Tween 20, and 1% (w/v) BSA.

3.3.3.12 Assessment of conjugate pad with varied HRP concentrations

Figure 3.34 shows signals with a range of concentration of HRP conjugate. Since HRP concentrations higher than 13.3 µg/mL showed high nonspecific signals (Figure 3.34b), these concentrations were not selected as optimal conditions. In the following study, thus, lower range of HRP concentration was tested.

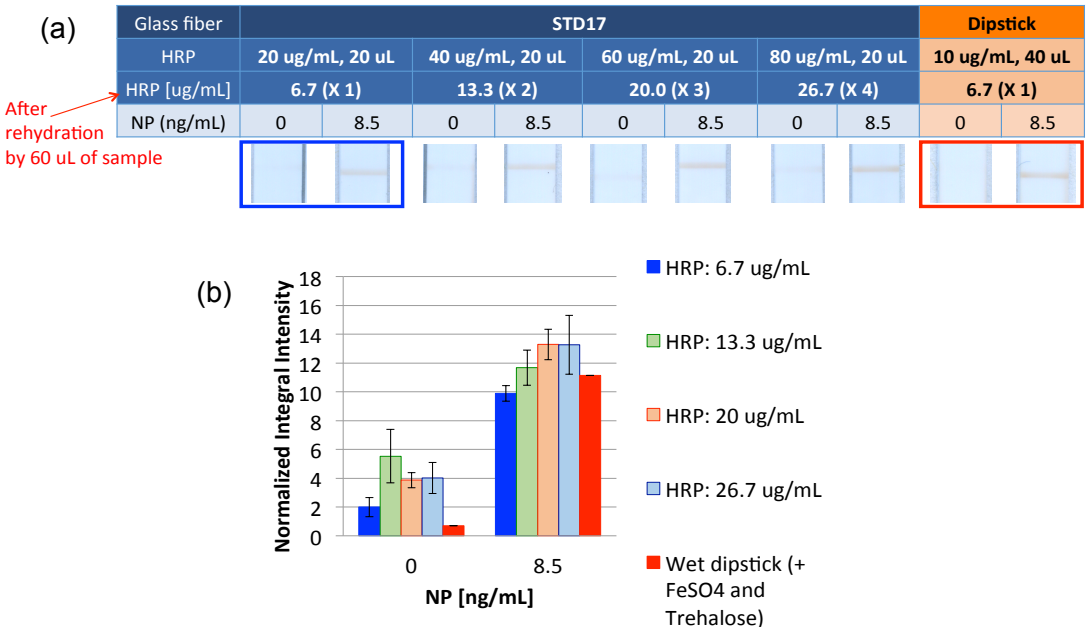

Figure 3.34. Assessment of conjugate pad with varied HRP concentrations. (a) Scanned images of signals are shown. Blue table shows results by conjugate pad (n=4). Red table shows results by dipstick format using wet reagents (n=1). (b) Normalized signal intensities with each condition are shown. HRP conjugate was mixed with 10 mM $FeSO_4$, 4% trehalose, and 0.1% BSA in PBS. 20 µL of the mixed solution was used for drydown on a glass fiber pad (21.5 × 4.5 mm). For pre-blocking of glass fiber pad, a solution of 1% BSA and 0.05% Tween 20 in PBS was used. Glass fiber pads were soaked in the pre-blocking solution, shaken for 1h, and dried in 37°C overnight. Premixed sample of recombinant NP (20 µL in lysis buffer) and HRP conjugate (40 µL of 10 µg/mL in PBS), running buffer as washing solution (20 µL), DAB (20 µL of 122 µg/mL in PBST) with sodium percarbonate (0.0125 w/v%) as a source of H_2O_2, and chase buffer were applied sequentially. Lysis buffer consists of 10 mM PBS, 0.05% Tween 20, 1% (w/v) BSA, and 5% (v/v) Triton X-100. Running buffer consists of 10 mM PBS, 0.05% Tween 20, and 1% (w/v) BSA.

Figure 3.35a shows scanned images of each signal by varied drydown conditions. Quantified signal intensities (Figure 3.35b) show that 20 µg/mL of HRP-IgG showed similar signal intensities compared to signals by wet dipstick format. This condition was used as our optimized drydown condition.

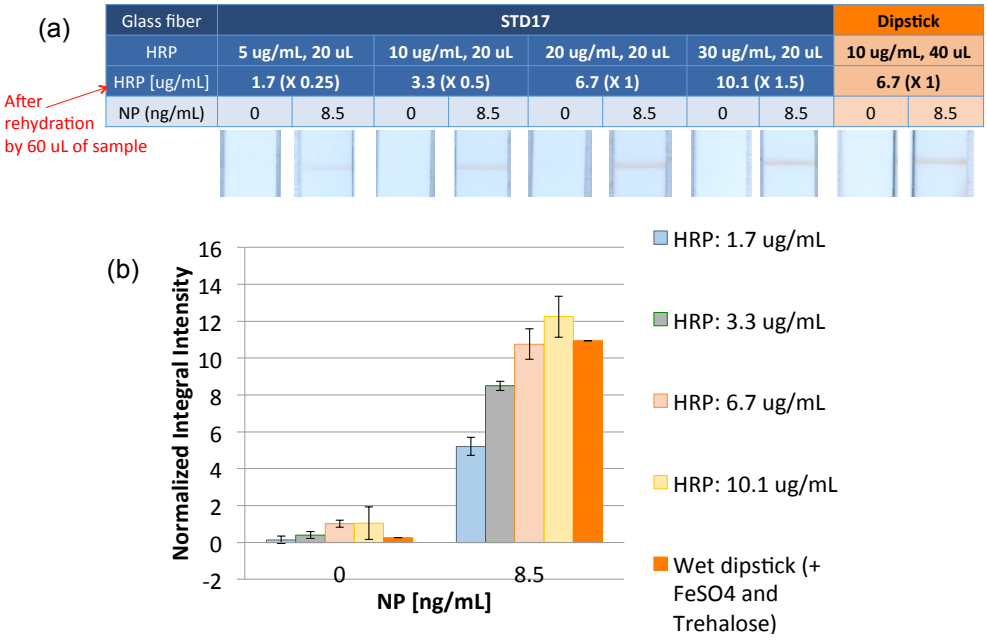

Figure 3.35. Assessment of conjugate pad with lower HRP concentrations. (a) Scanned images of signals are shown. Blue table shows results by conjugate pad (n=4). Red table shows results by dipstick format using wet reagents (n=1). (b) Quantified signal intensities are shown. HRP was mixed with 0.01M $FeSO_4$, 4% trehalose, and 0.1% BSA in PBS. 20 µL of the mixed solution was used for drydown on a glass fiber pad (STD17, 21.5 × 4.5 mm). Premixed sample of recombinant NP (20 µL in lysis buffer) and HRP conjugate (40 µL of 10 µg/mL in PBS), running buffer as washing solution (20 µL), DAB (20 µL of 122 µg/mL in PBST) with sodium percarbonate (0.0125 w/v%) as a source of H_2O_2, and chase buffer were applied sequentially. Lysis buffer consists of 10 mM PBS, 0.05% Tween 20, 1% (w/v) BSA, and 5% (v/v) Triton X-100. Running buffer consists of 10 mM PBS, 0.05% Tween 20, and 1% (w/v) BSA.

3.3.3.13 Summary of the assessments of conjugate pad using HRP-IgG

Figure 3.36 shows a summary of the assessments of conjugate pad using HRP-IgG. Our current best condition with 20 µg/mL of HRP-IgG showed signal intensities comparable to signals by wet dipstick format. However, this condition did not show the same sensitivity in an integrated 2DPN device (data not shown, other members in our lab investigated) because flow rate, volume of each reagent, and washing efficiency in 2DPN were different compared to the simpler prototype that was developed herein. Therefore, further optimization was investigated for an integrated 2DPN device.[68]

(a)

	Current best	Tested conditions
HRP -Ab [ug/mL]	20	10-120
FeSO4 [mM]	10	10
Trehalose [%]	4	4
BSA [%]	0.1	0.1
Glass fiber	STD17	STD17, 8950, 8964
Blocking of glass fiber	Yes	No, Yes
Dextran [%]		
Drydown method	Vacuum	Vacuum, Lyophilization

(b)

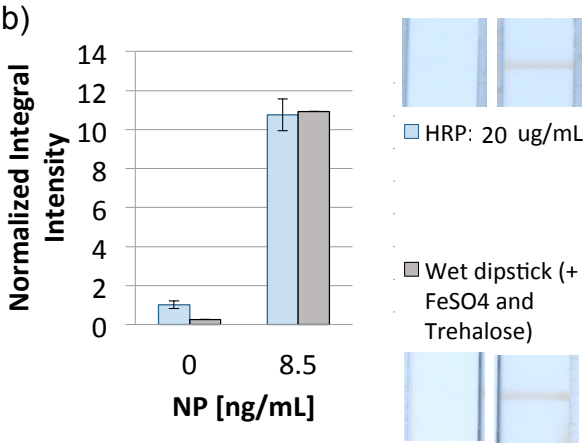

Figure 3.36. Summary of conditions tested for drydown of HRP-IgG. (a) Current best condition and tested conditions are shown. (b) Signal intensity with the current best condition for drydown of HRP-IgG (n=3) was compared with the signal intensity by wet dipstick format (n=1). HRP conjugate was mixed with 10 mM $FeSO_4$, 4% trehalose, and 0.1% BSA in PBS. 20 µL of the mixed solution was used for drydown on a glass fiber pad (STD17, 21.5 × 4.5 mm).

3.3.3.14 Streptavidin poly-HRP to increase the ratio of HRP in assay stack

So far, the following procedure has been tested for HRP/DAB assay: add (1) a mixture of NP sample and HRP-IgG conjugate, (2) wash buffer, (3) DAB solution including H_2O_2, and (4) chase buffer (H_2O_2 in PBST) using 96-well plate to sequentially apply each reagent. HRP-IgG showed better LOD than gold nanoparticles-based assay for both recombinant NP and virus samples. To further improve the sensitivity, streptavidin poly-HRP was investigated as a new assay label (Figure 3.37). Streptavidin poly-HRP is polymer of HRP molecules that are covalently conjugated to streptavidin to increase the molar ratio of HRP on the conjugate. To apply the streptavidin poly-HRP for sandwich immunoassay, biotinylated detection antibody (biotin-IgG) was used as a secondary antibody.

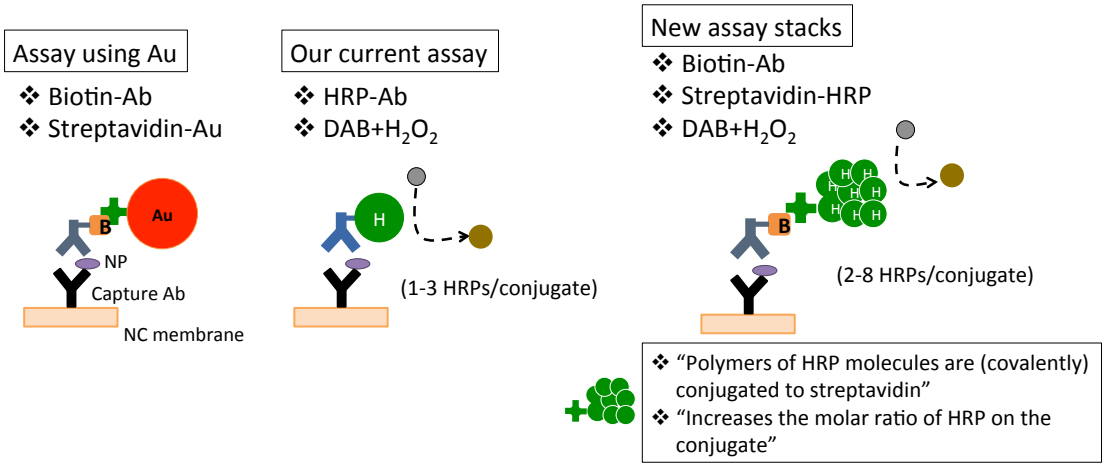

Figure 3.37. Assay stacks for influenza A NP detection. For Au nanoparticles-based assay, biotinylated detection antibody (biotin-IgG) and streptavidin-coated gold nanoparticles (streptavidin-Au) were used (LOD was 1.4 × 10^5 $TCID_{50}$/mL). To improve the sensitivity, HRP-IgG and DAB/H_2O_2 solution were used for the current assay stack (LOD was 2.4 × 10^4 $TCID_{50}$/mL). To further improve the sensitivity compared to commercial kit (5.0 × 10^4 $TCID_{50}$/mL was detectable by BD kit), streptavidin poly-HRP (streptavidin-HRP) was used in a new assay stack. Streptavidin-HRP is polymer of HRP molecules that are covalently conjugated to streptavidin to increase the molar ratio of HRP on the conjugate. For this streptavidin-HRP system, biotin-IgG was used as a secondary antibody.

3.3.3.15 LOD analysis before optimizing the assay with streptavidin poly-HRP

Although each condition was not optimized for the assay with streptavidin poly-HRP, LOD was measured to know the performance of the new assay stack compared to the previous assay with HRP-IgG. Figure 3.38a shows results by a range of concentrations of influenza A virus. As shown in Figure 3.38b, the streptavidin poly-HRP assay resulted in higher signal intensities compared to LOD of the previous HRP-IgG assay and commercially available BD kit. Each reagent concentration for the streptavidin poly-HRP assay was improved in the section 3.3.3.17.

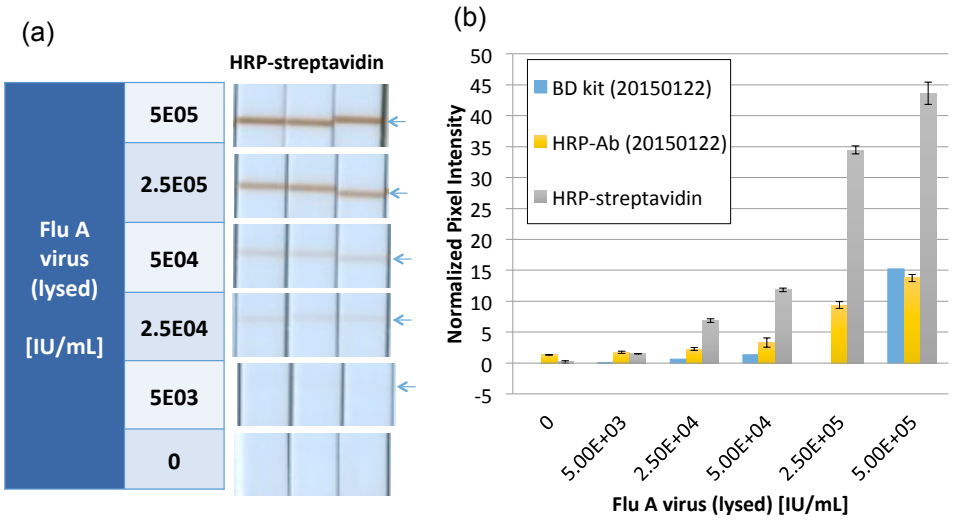

Figure 3.38. LOD analysis of the streptavidin-HRP assay. (a) Scanned images of signal using a range of concentrations of influenza A virus and (b) quantified signal intensities including previous results by HRP-IgG assay and BD kit are shown (n=3). Virus sample (20 µL in lysis buffer), biotin-IgG (20 µL of 5 µg/mL in running buffer), and streptavidin-HRP (40 µL of 2 µg/mL) were premixed and then applied. After that, running buffer as washing solution (20 µL), DAB (20 µL of 122 µg/mL in PBST) with sodium percarbonate (0.0125 w/v%) as a source of H_2O_2, and chase buffer (20 µL of 0.0125 w/v% of sodium percarbonate in PBST) were applied sequentially. Lysis buffer consists of 10 mM PBS, 0.05% Tween 20, 1% (w/v) BSA, and 5% (v/v) Triton X-100. Running buffer consists of 10 mM PBS, 0.05% Tween 20, and 1% (w/v) BSA.

3.3.3.16 Estimation of costs and amount of HRP in two systems

Figure 3.39 shows a summary of the streptavidin poly-HRP assay and the HRP-IgG assay to compare their costs and expected amount of HRP. Total cost/test of the detection antibody and HRP in the streptavidin poly-HRP assay and the HRP-IgG assay are ~$0.09 and ~$0.27, respectively. In addition, expected amount of HRP per assay is higher with the streptavidin poly-HRP assay (75~300 nM) compared to the HRP-IgG assay (62~190 nM). Therefore, the streptavidin poly-HRP assay has a potential to increase the molar ratio of HRP with lower cost.

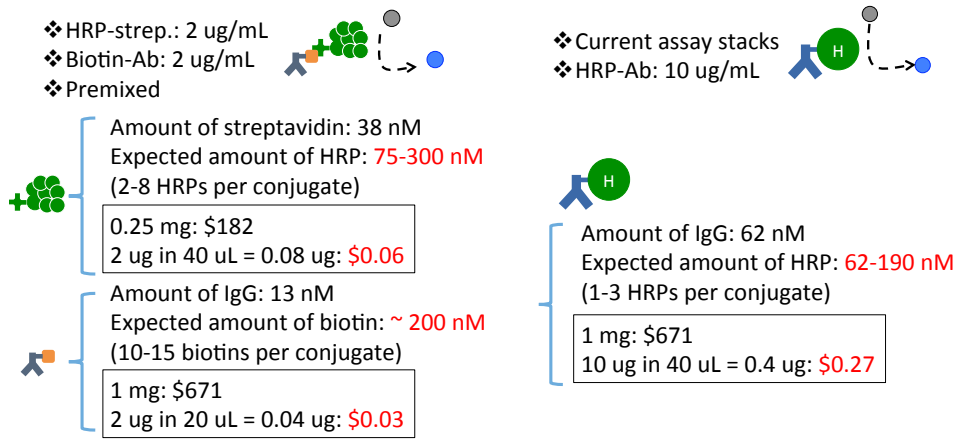

Figure 3.39. Expected amount of HRP and total cost per test in the new and previous assay.

3.3.3.17 Optimization of the streptavidin poly-HRP assay

Figure 3.40 shows signal intensities (specific signal subtracted by nonspecific signal) using a range of concentrations of each reagent to optimize the streptavidin poly-HRP assay. Streptavidin poly-HRP concentration was varied from 0.25 to 3.00 μg/mL and 0.5 μg/mL showed high signal intensity with low standard deviation (SD) (Figure 3.40a). High SD was observed by 3.00 μg/mL of streptavidin poly-HRP because high concentration of HRP was hard to be fully rinsed by washing step and caused high background. Figure 3.40b shows a range of DAB concentrations and 50 μg/mL showed higher signal intensity than the other concentrations. Higher DAB concentrations than 50 μg/mL showed lower signal intensities, which were also due to high background. Concentration of biotinylated detection IgG was varied from 0.25 to 8.00 μg/mL and 2.00 μg/mL was optimal concentration (Figure 3.40c). Higher concentrations than 2.00 μg/mL resulted in high nonspecific signal, which disrupts LOD improvement. A range of sodium percarbonate concentrations was also assessed and 0.0125 w/v% was optimal to achieve high signal intensity with low nonspecific signal (Figure 3.40d). High sodium percarbonate

concentration produced high concentration of H_2O_2 and it would lessen the enzymatic activity of HRP, which leads to lower signal intensity.

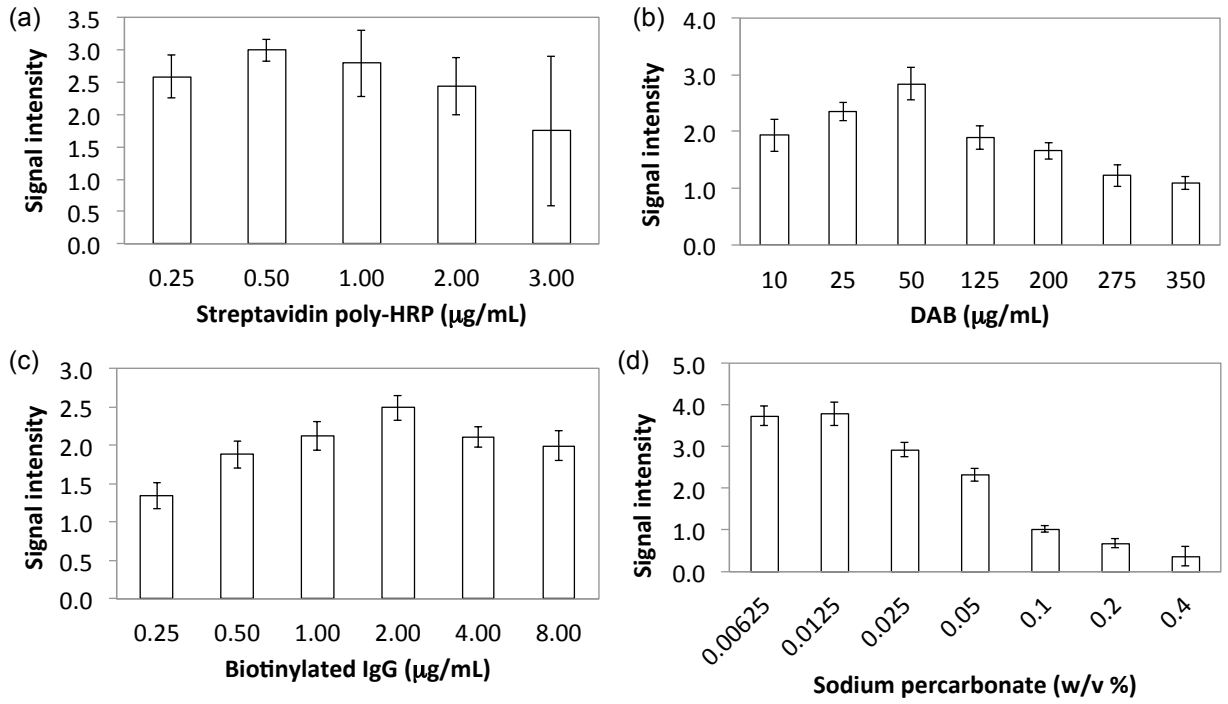

Figure 3.40. Optimization of reagent concentration in the streptavidin poly-HRP assay. Signals using a range of concentrations of (a) streptavidin poly-HRP, (b) DAB, (c) biotinylated detection IgG, and (d) sodium percarbonate are shown (n=4). For streptavidin poly-HRP, DAB, biotinylated detection IgG, and sodium percarbonate, 0.5 μg/mL, 50 μg/mL, 2.0 μg/mL, and 0.0125% were optimal concentrations, respectively. These optimal concentrations were used for each optimization process. Specific signal from positive sample (2.5×10^4 $TCID_{50}$/mL) was subtracted by nonspecific signal from negative sample (0 $TCID_{50}$/mL).

3.3.3.18 LOD analysis of the improved streptavidin poly-HRP assay

The clinically-relevant range of influenza A virus is approximately $1.0 \times 10^3 \sim 1.0 \times 10^7$ IU/mL (virus concentration in IU/mL in this study is based on the value provided by Virapur. IU/mL=$TCID_{50}$/mL).[69,70] However, our preliminary results in wet dipstick format using gold nanoparticles-based assay showed 10^3-fold higher (worse) LOD compared to the lowest clinical relevant range. To improve the assay sensitivity, we tested detection antibody directly conjugated to HRP (HRP-IgG) to enhance the signal (Figure 3.41a). HRP-IgG is conjugated using periodate-

oxidized HRP (communication from HyTest) and typically, molar ratios of 4:1 to 15:1 (enzyme:antibody) give conjugates acceptable for ELISA techniques.[71] The LOD was 2.4×10^4 $TCID_{50}$/mL, which was approximately 10-fold better than our gold nanoparticles-based assay and 10-fold worse than the lowest clinical relevant range. The streptavidin poly-HRP assay was tested to increase the number of HRP copies in the assay stack without increasing the concentration of detection antibody (Figure 3.41b). Streptavidin poly-HRP contains 2-8 HRPs per streptavidin (communication from Thermo Fisher Scientific). Biotin-IgG is made using biotin-isothiocyanate for biotinylation (communication from HyTest). Typically, molar ratios of about 2:1 to about 50:1 (biotin:antibody) can be available for biotinylation.[71] Biotin-IgG and Pierce streptavidin poly-HRP were premixed with virus sample and then applied to the strip. The improved streptavidin poly-HRP assay showed very low nonspecific signal, which would be due to the concentration of detection antibody (2 μg/mL) that was lower than the concentration (10 μg/mL) in the HRP-IgG assay. Figure 3.41c shows LODs of these assays, showing LOD of 8.2×10^3 $TCID_{50}$/mL in the streptavidin poly-HRP assay (LOD was calculated by the previously developed MATLAB script[66]). This LOD was still higher than the lowest clinically relevant range (1.0×10^3 $TCID_{50}$/mL). The 2DPN could be a platform to improve LOD because the reagent delivery can be modified. For example, the DAB amplification solution can be directly applied to the capture region to avoid the loss of the reagent while decreasing assay time.

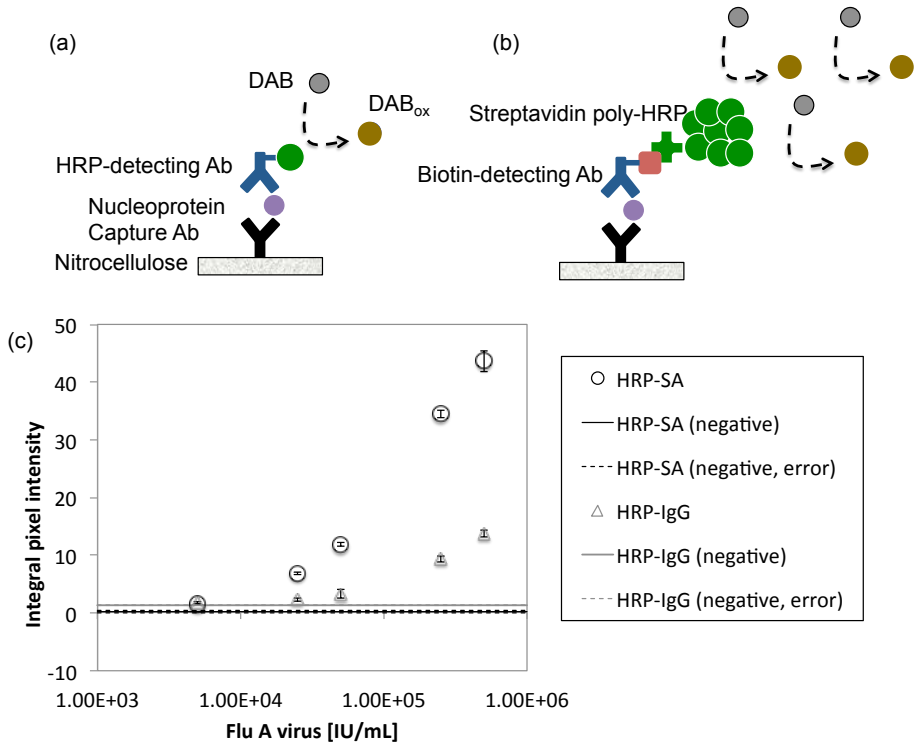

Figure 3.41. LOD assessment of HRP/DAB assay for influenza A NP detection. Schematic of assay stacks in (a) HRP-IgG assay and (b) streptavidin poly-HRP (HRP-SA) assay, and (c) LOD comparison of both assays are shown (n=4). Calculated LODs of HRP-IgG assay and HRP-SA assay were 2.4×10^4 (lower and upper 95% CI = 1.4×10^4 and 3.3×10^4) and 8.2×10^3 (lower and upper 95% CI = 4.1×10^3 and 1.2×10^4) IU/mL, respectively (IU/mL=$TCID_{50}$/mL).

3.3.3.19 Patient sample and SNM for influenza A assay

Patient sample, simulated nasal matrix (SNM) and PBST were tested as dilution buffers for influenza A assay (Figure 3.42). Signal intensities with positive sample were decreased by SNM compared to the signals using patient sample and PBST. Although patient sample also resulted in lower signal than the signal using PBST, nonspecific signals with patient sample were very low. This is important to achieve improved LOD. As a conclusion, patient sample would not have significant impact on specific/nonspecific signal in influenza A assay.

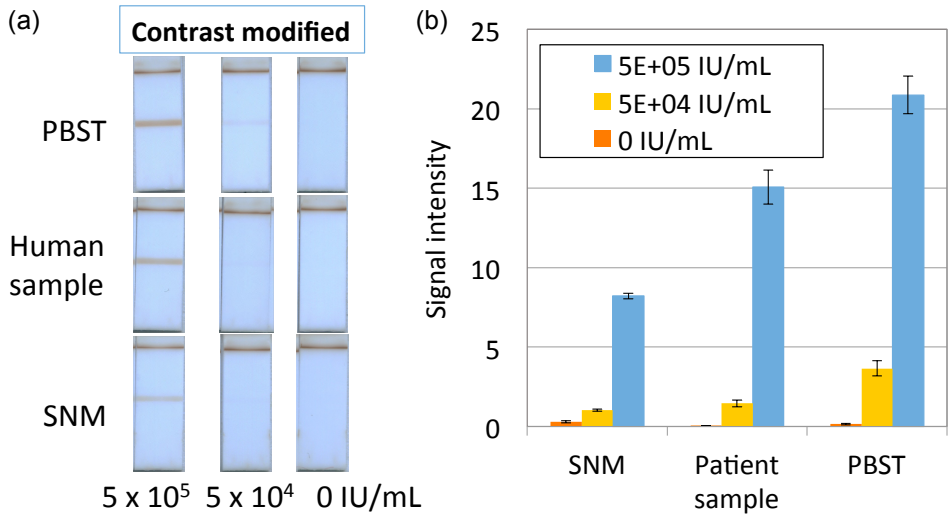

Figure 3.42. Assessment of dilution buffer for influenza A assay. Samples of PBST, human sample and simulated nasal matrix (SNM) were mixed with virus sample. (a) Scanned images of strips and (b) quantified signal intensities are shown (n=4). Virus sample (20 µL in dilution buffer with 5% Triton X-100), biotin-IgG (20 µL of 2 µg/mL in running buffer), and streptavidin-HRP (40 µL of 0.5 µg/mL in running buffer) were premixed and then applied to each LFT strip. Running buffer as washing solution (20 µL), DAB (20 µL of 50 µg/m in PBST) with sodium percarbonate (0.0125 w/v%) as a source of H_2O_2, and chase buffer (20 µL of 0.0125 w/v% sodium percarbonate in PBST) were then applied sequentially.

3.3.3.20 Prototype of POC device with dry storage conjugate pad

Figure 3.43a shows a schematic diagram of a prototype POC device, which requires extra user steps (i.e. not fully automated device). Detailed protocols are shown in the Methods section. Wet dipstick format was also performed as positive control. In the dipstick format, 0.02 µg (40 µL) of streptavidin poly-HRP and 0.04 µg (20 µL) of biotin-IgG were used. To optimize the concentration of streptavidin poly-HRP and biotin-IgG in the conjugate pad of the prototype, varied amounts of each reagent were evaluated; 0.02~0.08 µg (i.e. 1~4-fold higher than the concentration in the dipstick format) of streptavidin poly-HRP and 0.04~0.12 µg (i.e. 1~3-fold higher than the concentration in the dipstick format) of biotin-IgG were assessed. Figure 3.43b, 3.43c, and 3.43d show signal intensities by 1, 2 and 3-fold higher biotin-IgG, respectively. Compared to the specific signal in the dipstick format, several conditions showed better signal

intensities with the conjugate pad. When the same streptavidin poly-HRP concentration was used for both dipstick format and prototype, the prototype showed lower signal intensity than the dipstick format. This could be due to the low rehydration efficiency and thus lower amount of HRP that passed through the capture region compared to the dipstick format. Nonspecific signal by 3~4-fold higher streptavidin poly-HRP concentration in the prototype was higher than the nonspecific signal in dipstick format. Therefore, 2-fold higher streptavidin poly-HRP and 1~2-fold higher biotin-IgG concentrations, compared to the dipstick format, were optimal conditions for the dry conjugate pad.

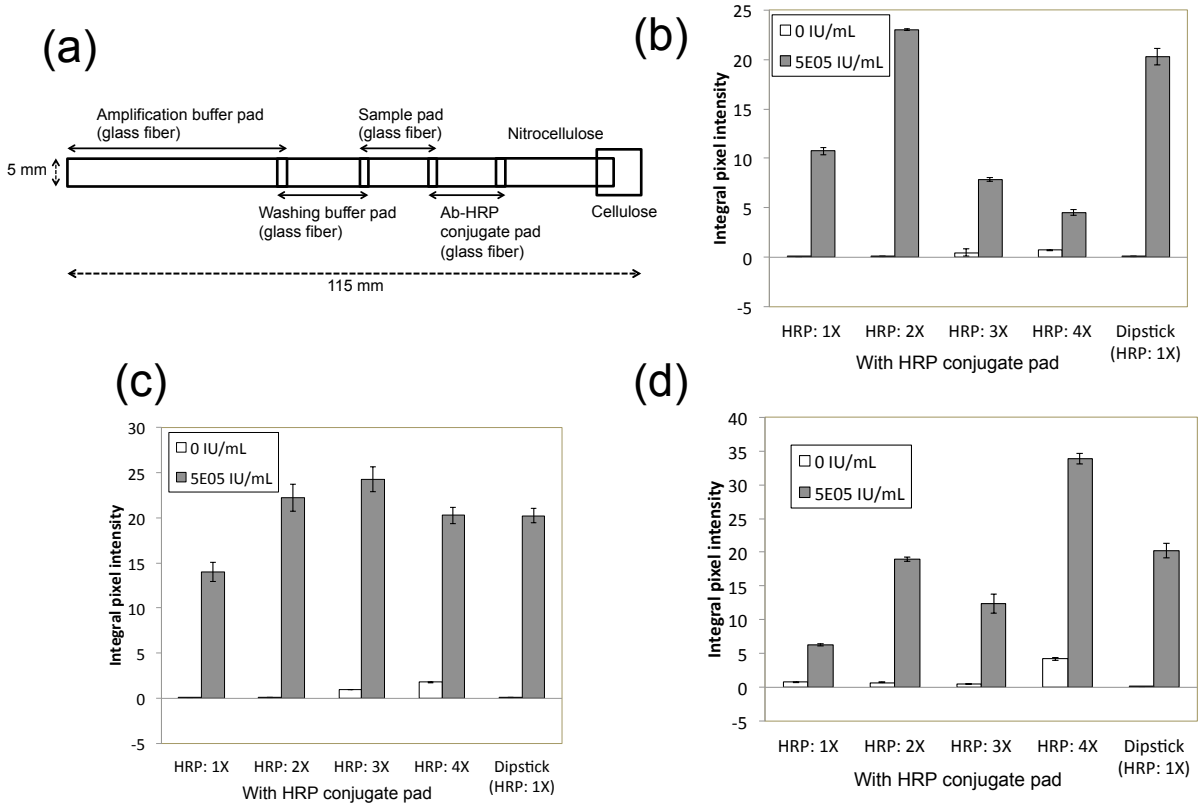

Figure 3.43. Assessment of antibody-HRP conjugate pad in the prototype POC device. (a) Schematic diagram of the prototype with antibody-HRP conjugate pad is shown. Signal intensities by the prototype with (b) 0.04 μg (1X), (c) 0.08 μg (2X), and (d) 0.12 μg (3X) of biotin-IgG are shown (n=4). HRP concentration was varied from 0.02 to 0.08 μg (1~4X). 1~4X means 1~4-fold higher than the concentration in the dipstick format. The dipstick format was performed as positive control (0.02 μg of HRP and 0.04 μg of biotin-IgG were used as 1X reagent concentration).

LOD of the prototype with the optimized antibody-HRP conjugate pad was assessed and compared with the dipstick format and a commercially-available kit (BD Directigen EZ Flu A+B). LODs of the dipstick format, prototype, and commercial kit were 6.7×10^3, 1.3×10^4, and 6.0×10^4 $TCID_{50}$/mL, respectively (Figure 3.44). The dipstick format achieved 10-fold better LOD than the commercial kit while the prototype showed only ~5-fold better LOD. The lower sensitivity of the prototype compared to the dipstick format could be due to insufficient wash and excessive delivery of the amplification buffer. Either of these problems could lead to high background and nonspecific signal. A fully-automated 2DPN assay with HRP-IgG conjugate pad was reported.[68]

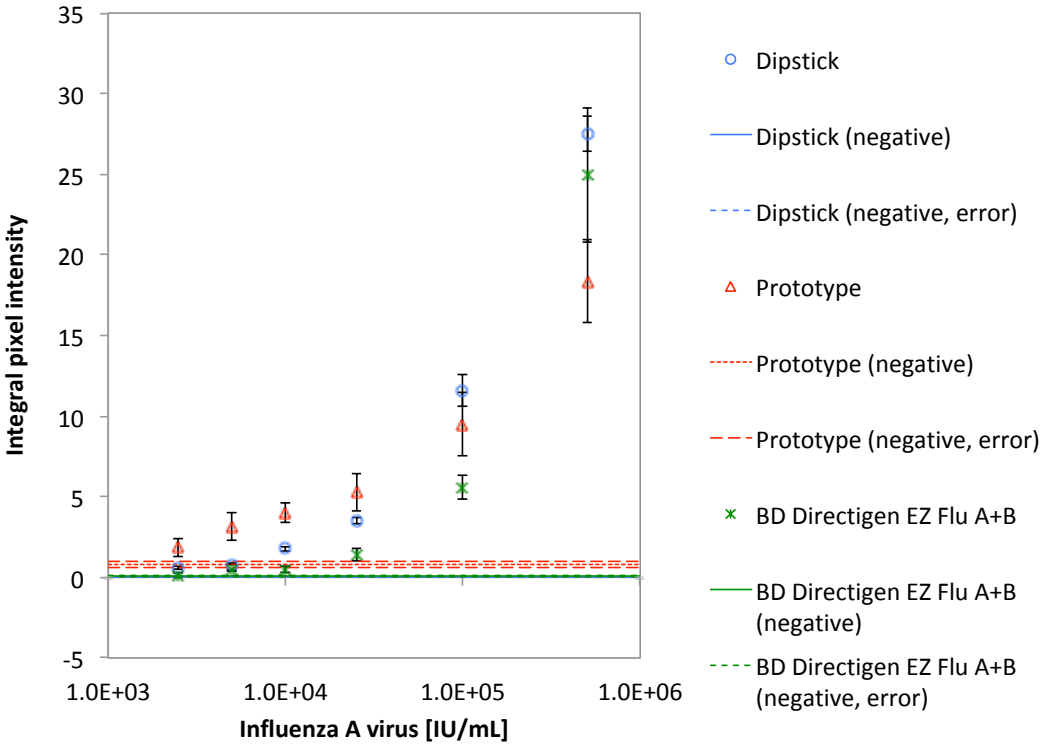

Figure 3.44. LOD assessment of the prototype with the optimized antibody-HRP conjugate pad. LODs of the dipstick, prototype, and commercial kit were 6.7×10^3 (lower and upper 95% CI = 3.5×10^3 and 9.4×10^3), 1.3×10^4 (lower and upper 95% CI = 4.8×10^3 and 2.3×10^4), and 6.0×10^4 (lower and upper 95% CI = 2.4×10^4 and 9.6×10^4) IU/mL, respectively (IU/mL=$TCID_{50}$/mL, n=4).

3.3.4 Conclusions

The work presented in this section demonstrated a chemically-amplified influenza A NP immunoassay, which achieved a 10-fold better LOD compared to a commercially available RDT. The prototype of a POC diagnostic device with antibody-HRP conjugate pad showed ~5-fold LOD improvement than the commercial kit. A fully automated assay device was reported based on this study.[68]

4 SPECIFIC AIM 2: INVESTIGATE REAGENT DELIVERY FORMAT

4.1 MOTIVATION AND GOALS

Recently, the Fu group investigated two types of reagent delivery formats in a sandwich immunoassay for malarial protein detection: a "premixed format", which is similar to what occurs in conventional LFTs, and in a "sequential delivery" of reagents, which is a feature that the 2DPN can provide.[55] They demonstrated a lower LOD with the sequential format compared the premixed format, attributing the advantage to the multivalent binding sites on the malarial protein and detection antibodies. Their mathematical model of the assay reproduced the experimental binding profiles (the intensity of the color from the leading to the trailing edge of the capture lines). The model has the potential to improve the sensitivity by customizing the reagent delivery format optimal for the number of binding sites available.

The goal of Specific Aim 2 was to improve the reagent delivery format specifically for the influenza A NP assay and to develop a computational model to predict assay performance. Since binding rate constants in our assay would be different from those in the malarial assay, it was assumed that the reagent delivery format for the influenza A NP assay could be optimized to improve LOD of the assay. In addition, modeling of the assay might allow prediction of a potential global minimum for the LOD. Since our system is a common sandwich immunoassay, such a model also can be used as a universal design tool for other protein detection systems.

4.2 GOAL 1: OPTIMIZE REAGENT DELIVERY FORMAT

4.2.1 Introduction

This section is to investigate the reagent delivery formats (the premixed and sequential delivery formats) for optimization of the assay to improve LOD. The following sections demonstrate comparisons of the premixed and sequential delivery, which motivated us to develop a related preliminary computational model.

4.2.2 Methods

Lateral flow tests (LFTs) were performed by applying wet reagents using a 96-well plate until the fluid was drawn from each well (the "dipstick" format). Two reagent delivery formats were compared. The premixed format consisted of the following reagents: (1) 40 μL of HRP-conjugated detection antibody or the mixture of 20 μL of biotin-detection antibody and 40 μL of Pierce streptavidin poly-HRP, which are both premixed with 20 μL of influenza A virus; (2) 20 μL of the running buffer as washing solution; and (3) 20 μL of DAB with 0.0125% (w/v) sodium percarbonate. On the other hand, the sequential format consisted of the following reagents: (1) 20 μL of influenza A virus; (2) 40 μL of HRP-conjugated detection antibody or the mixture of 20 μL of biotin-detection antibody and 40 μL of Pierce streptavidin poly-HRP; (3) 20 μL of the running buffer as washing solution; and (4) 20 μL of the DAB solution.

4.2.3 Results and Discussion

The Fu group previously compared reagent delivery in the premixed and sequential formats for a malarial antigen assay.[55] To investigate and optimize reagent delivery in our influenza NP assay, we compared the two reagent delivery formats (Figure 4.1). For the premixed format, HRP-IgG (Figure 4.1b) or biotin-IgG mixed with streptavidin poly-HRP (Figure 4.1e) were premixed with

virus sample. On the other hand, in the sequential format, HRP-IgG (Figure 4.1a) or biotin-IgG mixed with streptavidin poly-HRP (Figure 4.1d) were applied to the LFT after running virus sample. The malarial antigen assay, which utilized gold-nanoparticles-labeled detection antibody, indicated that the assay sensitivity was 4~10-fold better by the sequential format.[55] However, in contrast, Figure 4.1c (using HRP-IgG) and 4.1f (using streptavidin poly-HRP) show better sensitivity ($p<0.05$) using the premixed format in both assay stacks. This suggests that the reagent delivery format affects the signal intensity, which, in turn, seems to depend on binding rate constants in each assay system. This indicates a route for optimizing the reagent delivery format in LFTs for all sandwich assay systems. To elucidate the underlying mechanism, additional investigation of binding kinetics was reported in the following section using a mathematical model.

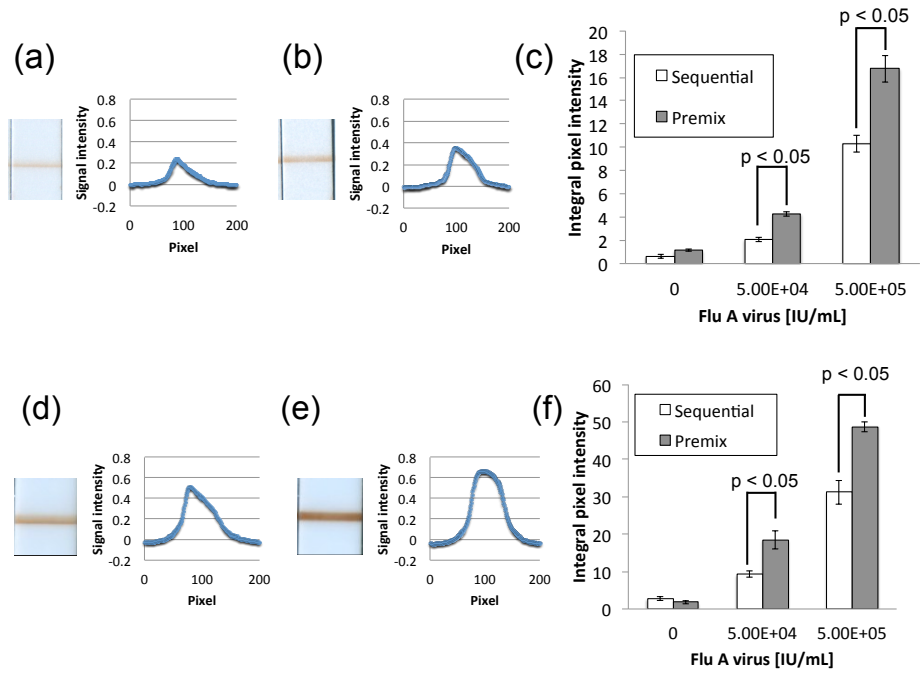

Figure 4.1. Comparison of reagent delivery formats. Signal intensities by assay stack with (a-c) HRP-IgG and (d-f) biotin-IgG mixed with streptavidin poly-HRP. Scanned images (left) and signal profiles (right) are shown for the sequential (a and d) and premixed (b and e) format (using 5.0×10^5 IU/mL of virus). A range of virus concentrations was used to quantify signals in both assay stacks (c and f, n=4). IU/mL=$TCID_{50}$/mL.

4.2.4 Conclusions

This work presents chemically-amplified influenza A NP immunoassay with improved reagent delivery format. The premixed format showed better sensitivity compared to the sequential format. We attempted to optimize the reagent delivery format to achieve high specific signal and low nonspecific signal. To elucidate the underlying mechanism of the reagent delivery format, a preliminary mathematical model to predict performance of the HRP/DAB assay was studied in the following section.

4.3 Goal 2: Develop Computational Model of a Flu Nucleoprotein Lateral Flow Assay to Predict Optimal Assay Condition

4.3.1 Introduction

Previous mathematical model studies for microfluidic-based immunoassays have investigated the effects of flow rate and binding constants in pressure-driven flow systems.[51] Lateral flow sandwich immunoassays have also been investigated using a model to predict binding signal with a single set of binding rate constants.[52] Recently, the Fu group investigated two types of reagent delivery formats in a sandwich immunoassay for malarial protein detection.[55] To predict the performance of our influenza A NP assay, the previously-developed model was provided by the Fu group and applied to the influenza assay by modifying some key parameters.

4.3.2 Methods

A previously-developed model of lateral flow sandwich immunoassay, which was to predict test line development and signal intensities using COMSOL Multiphysics (Burlington, MA)[55], was modified and applied to the influenza NP assay. For simplicity, the analyte was assumed to bind up to one capture species and up to one detection species at a time, with 4 sets of binding rate

constants. Effective association and dissociation rate constants were measured by bio-layer interferometry using an Octet RED96 (Pall ForteBio, Fremont, CA, USA). Darcy flow was utilized in the model within a duct (9 × 0.135 mm) with a downstream detection region (0.7 mm length) that included uniformly distributed immobilized capture sites.

Equation 4.1 shows related equation of Darcy's law:

$$Q = -\frac{\kappa A(p_b - p_a)}{\mu L} \tag{4.1}$$

where Q represents total discharge, κ represents permeability of the medium, A represents cross-sectional area to flow, $p_b - p_a$ represents total pressure drop, μ represents viscosity, and L represents the length over which the pressure drop occurs.

The bulk porosity modeled was 0.8, corresponding to the porosity of the nitrocellulose membrane (according to specifications from Millipore). Values in the model parameters were corresponding to experimental data. The capillary pressure for Darcy flow (4×10^3 Pa) was based on the flow rate of nitrocellulose membrane. The timing of the reagent input and total assay time (30 min) for the model were based on our experimental data. The Michaelis constant K_M and the constant k_{cat}/K_M (catalytic efficiency) of HRP with DAB as input parameters were based on measured values by absorbance detection using a previously-developed method.[72]

To modify the previously-developed model for sandwich immunoassay to apply for the influenza NP assay, we first determined whether the influenza recombinant NP (Brisbane/10/2007/H3N2, IRR) used in the model is a monomer in PBST. Analytical ultracentrifugation (AUC) was used to measure the range of observed sedimentation coefficients. Experimental and model data were

directly compared using an experimentally-derived calibration curve of the concentration of oxidized DAB (DAB_{ox}) and signal intensity.

4.3.3 Results and Discussion

4.3.3.1 Epitopes of NP to antibody provided by HyTest

Since the number of epitopes is critical to understand the binding reaction between an antibody and an antigen, a previously-reported work was referred to understand the structure of NP.[73] In this report, the authors showed that (1) trimer would be the most favorable structure of influenza NP and (2) monomer of NP has head and body region (Figure 4.2a). HyTest indicated that each monoclonal antibody (MAb) has each unique binding site (Figure 4.2b. For example, "InB36" would bind to "Fragment 1" of influenza NP). If most part of residues are conserved among different strains and types of influenza NP, it can be assumed that the head region and body region are binding sites for detection Ab and capture Ab, respectively (Figure 4.2, highlighted as red and blue). Therefore, trimer of NP would have 3 binding sites for each antibody.

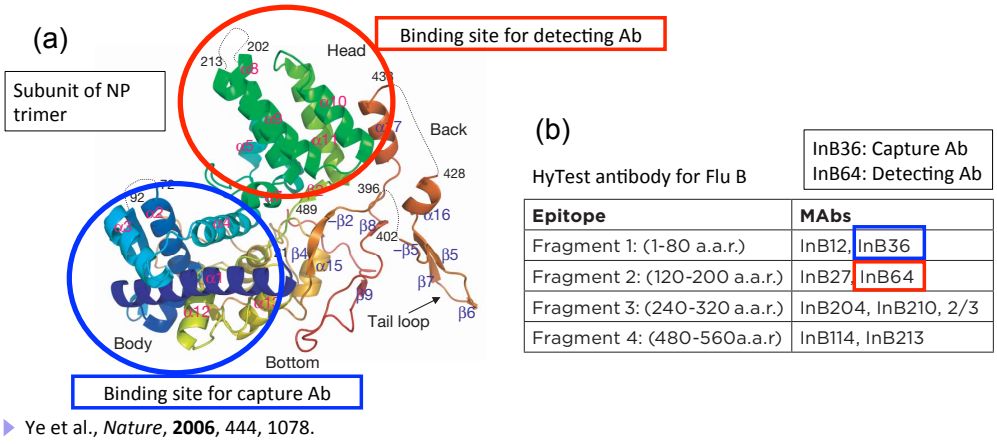

Figure 4.2. Structure and epitopes of NP. (a) Structure of subunit of influenza A NP trimer that has head (red) and body (blue) region (Ye et al., *Nature*, 2006, 444, 1078) and (b) epitopes for each MAb of Flu B (provided by HyTest) are shown.

4.3.3.2 Recombinant NP structure

In addition, dynamic light scattering (DLS) was used to see if our recombinant NP had the trimer structure as shown in previously published work.[73] Figure 4.3a and 4.3b show measurements made by Ye et al. in that previous work. Figure 4.3a shows a chromatogram result, which indicates that wild type of recombinant NP had oligomer rather than monomer. Figure 4.3b shows that the trimer was the most common structure in their sample, although monomers and larger oligomers were also present. To compare to their study, we used DLS to tested our NP sample in the following sections.

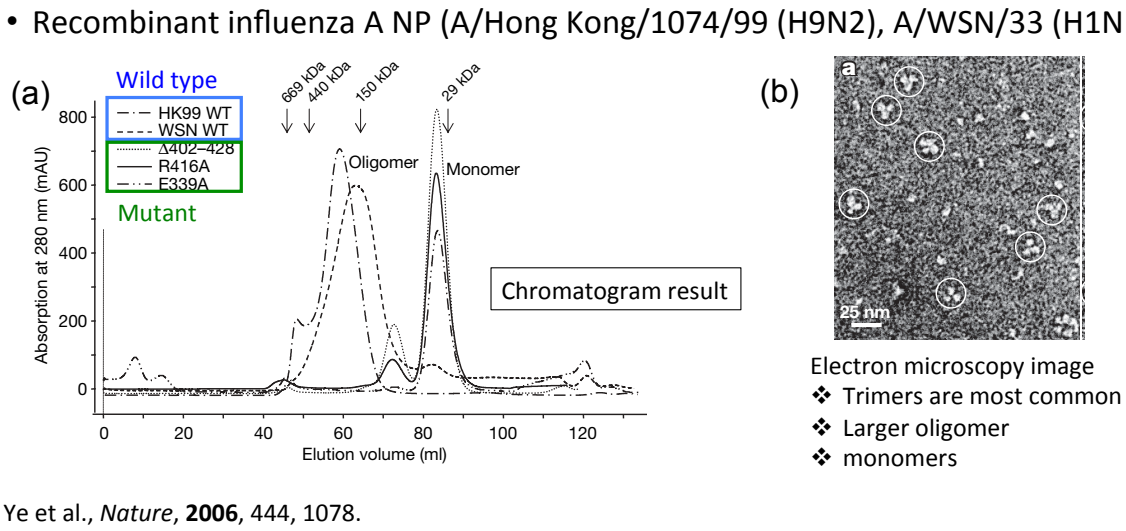

Figure 4.3. Structure of recombinant influenza A NP. (a) Chromatogram and (b) microscopic measurements of recombinant NP structure are shown (Ye et al., *Nature*, 2006, 444, 1078).

4.3.3.3 Viscosity and density of buffers to measure the size of NP by DLS

To apply a mathematical model to the influenza A NP assay to compare the premixed and sequential reagent delivery formats, binding kinetics of antibodies and NP should be measured. To do so, it is important to know if the NP in our assay buffer was monomeric or multimeric. DLS is a way to measure the size and polydispersity of size of particles in solution. To utilize DLS, density and viscosity of each buffer should be measured. At first, density of PBS, PBST

(0.05% Tween 20 in PBS), and 5% Triton X-100 in PBST were measured using density meter at MolES facility (DMA 5000 M, Anton Paar, Ashland, VA). Using the measured density, viscosity was measured by viscometer (AMVn, Anton Paar), which was also at MolES facility. Table 1 shows the measured values.

Table 1: Summary of parameters for each buffer

	PBS	PBST	5% Triton X-100 in PBST
Density [g/cm^3]	1.005294	1.005286	1.009339
Temperature [°C]	20.001	20.001	20.001
Viscosity [cP]	1.0197 ± 0.0011	1.0236 ± 0.0012	1.4376 ± 0.0001

Using parameters in Table 1, DLS was tested to measure the size of recombinant NP in each buffer. Table 2 shows critical micelle concentration (CMC) of each detergent. Since concentrations of each detergent used in our NP assay are higher than their CMC, they would form micelles in each buffer. Since DLS can detect the micelle, interpretation of the measurement is critical to see if the measured value is the size of micelles or NPs.

Table 2: CMC of each detergent in assay buffers for NP detection

	CMC [mM]	Used concentration [v/v%]	MW [g/mol]	Density [g/L]	Used concentration [mM]
Triton X-100	0.3	5	647	1070	82.689
Tween 20	0.059	0.05	1228	1100	0.448

4.3.3.4 DLS to measure the size distribution of recombinant NP

At first, each buffer without recombinant NP was measured (Figure 4.4). Previous results (data not shown) showed that 0.05% Tween 20 in PBS formed micelles because the concentration of Tween 20 was higher than CMC (Table 2). Therefore, 25, 50 and 80% CMC of Tween 20 were

used. Figure 4.4 shows that 25-80% CMC of Tween 20 in PBS had particles (~10 nm), which might be not micelles because the concentration was lower than its CMC.

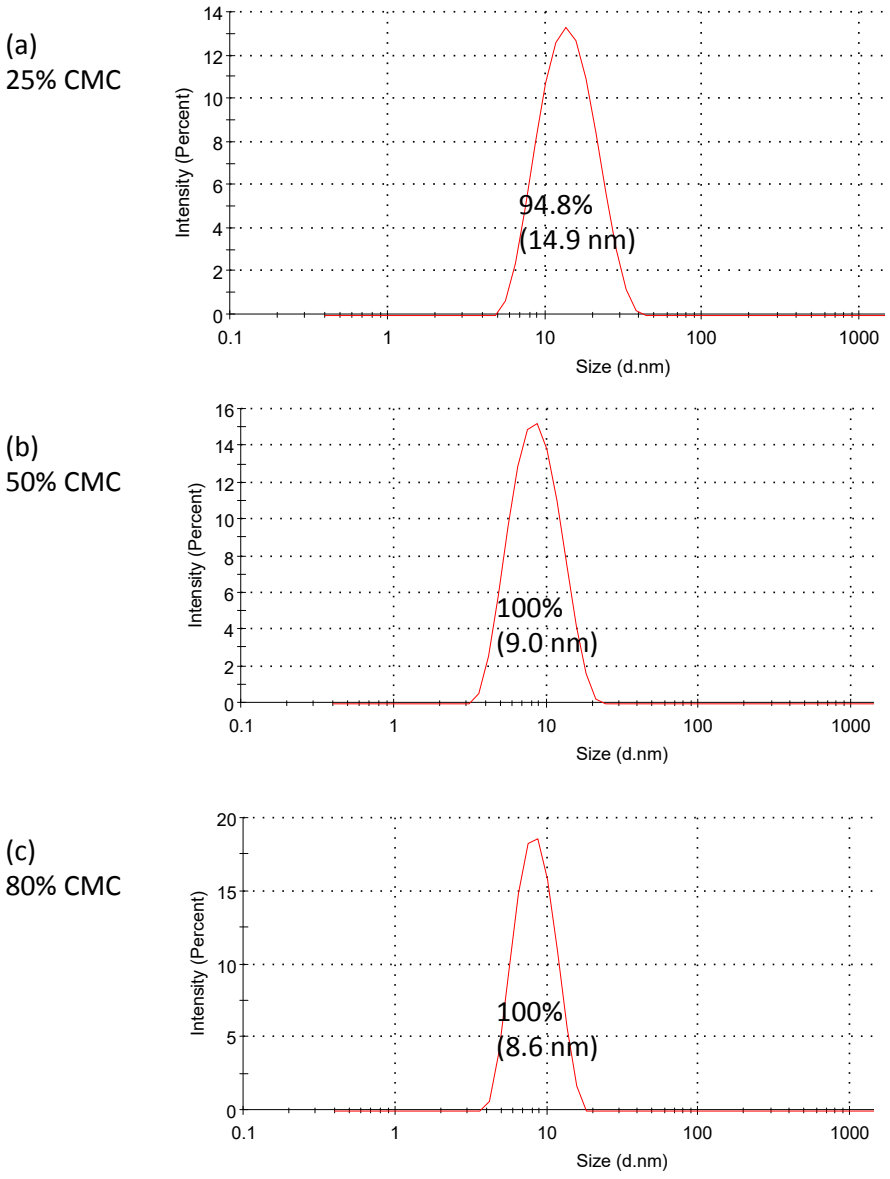

Figure 4.4. Size distribution of PBS including Tween 20. (a) 25%, (b) 50%, and (c) 80% CMC of Tween 20 in PBS were measured. Malvern Zetasizer nano ZS was used for the measurement. A 0.22 µm filter was used to filter 1 mL of each buffer before DLS measurement.

Figure 4.5 shows the size distribution of the recombinant NP (14 nM) in PBS with a range of Tween 20 concentrations (0-80 % CMC). Figure 4.5a shows the size distribution of recombinant

NP in PBS without Tween 20. The solution was filtered by 0.22 μm filter and the average diameter of measured particle was 215.2 nm. The small peak at 1.7 nm would be background noise, which might be due to air bubbles. As shown in Figure 4.5b, 4.5c and 4.5d, increasing the concentration of Tween 20 helped to dissolve the NP oligomers and aggregates, which would be distributed in a range between 200-700 nm. In the sample in which Tween 20 was at a concentration at 80% of its CMC, one peak was obtained at the average size of 9.0 nm, which was close to the expected diameter of monomeric NP (7 nm). Therefore, the recombinant NP in PBST, which has higher Tween 20 concentration than 80% CMC, would be mostly dispersed as monomers. To investigate the size distribution in deep, sedimentation velocity measurement was tested in the following section.

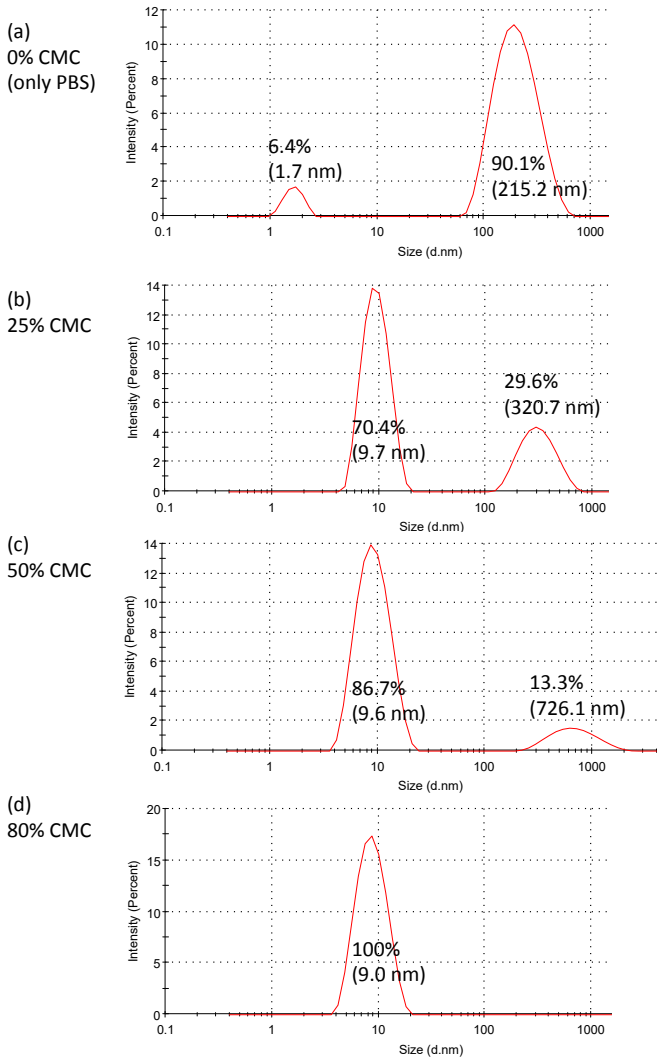

Figure 4.5. Size distribution of recombinant NP (14 nM) measured by DLS (Malvern Zetasizer nano ZS). (a) 0%, (b) 25%, (c) 50%, and (d) 80% CMC of Tween 20 in PBS were used.

4.3.3.5 AUC to measure sedimentation velocity of NP

DLS showed a size distribution including both NP and micelles formed by surfactant, which made data interpretation challenging. Therefore, analytical ultracentrifugation (AUC) was tested as an alternative method to measure the size distribution of NP in PBST. At first, optical density (OD) of NP in PBST was measured to know appropriate wavelength for the absorbance measurement in AUC.

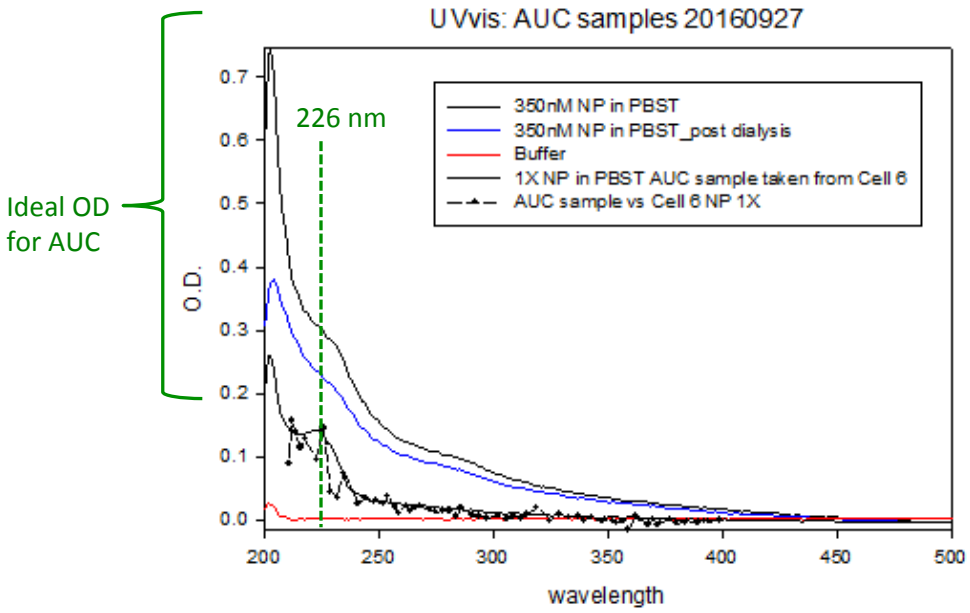

Figure 4.6. Optical density of recombinant NP (350 nM) in PBST. Samples (1) before and (2) after dialysis with PBST, (3) PBST only, and (4) a sample taken from AUC cell were measured. UV-visible spectrophotometer (Evolution 220, Thermo Fisher) at MolES facility was used.

Figure 4.6 shows absorption spectrum of each sample. A 350 nM NP in PBST sample showed a bump at ~230 nm. After dialysis with PBST, overall OD decreased because the NP concentration would be decreased. Dialyzed NP sample was then set up in AUC system (ProteomeLab XL-1, Beckman Coulter, Brea, CA). However, the AUC system did not detect enough OD from the dialyzed sample. Ideal OD for AUC is above 0.2 and the dialyzed sample showed ~0.24 OD at 226 nm. Therefore, the sample was taken from the cell of AUC system and then its OD was measured again (Figure 4.6). However, OD was much lower than the OD of the sample before setting up in the AUC system. The reason was not clear, but John Sumida (a technician at MolES facility) suggested running AUC using the same sample because the sample still showed OD slightly higher than the ideal OD at 226 nm.

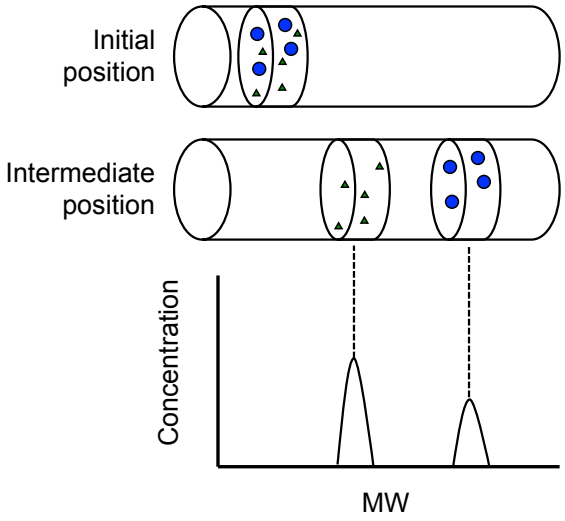

Figure 4.7. Mechanism of analytical ultracentrifugation (AUC). Protein sample is fractionated by mass using ultracentrifugation. The mass can be calculated from sedimentation coefficient, which is based on the speed of sedimentation.

Figure 4.7 shows a schematic diagram of AUC and Equation 4.2 shows related equation to calculate the mass of protein. Protein sample is separated by its mass using ultracentrifugation. The mass can be calculated from sedimentation coefficient, which is based on the speed of the sedimentation. Equation 4.2 shows related equation to calculate the mass of protein:

$$s = \frac{dr/dt}{\omega^2 r} = \frac{M \cdot (1 - \bar{\nu}\rho)}{N_A f_t} \tag{4.2}$$

where s represents sedimentation coefficient, r represents radial position, ω represents angular velocity (rpm), M represents mass of protein, $\bar{\nu}$ represents partial specific volume, ρ represents solvent density, N_A represents Avogadro constant, and f_t represents frictional force.

Figure 4.8 shows the size distribution of recombinant NP measured by AUC, indicating that 41% was monomer (65 kDa), 18% was dimer (116 kDa), and rest of the sample (41%, 170-3000 kDa)

included trismers, tetramers, pentamers, and noise. Tween 20 in PBST would help to dissolve NP aggregates into monomer and dimer. Since 5% Triton X-100 is used in PBST as lysis buffer in the NP assay, NP in lysis buffer would be mostly monomers. This is important and useful information to apply for the mathematical modeling to compare the premixed and sequential reagent delivery formats.

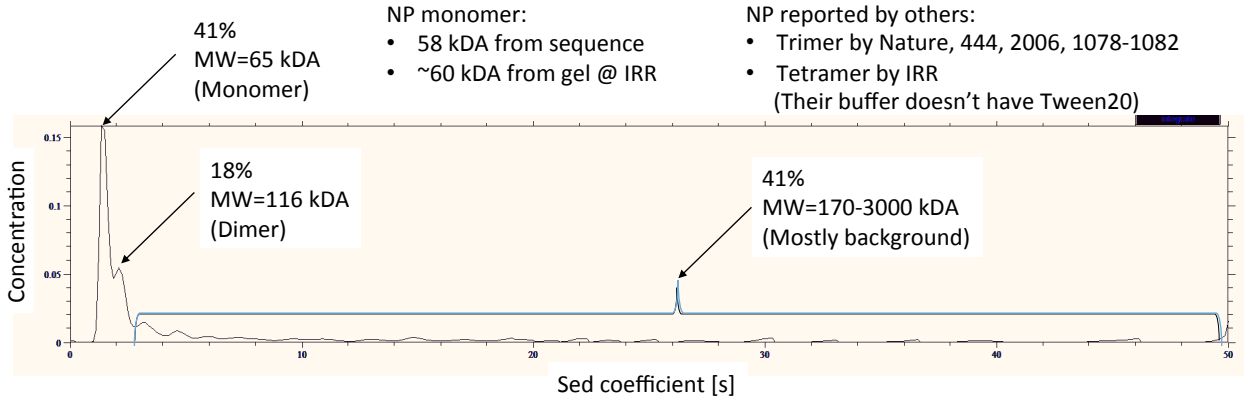

Figure 4.8. Size distribution of recombinant NP (350 nM) measured by AUC system (ProteomeLab XL-1, Beckman Coulter). The result indicated that 41% was monomer (65 kDa), 18% was dimer (116 kDa), and rest of the sample (41%, 170-3000 kDa) included trismers, tetramers, pentamers, and noise.

4.3.3.6 SPR to measure the binding kinetic of NP and its antibodies

Next step is to measure the binding kinetic of NP and its antibodies. Because of the availability for training in MolES facility, SPR was selected as a measurement method. Figure 4.9 shows responses obtained by injection of NP sample in PBST on each surface. Au surface, as a standard surface for SPR, showed nonspecific absorption of NP even after regeneration reagent (chemicals to wash out the surface of the biosensor so that it can be used in another assay) was injected (Figure 4.9a). As an alternative surface, anti-mouse IgG was immobilized on the surface to capture anti-NP mouse IgG. However, the anti-mouse IgG surface also showed nonspecific absorption of NP (Figure 4.9b). Lastly, streptavidin-oligo surface was used to immobilize biotinylated anti-NP mouse IgG, but the streptavidin-oligo surface also resulted in nonspecific

binding of NP sample (Figure 4.9c). This could be due to the characteristic of recombinant NP that would be sticky to any surface because of its oligomers (170-3000 kDa, shown in Figure 4.8). As an alternative approach, Octet system at MolES facility was used since it was assumed to have smaller surface area than SPR, which would not have bigger impact on nonspecific binding of NP.

4.3.3.7 Octet system to measure the binding kinetic of NP and its antibodies

SPR showed high nonspecific absorption of NP and did not work for quantification of binding kinetics. As an alternative method, Octet system at MolES facility was tested. Octet system uses optical analytical technique that analyzes the interference pattern of white light reflected from two surfaces: a layer of immobilized protein on the biosensor tip and an internal reference layer. Any change in the number of molecules bound to the biosensor tip causes a shift in the interference pattern that can be measured in real-time. Streptavidin-coated tip was used to immobilize the biotinylated IgG (capture or detection IgG) and then the binding rates of recombinant NP and another IgG (capture or detection IgG) were measured (Figure 4.10). Figure 4.10a shows a response from a dilution series of NP after immobilizing biotinylated IgG on the tip. No-biotinylated IgG control showed nonspecific absorption of NP on the tip, but the effect of the nonspecific absorption was smaller than the one in SPR to calculate the binding rates. Therefore, this noise was subtracted from the raw data to calculate binding rates. k^a (Figure 4.10b), k^b (Figure 4.10c), k^c (Figure 4.10d), and k^d (Figure 4.10e) were then measured. These measured values were used as input parameters in the preliminary mathematical model (Table 3).

(a) Au surface

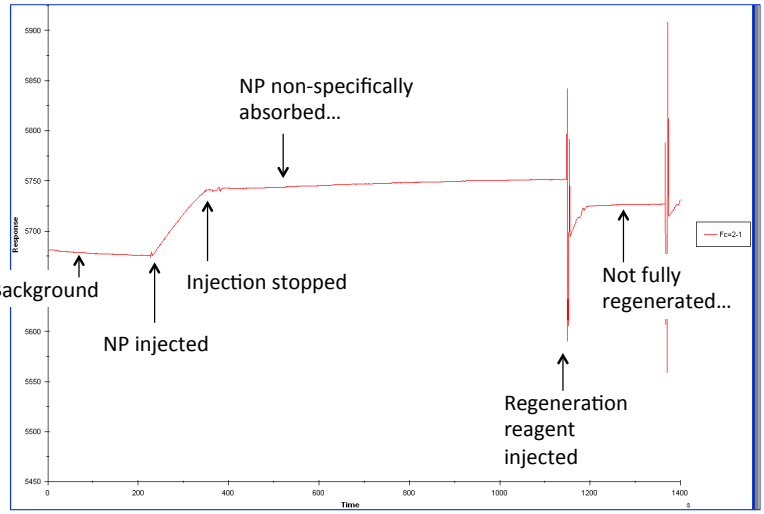

(b) Anti-mouse IgG surface

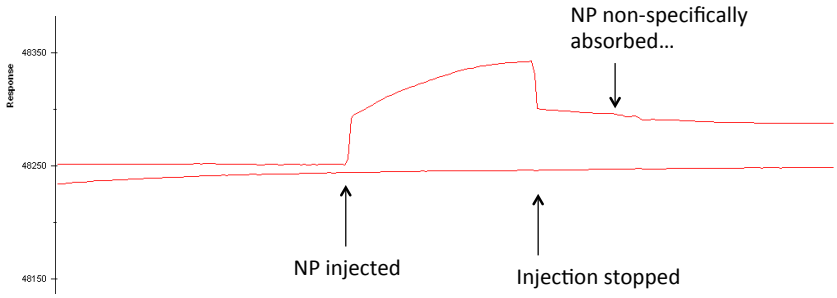

(c) Streptavidin-oligo surface

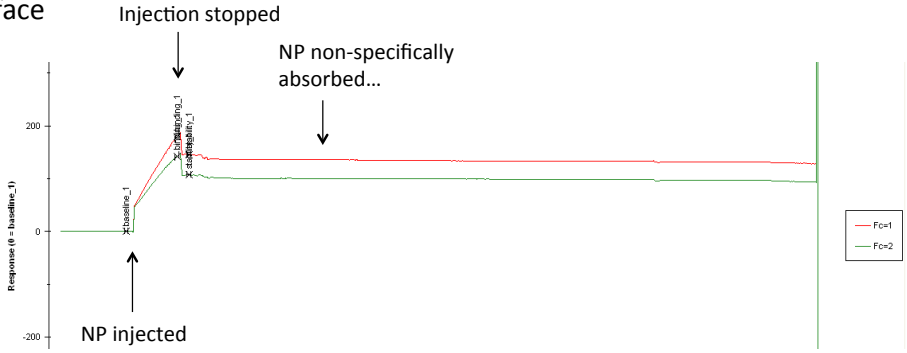

Figure 4.9. Responses obtained by injection of NP sample in SPR. NP in PBST was injected on (a) Au surface, (b) anti-mouse IgG surface, and (c) streptavidin-oligo surface. Biacore T100 (GE Healthcare) at MolES facility was used.

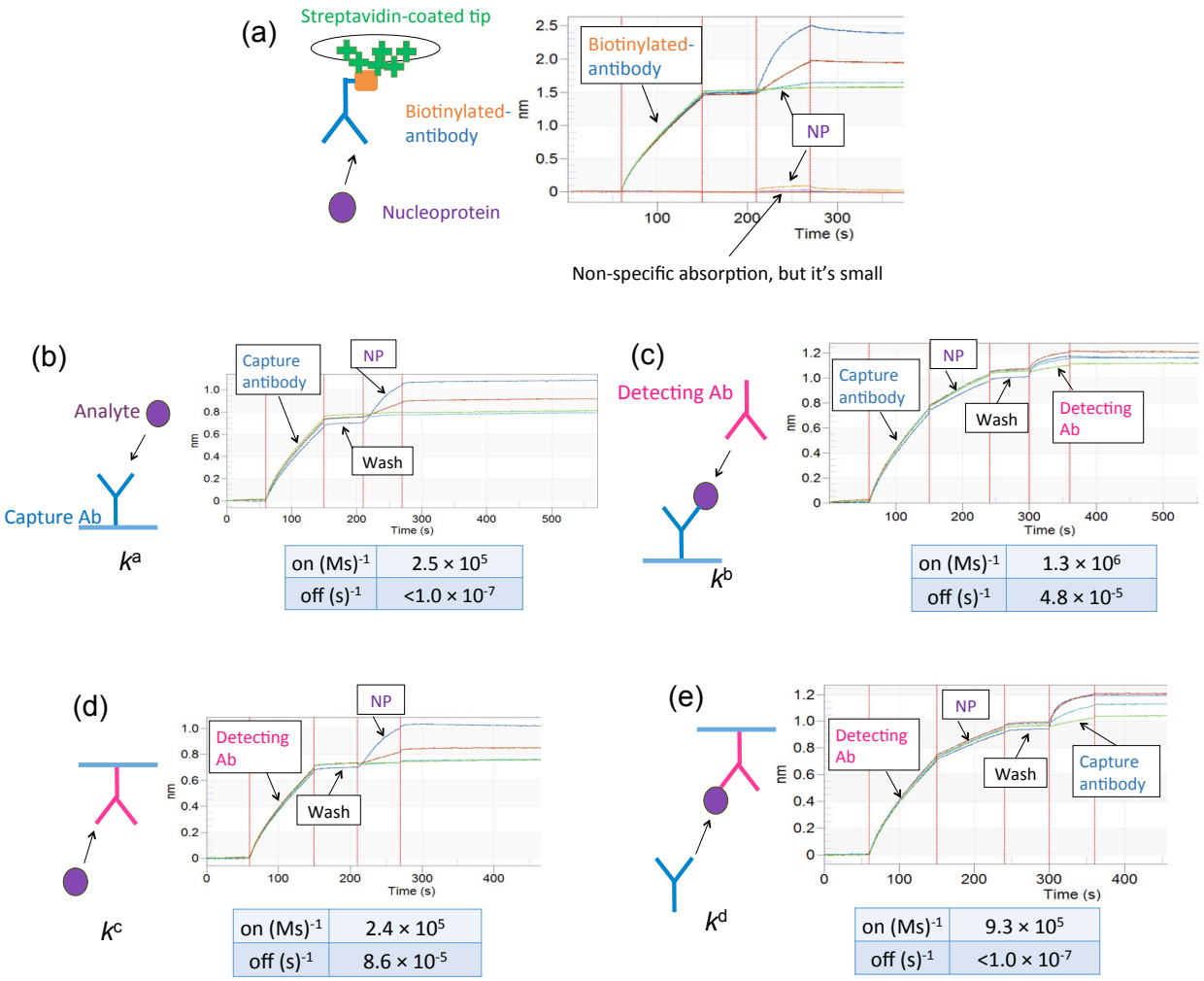

Figure 4.10. Binding rates in influenza NP assay measured by Octet system. (a) Evaluation of nonspecific binding of NP on the surface of Octet system. 0 and 15 nM biotinylated IgG and a range of NP concentration (4.9, 14.8, 44.3, and 133.0 nM) were tested. Nonspecific absorption of NP was observed, but the effect of the nonspecific absorption was smaller than the one in SPR. This noise was subtracted from the raw data to calculate binding rates. Reactions between (b) capture IgG and NP, (c) detection IgG and NP bound to capture IgG, (d) NP and detection IgG, and (e) capture IgG and NP bound to detection IgG were measured. 5 nM biotinylated IgG (capture or detection IgG) was immobilized on streptavidin-coated tip. For sandwich format (b and d), 50 nM NP and dilution series of IgG (5.6, 16.7, 50, and 150 nM of detection or capture IgG) were used. For non-sandwich format (a and c), 2.5, 7.4, 22.2, 66.7 nM of NP were measured. Buffer consists of 0.05% Tween 20 and 0.01% BSA in 10 mM PBS.

Table 3: Parameters used in the model

Parameter	Value	Unit	Description
kaon	1.00E+05	1/(Ms)	Binding rate constant
kbon	1.00E+06	1/(Ms)	Binding rate constant
kcon	1.00E+05	1/(Ms)	Binding rate constant
kdon	1.00E+06	1/(Ms)	Binding rate constant
kaoff	1.00E-07	1/s	Binding rate constant
kboff	9.00E-05	1/s	Binding rate constant
kcoff	5.00E-05	1/s	Binding rate constant
kdoff	1.00E-07	1/s	Binding rate constant
D_Ag	7.30E-11	m^2/s	Diffusion coefficient of antigen
density0_CapAb	7.00E-03	moles/m^3	Density of capture Ab
c0_Ag	1.00E-09	moles/m^3	Initial concentration of antigen
D_DetAb	1.00E-11	m^2/s	Diffusion coefficient of detection Ab
c0_DetAb	1.00E-05	moles/m^3	Initial concentration of detection Ab
D_AgDetAb	7.30E-11	m^2/s	Diffusion coefficient of antigen bound to detection Ab

4.3.3.8 Modeling of flu NP assay to compare premixed and sequential reagent delivery formats

Experimental and model data were directly compared using an experimentally-derived calibration curve of the concentration of oxidized DAB (DAB_{ox}) and signal intensity (Figure 4.11). Comparison of the experimental and model binding profiles showed coarse agreement to demonstrate the difference between the premixed and sequential delivery formats (Figure 4.12). Association and dissociation rate constants were varied in the model to investigate the cases that the premixed format showed higher signal intensity than the sequential format. The four sets of model rate constants satisfied the following condition in our system. The association rate constant of NP-capture antibody complex to detection antibody (k^b_{on}) was smaller than or equal to the association rate constant of NP-detection antibody complex to immobilized capture antibody (k^d_{on}). The binding rate constants measured by Octet system falls in this range ($k^b_{on} \approx k^d_{on}$). On the other hand, the modeled signal intensity with the premixed format was lower than the intensity with the sequential format when $k^b_{on} > k^d_{on}$. k^b_{on} (association rate of detection

antibody with NP bound to capture antibody) is related to the sequential reagent delivery format. k^{d}_{on} (association rate of capture antibody with NP bound to detection antibody) is related to the premixed reagent delivery format. Therefore, when $k^{b}_{on} > k^{d}_{on}$, it can be assumed that the sequential format can show better signal intensity compared to the premixed format. If our influenza NP antibodies had such condition (i.e. $k^{b}_{on} > k^{d}_{on}$), our assay would have shown better signal intensity with the sequential format, which is the same result compared to the previous work for the malarial assay.[55] This preliminary model should be further improved as a design tool to apply for any sandwich immunoassay with different antibody-analyte binding kinetic combinations, which would be useful to optimize the reagent delivery format to improve LOD in each system.

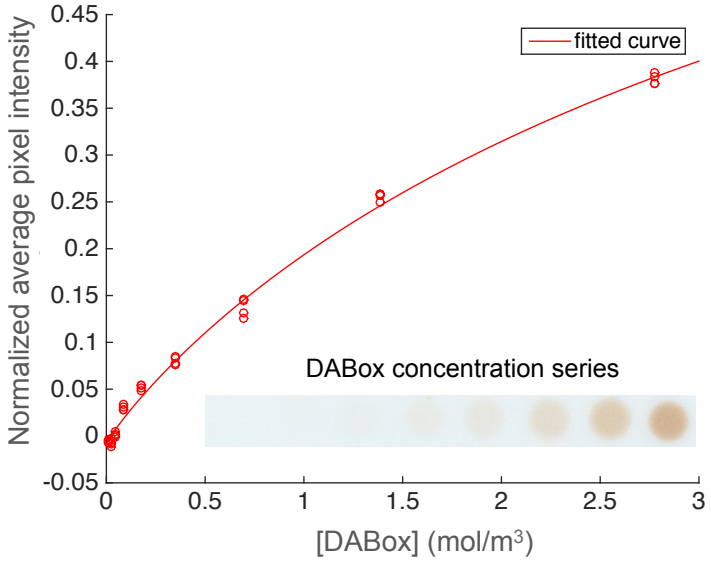

Figure 4.11. Calibration curve of the concentration of DAB_{ox} and signal intensity to apply for the preliminary model. The plot shows average signal intensity of 8 concentrations of DAB_{ox} on nitrocellulose (n=4) and a 4-PL fit to the data (solid line).

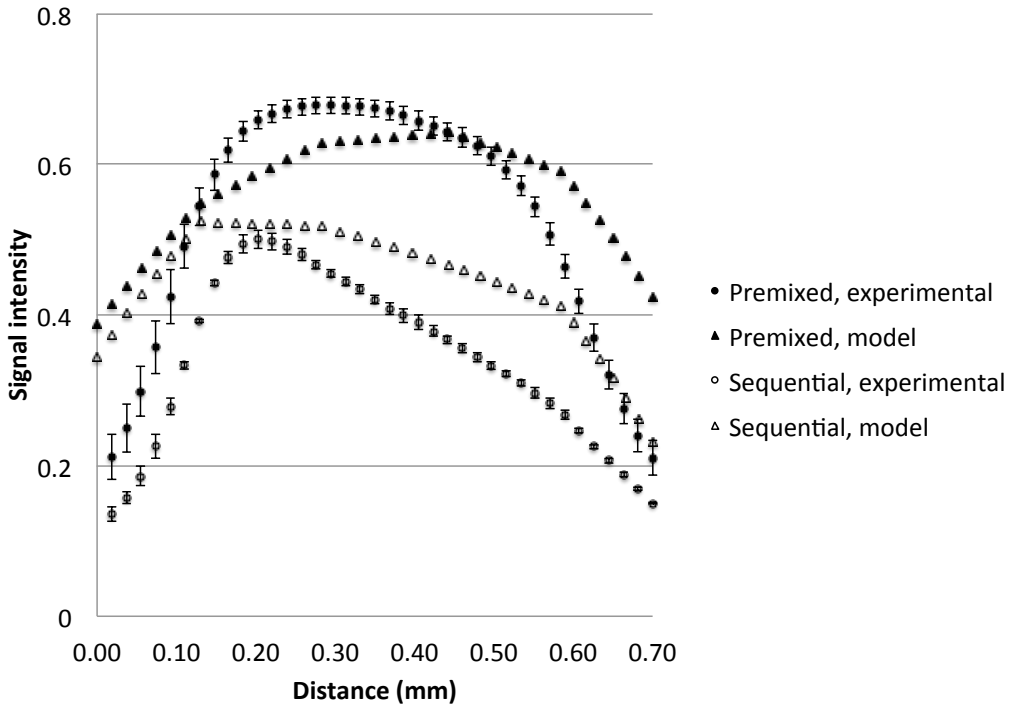

Figure 4.12. Experimental (circle) and model (triangle) binding profiles for the premixed (solid) and sequential (hollow) reagent delivery formats. The error bars for the experimental binding profiles represent the standard deviation (n=4). The experimental and model binding profiles showed rough agreement, but the model should be improved and evaluated by varying key parameters.

4.3.4 Future Experiments and Expected Results

To validate the model, some parameters should be varied both in the model and the experiment. Concentrations of each reagent (NP, detection antibody, capture antibody, DAB, etc.) would be easy to vary in the experiment to evaluate the model. H_2O_2 is also key factor in the reaction for signal amplification and thus it is also important parameter for the evaluation. A search algorithm should be implemented to perform the minimization of a goodness-of-fit function, the sum-squared error (SSE) between the experimental and model data. Once the experimental and model data showed good agreement, the model will be used to predict a potential global minimum LOD to improve the experimental LOD. It would be a possible option to collaborate

with a research group in Intellectual Ventures (Seattle, WA) since they are also working on a modeling approach to predict the assay performance in sandwich immunoassay.[5,54]

4.3.5 Conclusions

This work aims to elucidate the underlying mechanism of the reagent delivery format using a mathematical model of sandwich immunoassay with signal amplification to predict possible global minimum LOD of the system. The experimental and model binding profiles showed rough agreement and the model should be improved and evaluated by varying key parameters. We could also collaborate with a research group in Intellectual Ventures that has developed an extensive model of this sort.

5 SPECIFIC AIM 3: IMPROVE LOD THROUGH ISDA ("LFT-ISDA")

5.1 MOTIVATION AND GOALS

As described in the background section, our lab successfully demonstrated isothermal strand displacement amplification (iSDA) on a lateral flow format.[63,64] Based on this study, we designed a LFT enhanced using iSDA as a signal amplification reaction, with the goal of drastically improving the immunoassay sensitivity. We named this integrated assay LFT-iSDA. Like immuno-PCR, this version of LFT-iSDA used detection antibodies tethered to synthetic oligonucleotide (oligo) templates. Streptavidin can be used as a commercially-available universal tool to tether biotinylated detection antibodies and biotinylated oligo templates. Unlike immuno-PCR, the sandwich immunoassay formed under lateral flow on capture antibodies immobilized onto a nitrocellulose test strip. The iSDA signal amplification step was then performed in place and the amplified products containing a probe sequence (i.e. amplicons) were detected on lateral flow strips or analyzed by polyacrylamide gel electrophoresis (PAGE).

The goal of Specific Aim 3 is to further improve LOD of influenza A NP assay by LFT-iSDA. To validate LFT-iSDA, we compared the performance of LFT with our previous work with gold nanoparticle labels and horseradish peroxidase (HRP) using chromogenic substrates like diaminobenzidine (DAB).[35,68] We assessed false positive rates, which has proven to be a common problem with immuno-PCR assays, and demonstrated washing and blocking strategies to minimize the occurrence of false positives in the LFT-iSDA assay. We performed a manual implementation of LFT-iSDA, which was slow to run (~ 2 hours), but automation of LFT-iSDA is underway based on a two-dimensional paper network (2DPN) that is inexpensive, rapid, and

simple to use.[64,68] Ultimately, in our manual implementation of our model NP system, the LFT-iSDA was ~10,000-fold more sensitive than the conventional LFT. This is the first study of immuno-NAAT demonstrated on nitrocellulose membrane as a low-cost POC platform.

5.2 Goal 1: Perform a Proof of Concept of LFT-iSDA

5.2.1 Introduction

In our previous experience, not all porous materials support iSDA reactions. We evaluated the compatibility of nitrocellulose to support iSDA reactions in the context of the NP LFT. The following experiments were to perform a proof of concept of LFT-iSDA on nitrocellulose using a combination of experimental controls.

5.2.2 Methods

5.2.2.1 LFT strip fabrication

We verified LFT-iSDA with an influenza A NP lateral flow assay previously developed in our lab.[68] In brief, the lateral flow assay device consisted of a 4 mil-thick Mylar-backed porous nitrocellulose membrane (HF120, Millipore, Burlington, MA, USA) and a removable cellulose wicking pad (C083, Millipore) overlapped by 5 mm and attached to an adhesive-backed Mylar sheet (T-5501-10/1, Fralock, Valencia, CA, USA). Anti-influenza A NP monoclonal antibodies (1 mg/mL, InA108, HyTest, Turku, Finland) were striped to form a capture line using a reagent dispenser (Biojet HR Solenoid Dispenser, BioDot, Irvine, CA, USA). Striped cards were dried at 37 °C for 2 hours, cut to 5 mm-wide strips, and stored in sealed pouches (139-312, Medium Mylar Plate Pouches, Impak, Los Angeles, CA, USA) with 0.5 gram desiccant packs (01AP18J15, Impak) at room temperature.

5.2.2.2 iSDA reaction with master mix

Table 4 contains the sequences of the oligo templates, probes, and primers for the iSDA reaction. Oligo templates and primers were synthesized by Integrated DNA Technologies (IDT, Skokie, IL, USA). The synthetic oligo template was derived from a target sequence in *mecA* (a gene that confers methicillin resistance in *S. aureus* and other bacteria), which was previously shown to be a high-quality iSDA target sequence.[64] The iSDA reaction combined template and a "master mix," which consisted of 500 nM forward extension primer, 250 nM reverse primer, 50 nM each of forward and reverse bumper primer, 0.2 U/μL Bst 2.0 WarmStart DNA Polymerase (M0538, New England Biolabs, Ipswich, MA, USA), 1.6% v/v nicking endonuclease Nt.BbvCI-137 (mutant strain, New England Biolabs), 250 μM of each dNTP (N0447, New England Biolabs), 3.75 mM magnesium sulfate (B1003, New England Biolabs), 10 mM potassium phosphate (monobasic, P8709, Sigma, St. Louis, MO, USA), and 40 mM potassium phosphate (dibasic, P8584, Sigma) (pH 7.6). Detailed descriptions of the iSDA reaction was previously reported.[63,64]

Table 4: Sequences of oligo templates, primers and probes for iSDA

mecA template (oEH1099, without bumper site)	5Biosg//iSp18/AAAGATGGCAAAGATATTCAACTAACT ATTGATGCTAAAGTTCAAAAGAGTATTTATAACAAC ATGAAAAATGATTATGGCTCAGGTACTGCTATCCACC
mecA template (oEH1139, with bumper site)	5Biosg//iSp18/AAGATGGCAAAGATATTCAACTAACTAT TGATGCTAAAGTTCAAAAGAGTATTTATAACAACAT GAAAAATGATTATGGCTCAGGTACTGCTATCCACCCT CAAACAGGTGAATTATTAGCAC
Forward amplification primer (F) (CCTCAGC = nicking site)	5′–CCA TTA TAC TAC CTG TCT CCTCAGC GGC AAA GAT ATT CAA CTA AC–3′
Reverse amplification primer (R) (CCTCAGC = nicking site)	5′–TAG AAT AGT CAC TTA CTT CCTCAGC GCC ATA ATC ATT TTT CAT GTT–3′
Forward bumper primer (FB)	5′–GAT AAT AGC AAT ACA ATC GCA CA–3′
Reverse bumper primer (RB)	5′–GTG CTA ATA ATT CAC CTG TTT GA–3′
Capture probe (*pDNA[...]* = pyranosyl DNA)	4′–*pDNA*[CAAGAATC]–2′– HEG–5′–CTT TAG CAT CAA TAG TTA G–hexanol–3′
Biotin probe (A* = Super A®, ElitechGroup)	5′–GTT A*TA AAT A*CT CTT TTG A–biotin TEG–3′

5.2.2.3 LFT-iSDA test

The LFT-iSDA test procedure consisted of three primary steps: LFT, iSDA reaction, and amplicon detection (Figure 5.1A). Twelve tests were run at a time, starting with twelve parallel lateral flow tests (nitrocellulose strips and cellulose pads, described above) adhered to a "test card", which was laser-cut from 10 mil (0.25 mm) adhesive-backed Mylar (Fralock) on a CO_2 laser (VLS 3.60, Universal Laser Systems, Scottsdale, AZ). The immunoassay step was performed using the test card to sequentially place the parallel lateral flow tests into three rows of wells of a 96-well plate. The first row of wells contained 20 μL of solution containing recombinant influenza NP analyte (Brisbane/10/2007 [H3N2], International Reagent Resource, Center for Disease Control and Prevention, Atlanta, GA, USA) in lysis buffer premixed with 20 μL of biotinylated detection antibody (3IN5 InA245, HyTest) in running buffer, 20 μL of streptavidin solution (S4762, Sigma) or streptavidin-coated gold nanoparticles (Innova BioSciences, Cambridge, UK), and 10 μL of oligo template. Analyte and template concentrations were varied as described in the main text. The second and third rows of wells contained 20 μL of wash buffer and 40 μL of rinse buffer, respectively. The full volume of each well was observed to flow into each strip before placing the card into the next row. The running buffer contained 1% (w/v) BSA (A-3249, Sigma) in PBST (P3563, Sigma). The lysis buffer, needed for release of NP from viruses in practical application, contained 5% (v/v) Triton X-100 (T-9284, Sigma) in the running buffer. The wash buffer contained 0.8% Triton X-100 in the running buffer. The rinse buffer contained 1% (w/v) BSA and 0.05% Tween 20 (P9416, Sigma) in $KiPO_4$ buffer, which was chosen for compatibility with the iSDA reaction. Each reagent was diluted and calculated as both concentration and copies/test (Table 5).

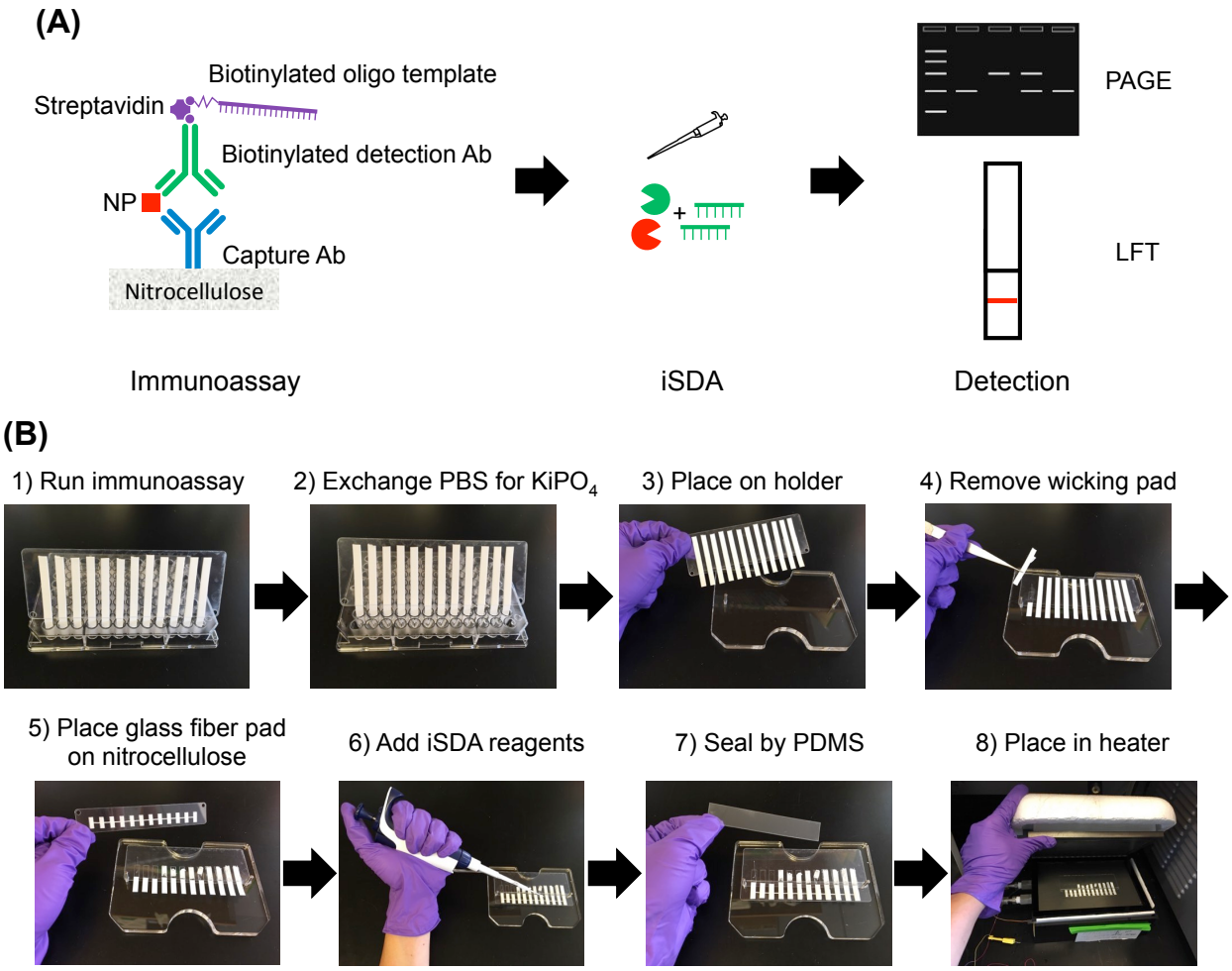

Figure 5.1. Schematic and procedures for LFT-iSDA. (A) Nitrocellulose, capture antibody, influenza A NP as a model analyte, biotinylated detection antibody, streptavidin, and biotinylated *mecA* template are used for a conventional lateral-flow-based immunoassay. After running the immunoassay, iSDA reagents are pipetted on a dry glass fiber pad that had been placed on the capture antibody. The assembly is then incubated at 50°C for 30 min. Amplified sample is then centrifuged out from the nitrocellulose and glass fiber pad to run PAGE or LFT to detect amplicons. (B) Experimental procedure of LFT-iSDA: 1) run immunoassay using the card-based dipstick format with 12 LFT strips and 96-well plate, 2) rinse away PBS using $KiPO_4$-based buffer, 3) place the card on holder, 4) remove wicking/waste pads from LFT strips, 5) place smaller card with glass fiber pads on nitrocellulose, 6) add iSDA reagents by pipetting on each glass fiber pad, 7) seal the card by PDMS, and 8) place the card in clam-shell heater at 50°C for 30 min.

Table 5: Reagent concentrations used in the manual LFT-iSDA assay

Unit	Detection Ab	Oligo template (oEH1139)	Streptavidin	Streptavidin-Au[a]
ng/mL	1.3	0.6	0.4	N/A
fmol/test	0.2	0.2	0.2	0.2
Copies/test	10^8	10^8	10^8	10^8

[a]Based on communication with Innova BioSciences (1 μL at OD 10 = ~9 x 10^8 beads)

Salmon sperm DNA (D9156, Sigma) was used as a real-time blocking agent as previously described.[74] The salmon DNA was heated at 95 °C for 10 min, then cooled to 4 °C immediately prior to use. Simulated nasal matrix (SNM) followed a previously-reported protocol; it contained 110 mM NaCl (S9888, Sigma), 1% (w/v) mucin from porcine stomach type III (M1778, Sigma), and 10 μg/mL human genomic DNA (G041, Promega, Fitchburg, WI, USA).[75] Both salmon sperm DNA and SNM were premixed with recombinant NP samples when used.

The iSDA reaction step was performed next (Figure 5.1B). As described above, the strips were placed in successive microplate wells that contained: 1) NP analyte premixed with detection antibody, streptavidin, and oligo template, 2) PBS-based wash buffer, and 3) $KiPO_4$-based rinse buffer. Second, the test card with 12 strips was placed on a custom holder and the cellulose waste pads were removed from each lateral flow test. Glass fiber amplification pads (8950, Ahlstrom, Stockholm, Sweden) were adhered to a laser-cut Mylar cover with PDMS-coated, Mylar-backed tape (ARclad® IS-7876, Adhesives Research, Glen Rock, PA, USA). The cover was placed on the test card using the holder, which aligned the amplification pads, and adhered to the test card using the PDMS tape. Next, 10 μL of the iSDA master mix was pipetted onto each glass fiber pad through laser-cut ports in the cover layer. The holes were then sealed with PDMS tape to prevent evaporation. The sealed test card was incubated at 50 °C for 30 minutes on a custom

"clamshell heater" with precision temperature control on two aluminum surfaces spaced 1/8 inch (3.2 mm) apart, which supported efficient iSDA amplification.

The amplicon detection step was performed next. The amplified fluid sample was recovered from each material (nitrocellulose strip and glass fiber pad) of each test by centrifugation and analyzed by LFT and/or PAGE to identify the presence of amplicons. Amplicon detection by LFT and PAGE were performed according to previously-reported protocols.[63,64] A schematic of the assay stack for amplicon detection by LFT is shown in Figure 5.2. Briefly, an amplicon test line and a flow control line were striped at 0.3 μL/cm on nitrocellulose using 400 μM hybrid pDNA-T20 (pyranosyl DNA covalently linked to 20 thymidine nucleotides) capture probe and 200 μM T20-biotin, respectively. The nitrocellulose was then guillotine-cut into 2.5-mm wide strips. For each material for each test, an 11 μL sample of amplified fluid was mixed with 7.4 μL of amplicon detection reagents, which consisted of 20 nM hybrid DNA-pDNA capture probe (ELITech Molecular Diagnostics, Bothell, WA, USA), 10 nM biotinylated DNA detection probe (ELITech Molecular Diagnostics), and 1.25 μL of 10 OD streptavidin-coated gold nanoparticles (Innova Biosciences); the resulted mixture was incubated at 49 °C for 30 min. The incubated samples were then mixed with 0.6 M NaCl and 0.8% v/v Triton X-100 and pipetted onto amplicon detection LFTs. Note that the 30-minute detection reagent incubation step would not be needed for the final automated LFT-iSDA assay, because the iSDA reaction has operated quite well in the presence of the amplicon detection reagents.[63,64]

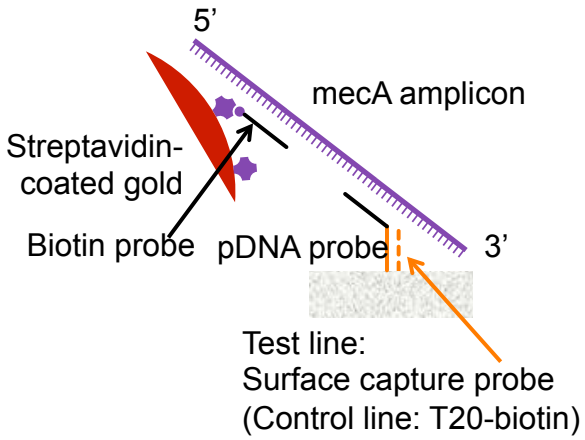

Figure 5.2. Schematic of the assay stack for LFT to detect amplicons. pDNA (pyranosyl DNA) capture probe linked to T20 (twenty repeats of thymidine) and T20-biotin were striped on nitrocellulose membrane as test and control line, respectively. Detection reagents consisted of biotin probe, DNA-pDNA capture probe, and streptavidin-coated gold nanoparticles. The detection reagents were mixed with amplicons and incubated at 49 °C for 30 min. The incubated amplicons were mixed with 0.6 M NaCl and 0.8% v/v Triton X-100 and then allowed to run the LFT.

5.2.3 Results and Discussion

5.2.3.1 LFT-iSDA using streptavidin to tether biotinylated detection antibody to the oligo template

We evaluated the compatibility of nitrocellulose to support iSDA reactions in the context of the NP LFT by immobilizing the biotinylated detection antibody on nitrocellulose. Streptavidin-coated gold nanoparticles were premixed with biotinylated oligo template and applied to the nitrocellulose strip in the dipstick format, followed by a $KiPO_4$-based rinsing step. iSDA was then performed as described in Figure 5.1B. The $KiPO_4$-based rinsing step is required to rinse the PBS away from the amplification zone, as it is not compatible with iSDA. Figure 5.3 shows how the amplicons and optical signals, which were observed by PAGE and gold nanoparticles, respectively, varied with positive and negative controls. The positive results demonstrated that the iSDA reaction was compatible with nitrocellulose. The no-template control, no-gold control, and no-detection-antibody control each did not show amplicons. The lack of amplicon

production in both the no-gold control and in the no-detection-antibody control indicated that streptavidin-coated gold nanoparticles were able to bridge the biotinylated oligo template to the previously-immobilized antibody. Although influenza A NP could bind nonspecifically to the sugar-phosphate backbone of single-stranded DNA,[76] these controls proved that NP itself did not bind to the template DNA in our experimental conditions.

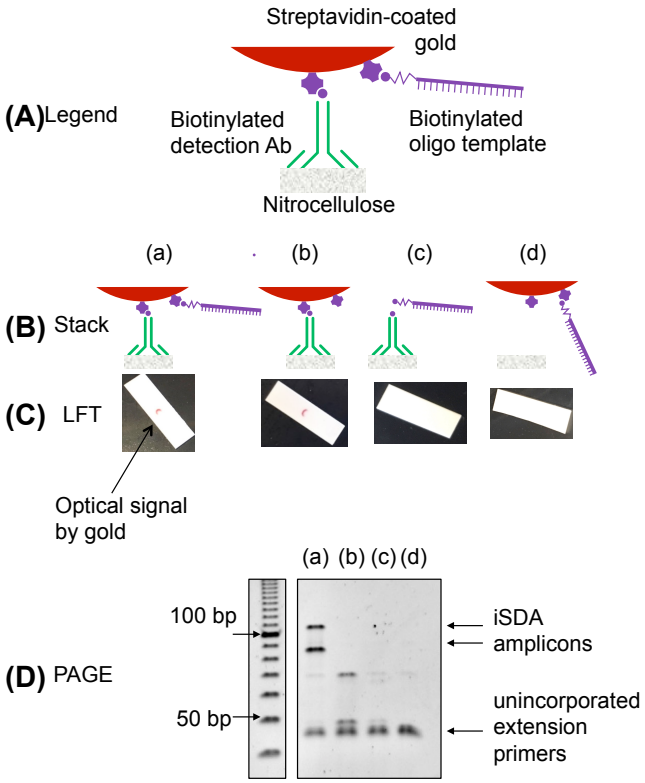

Figure 5.3. LFT-iSDA using a biotinylated detection antibody that had been previously immobilized on nitrocellulose. (A) Legend of schematic, (B) assay stack for each control, (C) scanned image of LFT, and (D) PAGE image are shown. (a) Positive sample, (b) no-*mecA*-template control, (c) no-streptavidin-coated gold-nanoparticles control, and (d) no-detection-antibody control were compared. Streptavidin-coated gold nanoparticles (20 µL) premixed with biotinylated *mecA* template (20 µL), wash buffer (20 µL), and rinse buffer (80 µL) were sequentially applied using the dipstick format using a 96-well plate. The wicking pads were removed right after rinsing step and 5 µL of iSDA reagents were pipetted onto each capture region. 1 mg/mL of biotinylated detection antibody was hand-spotted (0.5 µL) and dried at 37 °C for 2 h. 10^8 copies/test of each *mecA* template and gold nanoparticles were used. Nitrocellulose was rinsed by 80 µL of $KiPO_4$ including 1% BSA and 0.1% Tween 20.

Proof-of-concept of LFT-iSDA was demonstrated using the influenza A NP assay by adding an immobilized capture antibody, recombinant NP, detection antibody, streptavidin-coated gold nanoparticles, and the oligo (Figure 5.4). The no-NP control, no-gold control, and no-oligo-template control did not yield substantial amplicons, while positive samples using 10^9 NP copies/test produced amplicons (10^9 NP copies/test (8.5 ng/mL) is the same as or lower than expected LOD of commercially available rapid tests evaluated by the CDC[67] and our in-house experiment using BD Directigen™ EZ Flu A+B). The no-NP control, however, showed faint "nonspecific amplicons"; nonspecific binding of the detection reagents in the zone that is amplified using iSDA will limit the ultimate sensitivity of the assay. This issue could be due to nonspecific binding to the nitrocellulose by the streptavidin-coated gold nanoparticles at and near the capture region.

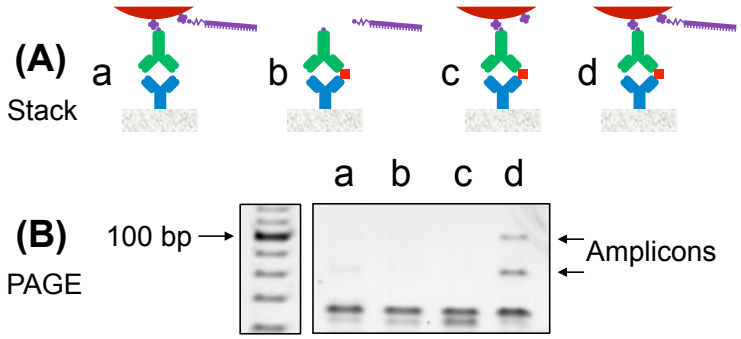

Figure 5.4. Proof of concept of LFT-iSDA using the full NP assay stack. (A) Assay stack for each control and (B) PAGE image are shown. Immunoassay was performed by sequential reagent delivery: (1) NP (20 µL) premixed with biotinylated detection antibody (20 µL), (2) wash buffer (20 µL), (3) streptavidin-coated gold nanoparticles (20 µL) premixed with biotinylated *mecA* template (20 µL), (4) second wash buffer (20 µL), and (5) rinse buffer (20 µL) were sequentially applied by dipstick format using 96-well plate. No-NP control (a), no-gold nanoparticles control (b), no-*mecA* template control (c), and positive sample (d) were compared. 10^8 *mecA* copies/test, 10^9 gold nanoparticles/test, 10^{11} biotinylated detection antibody copies/test (2 µg/mL), and 10^9 NP copies/test (8.5 ng/mL of recombinant NP) were used. Running buffer (1% BSA and 0.05% Tween 20 in PBS) was used as wash buffer. Running buffer with 0.8% Triton X-100 was used as buffer for *mecA* template and second wash. Rinse buffer was 1% BSA and 0.1% Tween 20 in $KiPO_4$.

To eliminate the negative effect of the gold nanoparticles, streptavidin was tested to replace with streptavidin-coated gold nanoparticles as the bridging molecule (Figure 5.5). Use of 10^8~10^9 streptavidin copies/test yielded amplicons from a positive NP sample and did not produce substantial "nonspecific amplicons" (Fig 5.5A). On the other hand, the assay stack with streptavidin-coated gold nanoparticles produced nonspecific amplicons (Fig 5.5B). Since streptavidin can be used as a commercially-available universal tool and is generally less expensive than gold nanoparticles, the streptavidin linking approach was used in the following experiments to demonstrate the performance of LFT-iSDA.

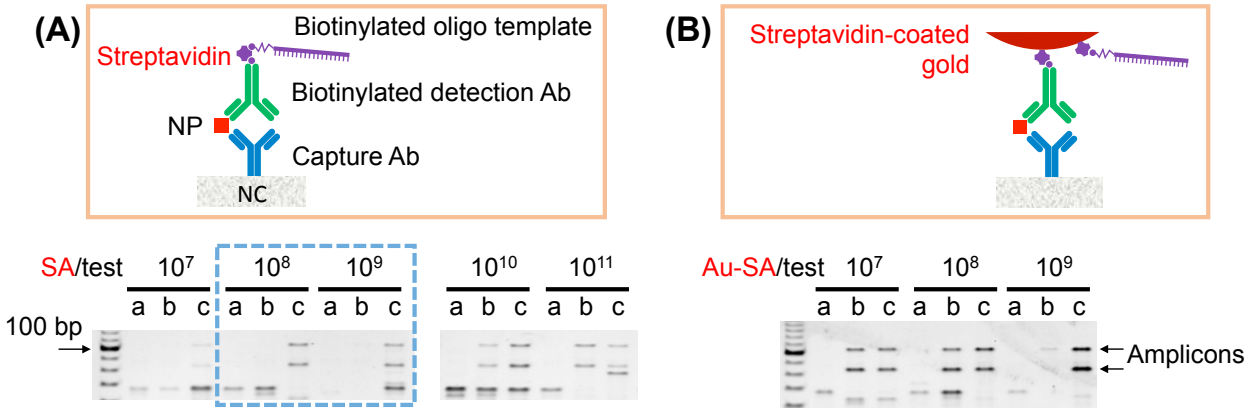

Figure 5.5. Comparison of streptavidin (SA) and streptavidin-coated gold nanoparticles (Au-SA) as linkers between the detection Ab and the oligo template for LFT-iSDA. Schematics of assay stacks (above) and images of the PAGE results (below) are shown. No-oligo template control (a), no-NP control (b), and all positive samples (c) were compared. 10^9 NP copies/test (8.5 ng/mL of recombinant NP) was used for (c). 10^8 *mecA* copies/test, 10^7~10^{11} streptavidin copies/test or 10^7~10^9 streptavidin-coated gold nanoparticles/test, and 10^{11} detection antibody copies/test were used. The blue dashed box indicates a working range of streptavidin copies/test that did not yield substantial nonspecific amplicons.

5.2.4 Conclusions

This work aims to further improve LOD of influenza A NP LFT by iSDA. Proof of concept of the LFT-iSDA was demonstrated on nitrocellulose membrane, while nonspecific signal in the

assay was still produced. The following section describes LOD of LFT-iSDA and possible approaches to reduce nonspecific signal.

5.3 Goal 2: Decrease Nonspecific Signal to Improve LOD

5.3.1 Introduction

Improving signal-to-background ratio is significantly important to improve LOD of the assay. The following experiments were to demonstrate blocking and washing strategies to reduce nonspecific signal. LOD of LFT-iSDA was compared with HRP/DAB assay and conventional gold nanoparticle-based assay. The reproducibility of LFT-iSDA was also validated using different type of nitrocellulose membrane with Dylan Guelig (student in our lab) to demonstrate the assay in another person's hands.

5.3.2 Methods

5.3.2.1 LFT-iSDA test

The LFT-iSDA test procedure is described in the previous section.

5.3.2.2 LFIA-HRP/DAB and LFIA-gold tests

The LOD of LFT-iSDA was compared to a previously-developed lateral flow immunoassay (LFIA)-HRP/DAB test and conventional LFIA-gold nanoparticle test.[68] Both of these assays were run on LFTs adhered to test cards in the same manner as for the immunoassay step of the LFT-iSDA test. As in that procedure, twelve parallel LFT strips were run by sequentially introducing fluids using rows of a 96-well plate, allowing all the fluid to be drawn from each well before moving to the next row. For the LFIA-HRP/DAB test, successive rows of wells contained: 1) 20 μL of recombinant influenza A NP in lysis buffer, 2) a mixture of 20 μL of biotinylated detection antibody (2 μg/mL) and 40 μL of Pierce streptavidin poly-HRP (0.5

μg/mL, 21140, Thermo Fisher Scientific, Waltham, MA, USA) in running buffer, 3) 20 μL of the running buffer as a wash step, and 4) 20 μL of DAB (50 μg/mL in PBST, D5905, Sigma) with 0.01% (w/v) sodium percarbonate (371432, Sigma) as a source of H_2O_2. For the LFIA-gold test, successive rows of wells contained: 1) a mixture of 20 μL of recombinant influenza A NP in lysis buffer and 20 μL of biotinylated detection antibody (10 μg/mL) in running buffer, 2) 20 μL of running buffer as a wash step, 3) 20 μL of streptavidin-coated gold nanoparticles (0.3 OD, Innova Biosciences), and 4) 40 μL of running buffer as a wash step.

5.3.2.3 Image acquisition and data analysis

Image data (600 dpi) was acquired from lateral flow strips with a high-resolution flatbed scanner (Perfection V700 Photo Scanner, Epson, Nagano, Japan) and a previously-reported custom script written in MATLAB (MathWorks, Natick, MA, USA).[77] The output of the script was the mean and standard deviation of signal intensities in a given color channel for the capture region of each scanned lateral flow strip. The green and blue channels in the RGB color space were used to quantify signals from gold nanoparticles-based assay and HRP/DAB assay, respectively. Another custom MATLAB script was used to perform LOD analysis, which consisted of generation of a four-parameter logistic curve fit to the signal intensities for each assay data set, estimation of LOD with 95% confidence intervals, and calculation of t-statistics.[66]

5.3.3 Results and Discussion

5.3.3.1 Reducing nonspecific signal using non-target DNA as blocking agent

To further improve the amplification efficiency, use of an oligo template with a bumper primer binding sequence was compared to the aforementioned results in which there was no bumper primer binding sequence on the oligo template. In iSDA, bumper primers hybridize to the target sequence outside of the extension primer binding sites and enhance strand displacement

activity.[63] Therefore, we assumed that the oligo template with a bumper site could achieve more effective amplification, although it might also increase nonspecific signal production. Figure 5.6 shows a comparison of oligo templates with and without the bumper site (oEH1139 and oEH1099, respectively). Compared to the results using oEH1099, oEH1139 showed very high specific and nonspecific signal while the no-template control did not yield nonspecific amplicons, suggesting that the reactions were not contaminated with amplicons from previous reactions. Nonspecific signal here would be due to nonspecific binding of the oligo template at and near the capture region. To further improve the assay sensitivity, the blocking/washing protocols used with oEH1139 must be improved to reduce nonspecific signal.

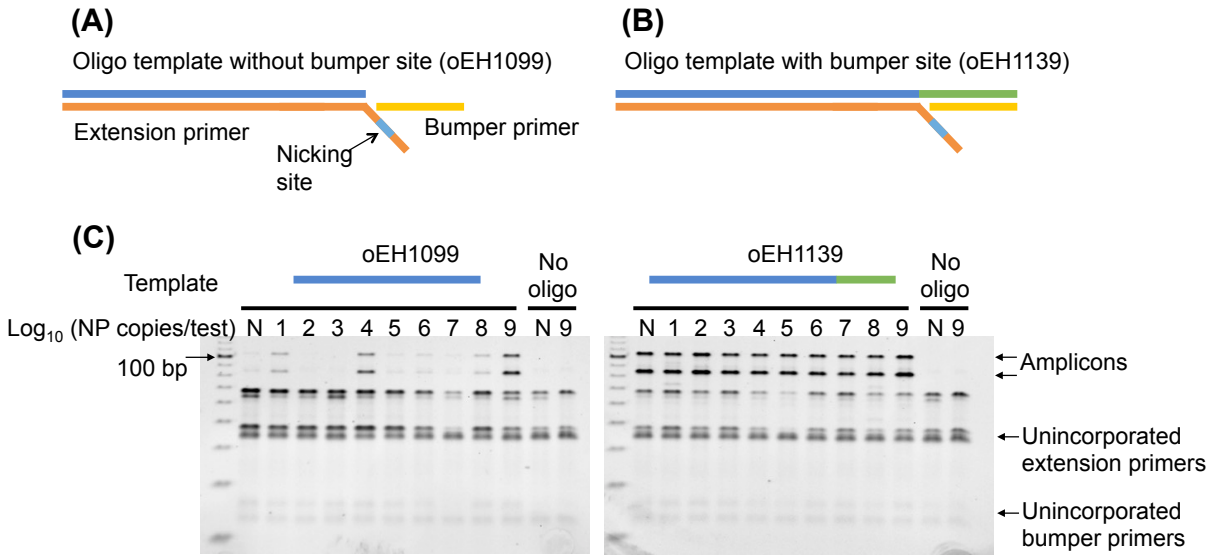

Figure 5.6. Effect of the presence of a bumper site on the oligo template on LFT-iSDA. Schematic of *mecA* oligo template (A) without and (B) with an added bumper site (oEH1099 and oEH1139, respectively), including extension and bumper primers, and (C) PAGE images obtained by both types of oligo template are shown. Immunoassay was performed by the following procedure: (1) NP (20 µL) premixed with biotinylated detection Ab (20 µL), streptavidin (20 µL), and biotinylated *mecA* oligo template (10 µL), (2) wash buffer (20 µL), and (3) rinse buffer (40 µL) were sequentially applied using the dipstick format in a 96-well plate. No-NP control (N) and positive samples (10^1~10^9 NP copies/test) were compared. No-oligo-template control was also tested. 10^8 *mecA* copies/test, 10^8 streptavidin copies/test, and 10^{11} detection antibody copies/test (2 µg/mL) were used.

Another approach to reduce nonspecific signals using denatured salmon sperm DNA as a nonspecific binding blocking agent was evaluated. Denatured fragmented salmon sperm DNA is known as an effective blocking agent in prehybridization/hybridization solutions for NAAT.[74] Moreover, a recent study showed the inhibition of recombinase polymerase amplification (RPA) by sheared salmon sperm DNA as background DNA.[78] Therefore, we evaluated the effect of denatured salmon sperm DNA as an additional real-time blocking agent for LFT-iSDA to mitigate nonspecific amplification (Figure 5.7). A range of concentrations of salmon sperm DNA was used with fixed copies/test of detection molecules. The molar ratio of oligo template to streptavidin to detection antibody was kept at 1:1:1 because free excess oligo template and/or detection antibody could cause false positives and/or false negatives. Figure 5.7 showed that higher concentration of denatured salmon sperm DNA reduced the nonspecific signal. This suggests that the negatively-charged salmon DNA blocks the surface of the capture region and/or the adjacent "free" nitrocellulose.

Denatured salmon DNA (μg/test)	1.0	0		0.2		0.5		1.0	
mecA (copies/test)	0	10^8							
NP (copies/test)	0	0	10^9	0	10^9	0	10^9	0	10^9

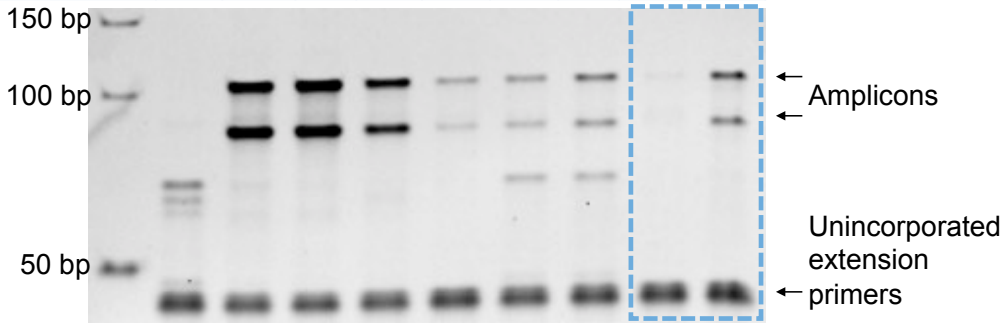

Figure 5.7. Effect of non-target DNA as blocking agent to reduce nonspecific signal imaged by PAGE. The salmon sperm DNA concentration was varied from 0 to 1.0 μg/test. First, salmon sperm DNA was denatured at 95°C for 10 min and cooled to 4°C. Denatured salmon sperm DNA was then mixed with the sample. Sample included a no-NP control and a positive sample (10^9 NP copies/test), which were compared. 10^8 *mecA* copies/test was mixed with 10^8 streptavidin copies/test and 10^8 detection antibody copies/test. The blue dashed box indicates a concentration of salmon sperm DNA that resulted in the lowest nonspecific signal.

5.3.3.2 Signal measurement of LFT-iSDA by LFT amplicon detection

LFT-iSDA with non-target DNA as a blocking agent was evaluated by both LFT amplicon detection (Figure 5.2) and PAGE. No-NP controls and positive NP samples (10^3-10^7 NP copies/test) were tested (Figure 5.8). PAGE showed specific signals with >10^5 NP copies/test (Figure 5.8A). Since no-template control (NTC) did not show the signal, nonspecific signals from no-NP control were not a contamination issue but due to nonspecific binding of templates at and near the capture region. The LFT amplicon detection (Figure 5.8B) was used to quantify the signal intensities. Based on the quantified signals (Figure 5.8C) and scanned image of amplicon LFT strips (Figure 5.8D), 10^5 NP copies/test (0.5 pg/mL) was the lowest NP concentration that could be detected. Since the lowest detectable NP (A/Brisbane/10/2007 (H3N2)) concentration reported by CDC using commercial kits was 54 ng/mL,[67] this observation suggests a potential for a highly sensitive protein detection. The current LFT-iSDA, however, is based on the manual implementation using purified recombinant NP sample without inhibitors in human nasal sample, such as mucin and human genomic DNA. Therefore, further investigation is required to validate the feasibility of LFT-iSDA with virus sample in human nasal matrix. The following section shows validation of LFT-iSDA in the presence of simulated nasal matrix (SNM), including the amplification inhibitors associated with such a sample.

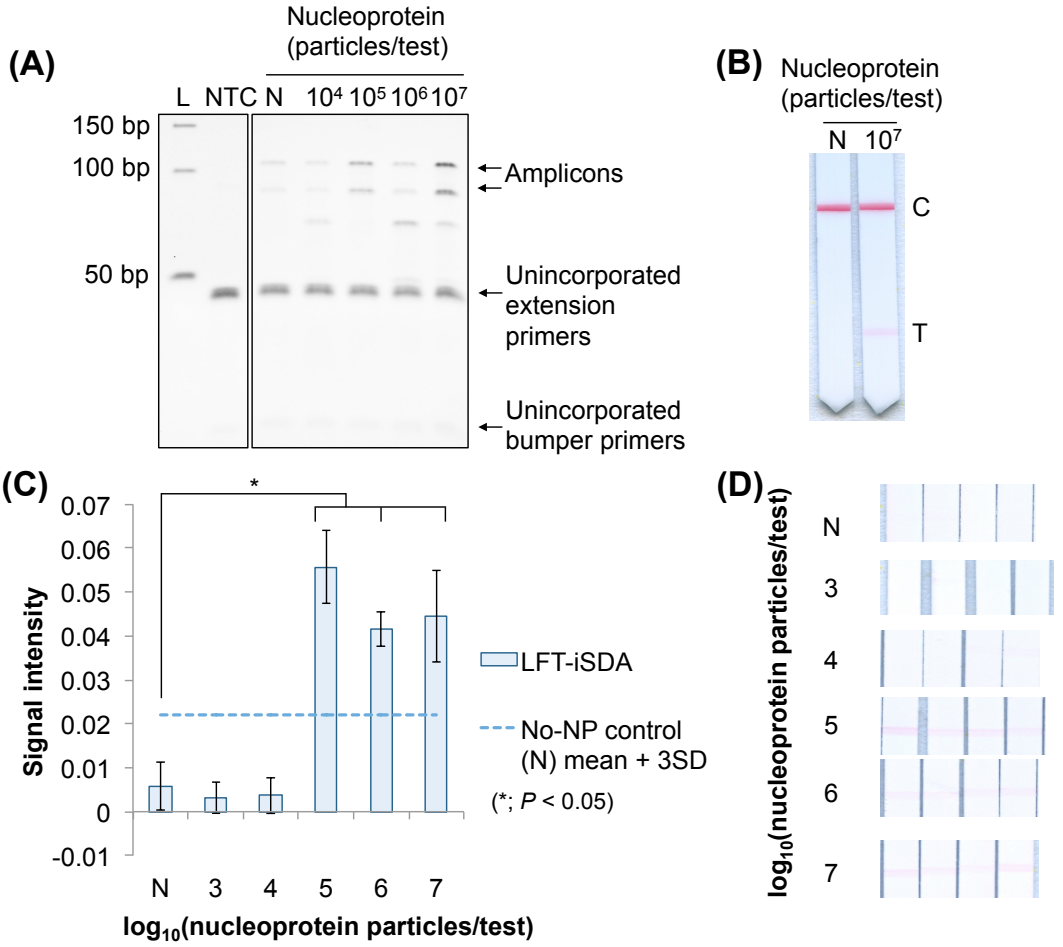

Figure 5.8. Signal measurement of LFT-iSDA with non-target salmon sperm DNA by LFT amplicon detection. PAGE image (A), scanned image of amplicon LFT strips (B), quantified signal intensities (C), and corresponding scanned image of strips (D) are shown. The denatured salmon sperm DNA (1.0 µg/test) was mixed with the NP sample. The no-NP control (N) and positive sample (10^3-10^7 NP copies/test) were compared. 10^8 *mecA* copies/test was mixed with 10^8 streptavidin copies/test and 10^8 detection antibody copies/test. Average signals for 10^5, 10^6 and 10^7 NP copies/test were significantly higher than no-NP control (*; $P < 0.05$, N=4).

5.3.3.3 LOD of LFT-iSDA compared to LFIA-HRP/DAB and LFIA-gold tests

The LOD of LFT-iSDA for influenza A NP was evaluated by signal quantification of LFT to detect iSDA amplicons. To evaluate the improvement possible with LFT-iSDA, a previously-developed LFIA-HRP/DAB test and a conventional LFIA-gold test were compared.[35,68] SNM was also used because complex biological samples could inhibit amplification and/or result in

nonspecific binding of the iSDA template oligo to the lateral flow material.[63,75] A preliminary result of LFT-iSDA using both SNM and denatured non-target salmon DNA showed poor sensitivity (Figure 5.9), indicating that the combination of SNM and non-target salmon DNA significantly decreased efficiency of the amplification.

Denatured salmon DNA (μg/test)	1.0							
SNM (%)	10							
mecA (copies/test)	0	10^8						
NP (copies/test)	0	0	10^4	10^5	10^6	10^7	10^8	10^9

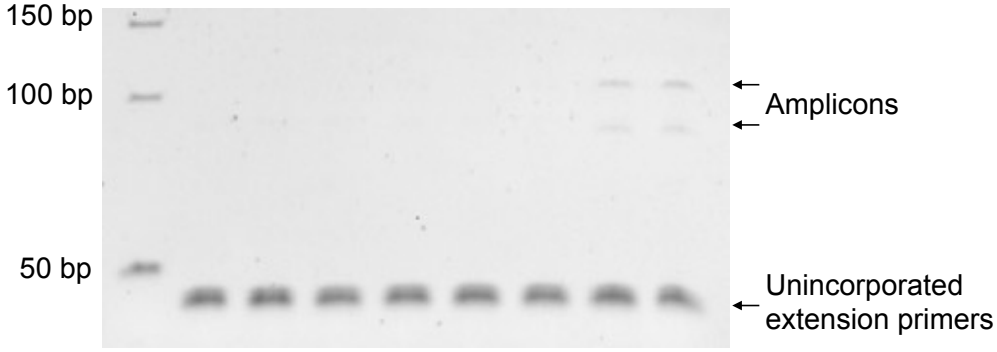

Figure 5.9. Effect of denatured non-target salmon DNA and SNM on LFT-iSDA. The denatured salmon sperm DNA (1.0 μg/test) and SNM were mixed with the NP sample. The no-NP control and positive sample (10^4-10^9 NP copies/test) were compared. 10^8 *mecA* copies/test was mixed with 10^8 streptavidin copies/test and 10^8 detection antibody copies/test. PAGE showed specific signals with > 10^8 NP copies/test, suggesting the decrease of the sensitivity compared to LFT-iSDA with only salmon DNA.

Therefore, SNM without non-target salmon DNA was premixed with NP sample to measure LOD of LFT-iSDA (Figure 5.10). The calculated LOD for this LFT-iSDA test was ~10,000-fold better than for the LFIA-gold test. Note that the current assay time for the manual LFT-iSDA is 40 min for immunoassay, 30 min for iSDA, 30 min for incubation of amplicons with probes, and 20 min for LFT to detect amplicons (2 hours total assay time). Since this is a manual implementation with wet reagents and purified recombinant NP sample, future work (underway) will include 1) validation with virus and human nasal swab samples, 2) integration of the LFT-

iSDA in a fully-automated 2DPN device, and 3) real-time detection using a fluorescence probe for faster sample-to-result times.

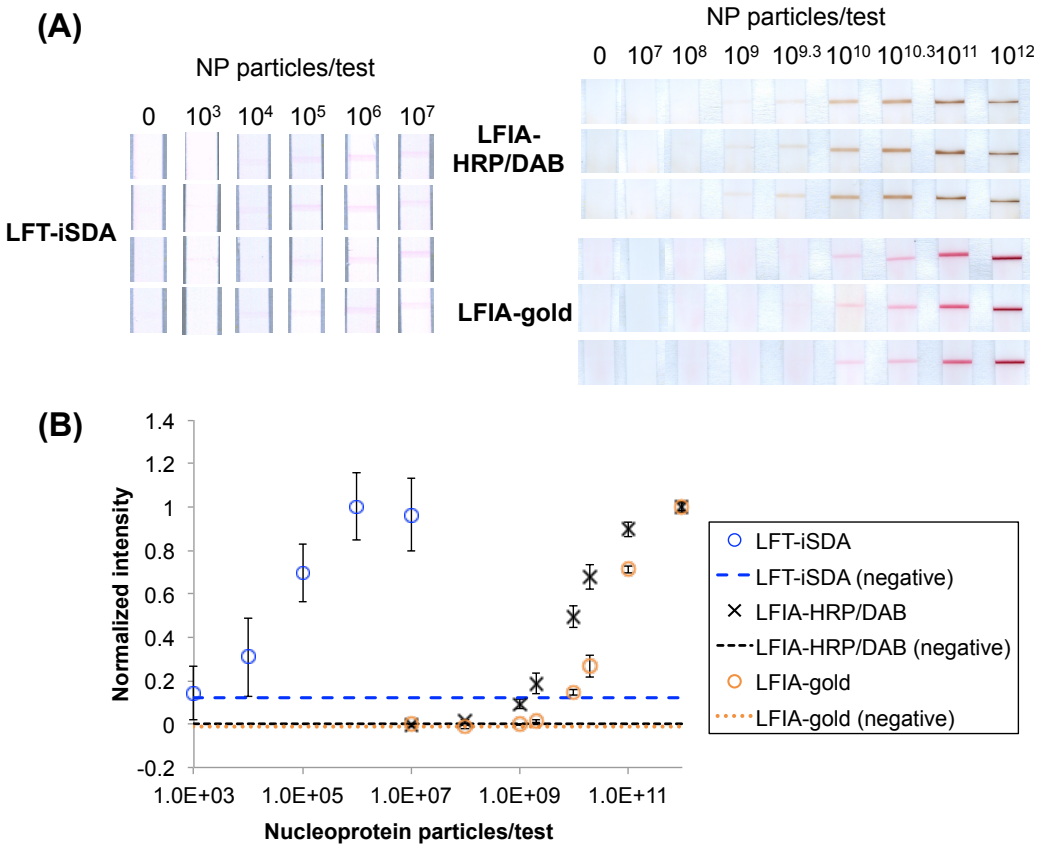

Figure 5.10. LOD of LFT-iSDA with SNM compared to HRP/DAB assay and gold (Au)-nanoparticle-based assay. Scanned images of each assay (A) and quantified signal intensities (B, normalized with the highest signal intensity in each assay) are shown. The final concentration of SNM in each test was 10% (v/v). The no-NP control and positive sample (10^3-10^{12} NP copies/test) were compared. 10^8 *mecA* copies/test was mixed with 10^8 streptavidin copies/test and 10^8 detection antibody copies/test. Calculated LOD for LFT-iSDA, HRP/DAB, and gold-nanoparticle-based tests were 5.2×10^4 (lower and upper 95% CI = 2.4×10^4 and 1.2×10^5), 7.2×10^8 (lower and upper 95% CI = 5.0×10^8 and 9.5×10^8), and 3.1×10^9 (lower and upper 95% CI = 2.4×10^9 and 3.9×10^9) NP copies/test, respectively (N=3~4).

5.3.3.4 Reproducibility of LFT-iSDA using different type of nitrocellulose

Since Millipore HF120 nitrocellulose membrane was expected to be out of stock (based on the communication with the company), new type of nitrocellulose membrane, CN95 (Sartorius, Goettingen, Germany) was validated for LFT-iSDA. Figure 5.11 shows the LFT-iSDA (1)

without SNM and salmon sperm DNA, (2) with salmon sperm DNA, and (3) with SNM. (1) showed significantly high nonspecific signals, which is the same issue of the assay using HF120. On the other hand, (2) and (3) showed decreased nonspecific and specific signals, indicating that optimization of reagent concentrations is required for the assay with CN95.

mecA (copies/test)	0	10^8								
SNM (%)	0	0			0			10		
Salmon DNA (µg/test)	0	0			1			0		
NP (copies/test)	0	0	10^5	10^7	0	10^5	10^7	0	10^5	10^7

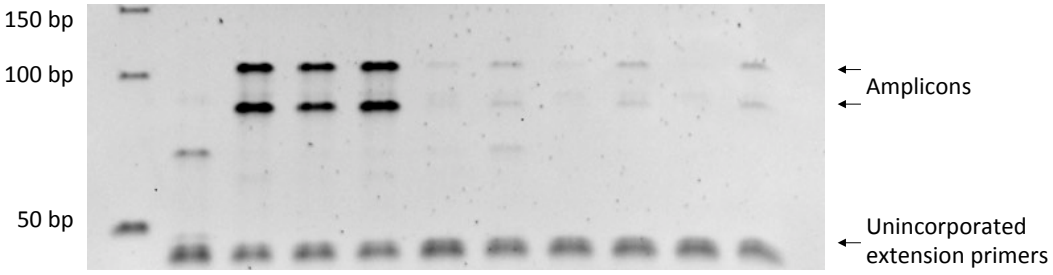

Figure 5.11. Validation of CN95 (nitrocellulose, Sartorius) for LFT-iSDA. The denatured salmon sperm DNA (1.0 µg/test) and SNM (10%) were tested. The no-NP control and positive sample (10^5 and 10^7 NP copies/test) were compared. NP sample was mixed with 10^8 mecA copies/test, 10^8 streptavidin copies/test, and 10^8 detection antibody copies/test.

Figure 5.12 shows the LFT-iSDA using varied salmon sperm DNA concentrations. Increasing salmon DNA decreased nonspecific signals and 0.75 µg/test salmon DNA showed specific signals from 10^5 and 10^7 NP copies/test, which were higher than nonspecific signals.

Therefore, 0.75 µg/test salmon DNA was used for LOD measurement of LFT-iSDA using CN95 (Figure 5.13, performed with Dylan Guelig to validate the reproducibility of the assay in another person's hands). LFT-iSDA using CN95 and salmon DNA showed specific signals from 10^6 NP copies/test, which was significantly higher than nonspecific signals. The sensitivity of LFT-iSDA with CN95 is ~10-fold worse than the sensitivity with HF120, but the assay has been

developed using HF120 and can be further improved using CN95. In addition, the signal intensities from 10^7 NP copies/test using CN95 were higher than any signals observed using HF120. Therefore, it is assumed that CN95 could support the amplification better than HF120. Optimization of the assay using CN95 for real-time fluorescence detection should be performed to develop an automated 2DPN integrated device.

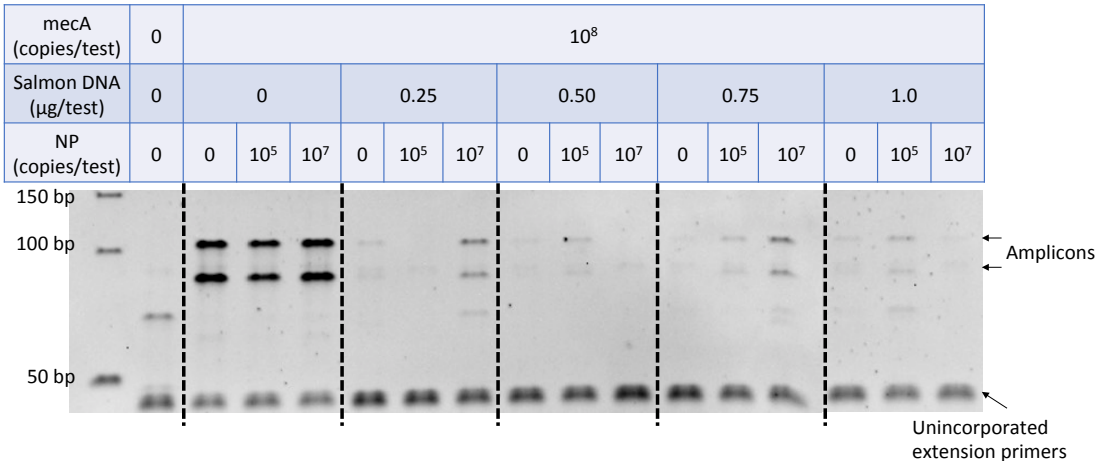

Figure 5.12. Effect of non-target denatured salmon sperm DNA as blocking agent for LFT-iSDA using CN95. Varied concentrations (0-1.0 µg/test) of denatured salmon sperm DNA were premixed with NP sample as blocking agent. 10^8 mecA copies/test, 10^8 streptavidin/test, and 10^8 detection Ab copies/test were premixed with NP sample. No-NP control and positive sample (10^5 and 10^7 NP copies/test) were tested.

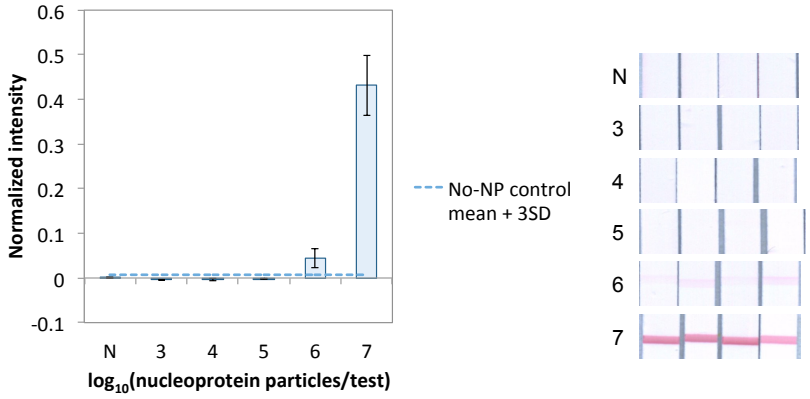

Figure 5.13. LOD measurement of LFT-iSDA using CN95 and salmon sperm DNA. Quantified signal intensities (left) and scanned images of LFT strips (right) are shown (N=4). A 0.75 µg/test salmon DNA solution was premixed with NP sample as blocking agent. 10^8 mecA copies/test, 10^8 streptavidin/test, and 10^8 detection Ab copies/test were premixed with NP sample. No-NP control (N) and positive sample (10^3-10^7 NP/test,) were tested.

5.3.4 Future Experiments and Expected Results

As described above, nonspecific signal has been reported as a common problem in immuno-NAAT. Table 6 shows typical blocking agents and methods to reduce nonspecific signal for immuno-NAAT (mostly for immuno-PCR). In addition to increasing the washing solution, a combination of detergents, proteins, non-target DNA, and normal goat serum would be applicable to reduce nonspecific signal in LFT-iSDA because those blocking agents are easily available for lateral flow assays.

Table 6: Blocking agents and methods for immuno-NAAT

Blocking agent/method	**Application**	**Reference #**
Increase/modify wash	Immuno-PCR	Analytica Chimica Acta 2016, 910, 12 [56]
DNAse I	Immunoliposome-PCR To degrade nonspecific DNA	J. Nanobiotechnology 2012, 10, 26 [79]
SDS + Tween 20	Immuno-PCR	Chem Com 2013, 49, (36), 3778 [80]
BSA	Immuno-PCR	Anal. Methods., 2015, 7, 99 [81]
Casein	Immuno-PCR	J. Virol. Methods, 2013, 187, 121 [82]
Nonfat milk	Immuno-PCR	Anal. Biochem., 2012, 431, 4 [83]
Salmon sperm DNA	Immuno-PCR	Biochem Biophys Res Commun 2005, 333, 1289, [84] and **our method (LFT-iSDA)**
Calf Thymus DNA	Immuno-PCR	Immune Network 2008, 8, 82 [85]
Normal goat serum	Immuno-PCR	Lett Appl Microbiol 1996, 23, 101 [86]

In addition, customizable non-target gene fragments, such as gBlocks Gene Fragments (IDT), would be a good alternative as blocking agent. For example, small amount of non-target DNA

fragment without nicking site would effectively block immunoassay and iSDA and not affect nicking, extension and displacement activity.

Direct conjugation of DNA template to detection antibodies is another approach to mitigate nonspecific reaction because the tetrameric structure of streptavidin would lead to the formation of heterogeneous detection molecule conjugates that could cause relatively low assay reproducibility.[56] A covalent antibody-DNA conjugation strategy, such as a previously-reported method using NHS-chemistry, is available for immuno-PCR and worth to apply for LFT-iSDA.[87]

Moreover, a background signal can be decreased by a proximity ligation assay (PLA). PLA uses two different DNA templates, which can be hybridized only when the two templates are close to each other.[57] For example, one template is conjugated to detection antibodies and the other is conjugated to capture antibodies, which would lead to very low probability that two DNA templates accidentally assemble each other and be hybridized. Therefore, PLA can extremely reduce the level of background signal in immuno-PCR and could be applied for LFT-iSDA.

5.3.5 Conclusions

This work aims to improve LOD of influenza A NP LFT by iSDA. We have demonstrated that LFT-iSDA can reduce the LOD of the assay by ~10,000-fold compared to the conventional gold-nanoparticle-based LFT immunoassay. This is the first demonstration of the immuno-NAAT on a nitrocellulose membrane, which allows an inexpensive paper-based membrane to become a platform for a highly sensitive protein detection. Although the current manual LFT-iSDA still has weaknesses (e.g. time-consuming process and nonspecific signal), the amplification method was validated as a platform that can work on nitrocellulose for protein detection. To further

improve the feasibility of this amplification method, immunoassay, iSDA, and amplicon detection should be integrated as an automated assay utilizing porous material networks to eliminate intermediate user steps. The integration of a fully-automated LFT-iSDA based on our previously-reported approaches[64,68] is underway.

6 CONCLUSION

6.1 SUMMARY OF WORK

Through the described works, we aimed to improve LOD of influenza A NP assay using signal amplification methods by absorbance-based detection and NAAT-based detection. In particular, through Specific Aim 1, we achieved 10-fold lower LOD compared to commercially available gold nanoparticle-based assay by enzymatic creation and precipitation of visible dyes using HRP and DAB. AuE and AgE were also investigated and their performance was compared. In Specific Aim 2, we aimed to optimize the reagent delivery format and to develop a computational model to predict a potential global minimum LOD in the assay. The premixed reagent format achieved better LOD compared to the sequential format, which would be due to a combination of binding kinetic constants in the system. To elucidate the underlying mechanism and predict behavior of the system, a preliminary mathematical model was developed and evaluated with experimental data. In Specific Aim 3, we aimed to further improve LOD of LFT by iSDA. This LFT-iSDA was the first demonstration of immuno-NAAT on nitrocellulose, which is a feasible platform for POC diagnostics. LFT-iSDA showed ~10,000-fold better LOD compared to conventional gold nanoparticles-based LFIA. This manually implemented LFT-iSDA should be integrated as a fully-automated 2DPN POC diagnostic device to reduce intermediate user steps.

6.2 PUBLICATIONS, PATENT APPLICATIONS, AND PRESENTATIONS

6.2.1 Publications:

- **K. Abe**, E. Heiniger, JD. Bishop, JR. Buser, S. Kumar, D. Guelig, and P. Yager, "Increased sensitivity for lateral flow tests through signal amplification by isothermal strand displacement amplification (LFT-iSDA)", *PLOS ONE*, manuscript under review.

- KG. Shah, V. Singh, PC. Kauffman, **K. Abe**, and P. Yager, "Mobile phone ratiometric imaging enables highly sensitive fluorescence lateral flow immunoassays without external optical filters", *Anal. Chem.*, 2018, 90 (11), 6967.[27]
- S. Huang, **K. Abe**, S. Bennett, T. Liang, P. D. Ladd, L. Yokobe, C. E. Anderson, K. Shah, J. Bishop, M. Purfield, P. C. Kauffman, S. Paul, A. E. Welch, B. Strelitz, K. Follmer, K. Pullar, L. Sanchez-Erebia, E. Gerth-Guyette, G. Domingo, E. Klein, J. A. Englund, E. Fu, and P. Yager, "Disposable autonomous device for swab-to-result diagnosis of influenza", *Anal. Chem.*, 2017, 89 (11), 5776.[68]

6.2.2 Patent Applications:

- **K. Abe**, JD. Bishop, JR. Buser, D. Guelig, E. Heiniger, A. Howell, S. Kumar, and P. Yager, "Increased sensitivity for lateral flow tests through signal amplification by isothermal strand displacement amplification (LFT-iSDA)", patent application serial number: 62/671,328, filed on 5/14/2018, UW reference: 48186.01US1.
- K. Shah, **K. Abe**, P. Kauffman, "Filter-free devices and systems for measuring fluorescence of a microfluidic assay and associated methods of use", patent application serial number: 15/589,804, filed on 5/8/2017, UW reference: 47699.02US2.

6.2.3 Oral/Poster Presentations:

- MicroTAS 2016 Dublin, Ireland, October 9 – 13, 2016

  "A disposable swab-to-result influenza rapid test device based on a 2-dimensional paper network"; S. Huang, S. Bennett, **K. Abe**, P. Ladd, T. Liang, K. Shah, P.C. Kauffman, S. Paul, M. Purfield, C.E. Anderson, L. Yokobe, B. Strelitz, K. Follmer, K. Pullar, L. Sanchez-Erebia, J. Englund, and P. Yager (**Oral**)

"Comparing the sensitivity of pre-mixed and sequential reagent delivery for an amplified influenza A nucleoprotein immunoassay"; **K. Abe**, P. Yager (**Poster**)

- Pacifichem 2015 Honolulu, HI, USA, December 15 – 20, 2015

  "Enzyme-based signal amplification for paper-based assays for influenza A detection"; **K. Abe**, P. Yager (**Oral**)

- MicroTAS 2014 San Antonio, TX, USA, October 26 – 30, 2014

  "Separation and Concentration of Proteins by Isoelectric Focusing without Carrier Ampholytes in a Nitrocellulose Membrane"; **K. Abe**, P. Kauffman, P. Yager (**Poster**)

- BMES 2014 Annual Meeting San Antonio, TX, USA, October 22 – 25, 2014

  "Chemical Signal Amplification for Paper-Based Assays for Influenza A Detection"; **K. Abe**, P. Yager (**Poster**)

- BMES 2013 Annual Meeting Seattle, WA, USA, September 25 – 28, 2013

  "Isoelectric Focusing as a Pre-Conditioning System for Paper-Based Analytical Devices"; **K. Abe**, P. Kauffman, P. Yager (**Poster**)

- Gordon Research Seminar (Microfluidics, Physics & Chemistry) Lucca, Italy, June 8 – 9, 2013

  "Isoelectric Focusing as a Pre-Conditioning System of Microfluidic Paper-Based Analytical Devices"; **K. Abe**, P. Kauffman, P. Yager (**Poster**)

7 REFERENCES

(1) Yager, P.; Edwards, T.; Fu, E.; Helton, K.; Nelson, K.; Tam, M. R.; Weigl, B. H. *Nature* **2006**, *442* (7101), 412–418.
(2) Yager, P.; Domingo, G. J.; Gerdes, J. *Annu. Rev. Biomed. Eng.* **2008**, *10* (1), 107–144.
(3) Sharma, S.; Zapatero-Rodríguez, J.; Estrela, P.; O'Kennedy, R. *Biosensors* **2015**, *5* (3), 577–601.
(4) Centers for Disease Control and Prevention (CDC). Rapid Influenza Diagnostic Tests https://www.cdc.gov/flu/professionals/diagnosis/clinician_guidance_ridt.htm (accessed Mar 2, 2018).
(5) Gasperino, D.; Baughman, T.; Hsieh, H. V.; Bell, D.; Weigl, B. H. *Annu. Rev. Anal. Chem.* **2018**, *11* (1), annurev-anchem-061417-125737.
(6) Drancourt, M.; Michel-Lepage, A.; Boyer, S.; Raoult, D. *Clin. Microbiol. Rev.* **2016**, *29* (3), 429–447.
(7) Bouricha, M.; Samad, M. A.; Levy, P.; Raoult, D.; Drancourt, M. *J. Travel Med.* **2014**, *21* (1), 12–16.
(8) Gubala, V.; Harris, L. F.; Ricco, A. J.; Tan, M. X.; Williams, D. E. *Anal. Chem.* **2011**, *84* (2), 487–515.
(9) Peeling, R. W.; Mabey, D. *Clin. Microbiol. Infect.* **2010**, *16* (8), 1062–1069.
(10) Ninove, L.; Tan, C.; Nougairede, A.; Zandotti, C.; Richet, H.; Charrel, R.; de Lamballerie, X. *Clin. Microbiol. Infect.* **2017**, *16* (6), 651–656.
(11) Fournier, P.-E.; Drancourt, M.; Colson, P.; Rolain, J.-M.; Scola, B. La; Raoult, D. *Nat Rev Micro* **2013**, *11* (8), 574–585.
(12) Nie, S.; Roth, R. B.; Stiles, J.; Mikhlina, A.; Lu, X.; Tang, Y.-W.; Babady, N. E. *J. Clin. Microbiol.* **2014**, *52* (9), 3339–3344.
(13) Francois, P.; Tangomo, M.; Hibbs, J.; Bonetti, E.-J.; Boehme, C. C.; Notomi, T.; Perkins, M. D.; Schrenzel, J. *FEMS Immunol. Med. Microbiol.* **2011**, *62* (1), 41–48.
(14) Boehme, C. C.; Nicol, M. P.; Nabeta, P.; Michael, J. S.; Gotuzzo, E.; Tahirli, R.; Gler, M. T.; Blakemore, R.; Worodria, W.; Gray, C.; Huang, L.; Caceres, T.; Mehdiyev, R.; Raymond, L.; Whitelaw, A.; Sagadevan, K.; Alexander, H.; Albert, H.; Cobelens, F.; Cox, H.; Alland, D.; Perkins, M. D. *Lancet* **2011**, *377* (9776), 1495–1505.
(15) Abdurrahman, S. T.; Emenyonu, N.; Obasanya, O. J.; Lawson, L.; Dacombe, R.; Muhammad, M.; Oladimeji, O.; Cuevas, L. E. *Pan Afr. Med. J.* **2014**, *18*, 277.
(16) Pai, N. P.; Vadnais, C.; Denkinger, C.; Engel, N.; Pai, M. *PLoS Med.* **2012**, *9* (9), e1001306.
(17) Novak-Weekley, S. M.; Marlowe, E. M.; Poulter, M.; Dwyer, D.; Speers, D.; Rawlinson, W.; Baleriola, C.; Robinson, C. C. *J. Clin. Microbiol.* **2012**, *50* (5), 1704–1710.
(18) DiMaio, M. A.; Sahoo, M. K.; Waggoner, J.; Pinsky, B. A. *J. Virol. Methods* **2012**, *186* (1–2), 137–140.
(19) Wong, R.; Tse, H. *Lateral flow immunoassay*; Springer: New York, 2009.
(20) Peeling, R. W.; Holmes, K. K.; Mabey, D.; Ronald, A. *Sex. Transm. Infect.* **2007**, *82* (suppl 5), v1.
(21) Huang, X.; Aguilar, Z. P.; Xu, H.; Lai, W.; Xiong, Y. *Biosens. Bioelectron.* **2016**, *75*, 166–180.
(22) Hu, J.; Wang, L.; Li, F.; Han, Y. L.; Lin, M.; Lu, T. J.; Xu, F. *Lab Chip* **2013**, *13* (22),

4352–4357.
(23) Anderson, C. E.; Shah, K. G.; Yager, P. *Methods Enzymol.* **2017**, *589*, 383–411.
(24) Sajid, M.; Kawde, A.-N.; Daud, M. *J. Saudi Chem. Soc.* **2015**, *19* (6), 689–705.
(25) Paterson, A. S.; Raja, B.; Garvey, G.; Kolhatkar, A.; Hagström, A. E. V; Kourentzi, K.; Lee, T. R.; Willson, R. C. *Anal. Chem.* **2014**, *86* (19), 9481–9488.
(26) Chen, H.; Hagström, A. E. V; Kim, J.; Garvey, G.; Paterson, A.; Ruiz-Ruiz, F.; Raja, B.; Strych, U.; Rito-Palomares, M.; Kourentzi, K.; Conrad, J. C.; Atmar, R. L.; Willson, R. C. *Sci. Rep.* **2016**, *6*, 24297.
(27) Shah, K. G.; Singh, V.; Kauffman, P. C.; Abe, K.; Yager, P. *Anal. Chem.* **2018**, acs.analchem.8b01241.
(28) Yang, Y.; Noviana, E.; Nguyen, M. P.; Geiss, B. J.; Dandy, D. S.; Henry, C. S. *Anal. Chem.* **2017**, *89* (1), 71–91.
(29) Qin, Z.; Chan, W. C. W.; Boulware, D. R.; Akkin, T.; Butler, E. K.; Bischof, J. C. *Angew. Chemie - Int. Ed.* **2012**, *51* (18), 4358–4361.
(30) Ji, Y.; Guo, W.; Zhao, L.; Li, H.; Lu, G.; Wang, Z.; Wang, G.; Liu, C.; Xiang, W. *J. Virol. Methods* **2011**, *175* (1), 120–124.
(31) Zhu, M.; Gong, X.; Hu, Y.; Ou, W.; Wan, Y. *J. Transl. Med.* **2014**, *12* (1), 352.
(32) Zhu, M.; Hu, Y.; Li, G.; Ou, W.; Mao, P.; Xin, S.; Wan, Y. *Nanoscale Res. Lett.* **2014**, *9* (1), 528.
(33) Yeo, S.-J.; Huong, D. T.; Hong, N. N.; Li, C.-Y.; Choi, K.; Yu, K.; Choi, D.-Y.; Chong, C.-K.; Choi, H. S.; Mallik, S. K.; Kim, H. S.; Sung, H. W.; Park, H. *Theranostics* **2014**, *4* (12), 1239–1249.
(34) Li, X.; Lu, D.; Sheng, Z.; Chen, K.; Guo, X.; Jin, M.; Han, H. *Talanta* **2012**, *100*, 1–6.
(35) Ramachandran, S.; Fu, E.; Lutz, B.; Yager, P. *Analyst* **2014**, *139* (6), 1456–1462.
(36) Martinez, A. W.; Phillips, S. T.; Butte, M. J.; Whitesides, G. M. *Angew. Chemie Int. Ed.* **2007**, *46* (8), 1318–1320.
(37) Martinez, A. W.; Phillips, S. T.; Whitesides, G. M.; Carrilho, E. *Anal. Chem.* **2010**, *82* (1), 3–10.
(38) Carrilho, E.; Martinez, A. W.; Whitesides, G. M. *Anal. Chem.* **2009**, *81*, 7091–7095.
(39) Martinez, A. W.; Phillips, S. T.; Whitesides, G. M. *Proc. Natl. Acad. Sci. U. S. A.* **2008**, *105* (50), 19606–19611.
(40) Pollock, N. R.; Rolland, J. P.; Kumar, S.; Beattie, P. D.; Jain, S.; Noubary, F.; Wong, V. L.; Pohlmann, R. A.; Ryan, U. S.; Whitesides, G. M. *Sci. Transl. Med.* **2012**, *4* (152), 152ra129.
(41) Fu, E.; Liang, T.; Spicar-Mihalic, P.; Houghtaling, J.; Ramachandran, S.; Yager, P. *Anal. Chem.* **2012**, *84* (10), 4574–4579.
(42) Grant, B. D.; Smith, C. A.; Karvonen, K.; Richards-Kortum, R. *Anal. Chem.* **2016**, *88* (5), 2553–2557.
(43) Clark, N. M.; Lynch, J. P. *Semin. Respir. Crit. Care Med.* **2011**, *32* (4), 373–392.
(44) Molinari, N. A. M.; Ortega-Sanchez, I. R.; Messonnier, M. L.; Thompson, W. W.; Wortley, P. M.; Weintraub, E.; Bridges, C. B. *Vaccine* **2007**, *25*, 5086–5096.
(45) Rudenko, L.; Sellwood, C.; Russell, C.; Herfst, S.; Gross, D.; Dingwall, R. *Vaccine* **2015**, *33*, 7037–7040.
(46) Dawood, F. S.; Iuliano, A. D.; Reed, C.; Meltzer, M. I.; Shay, D. K.; Cheng, P. Y.; Bandaranayake, D.; Breiman, R. F.; Brooks, W. A.; Buchy, P.; Feikin, D. R.; Fowler, K. B.; Gordon, A.; Hien, N. T.; Horby, P.; Huang, Q. S.; Katz, M. A.; Krishnan, A.; Lal, R.;

Montgomery, J. M.; Mølbak, K.; Pebody, R.; Presanis, A. M.; Razuri, H.; Steens, A.; Tinoco, Y. O.; Wallinga, J.; Yu, H.; Vong, S.; Bresee, J.; Widdowson, M. A. *Lancet Infect. Dis.* **2012**, *12* (9), 687–695.
(47) Chartrand, C.; Leeflang, M. M. G.; Minion, J.; Brewer, T.; Pai, M. *Ann. Intern. Med.* **2012**, *156* (7), 500–511.
(48) Dunn, J. J.; Ginocchio, C. C. *J. Clin. Microbiol.* **2015**, *53* (6), 1790–1796.
(49) WHO. WHO recommendations on the use of rapid testing for influenza diagnosis http://www.who.int/influenza/resources/documents/rapid_testing/en/ (accessed Dec 26, 2016).
(50) Kirby, B. *Micro- and nanoscale fluid mechanics : transport in microfluidic devices*; Cambridge University Press: New York, 2010.
(51) Zimmermann, M.; Delamarche, E.; Wolf, M.; Hunziker, P. *Biomed. Microdevices* **2005**, *7* (2), 99–110.
(52) Qian, S.; Bau, H. H. *Anal. Biochem.* **2003**, *322* (1), 89–98.
(53) Hsieh, H.; Dantzler, J.; Weigl, B. *Diagnostics* **2017**, *7* (2), 29.
(54) Gasperino, D. J.; Leon, D.; Lutz, B.; Cate, D. M.; Nichols, K. P.; Bell, D.; Weigl, B. H. *Anal. Chem.* **2018**, acs.analchem.8b00440.
(55) Liang, T.; Robinson, R.; Houghtaling, J.; Fridley, G.; Ramsey, S. A.; Fu, E. *Anal. Chem.* **2016**, *88* (4), 2311–2320.
(56) Chang, L.; Li, J.; Wang, L. *Anal. Chim. Acta* **2016**, *910*, 12–24.
(57) Ryazantsev, D. Y.; Voronina, D. V.; Zavriev, S. K. *Biochem.* **2016**, *81* (13), 1754–1770.
(58) Adler, M.; Wacker, R.; Niemeyer, C. M. *Analyst* **2008**, *133* (6), 702–718.
(59) Cao, H.; Fang, X.; Liu, P.; Li, H.; Chen, W.; Liu, B.; Kong, J. *Sci. Rep.* **2017**, *7* (1), 9312.
(60) Cao, H.; Fang, X.; Li, H.; Li, H.; Kong, J. *Talanta* **2017**, *164*, 588–592.
(61) Sarkar, S.; Sabhachandani, P.; Konry, T. *Trends Biotechnol.* **2017**, *35* (3), 186–189.
(62) Konry, T.; Smolina, I.; Yarmush, J. M.; Irimia, D.; Yarmush, M. L. *Small* **2011**, *7* (3), 395–400.
(63) Toley, B. J.; Covelli, I.; Belousov, Y.; Ramachandran, S.; Kline, E.; Scarr, N.; Vermeulen, N.; Mahoney, W.; Lutz, B. R.; Yager, P. *Analyst* **2015**, *140* (22), 7540–7549.
(64) Lafleur, L. K.; Bishop, J. D.; Heiniger, E. K.; Gallagher, R. P.; Wheeler, M. D.; Kauffman, P.; Zhang, X.; Kline, E. C.; Buser, J. R.; Kumar, S.; Byrnes, S. A.; Vermeulen, N. M. J.; Scarr, N. K.; Belousov, Y.; Mahoney, W.; Toley, B. J.; Ladd, P. D.; Lutz, B. R.; Yager, P. *Lab Chip* **2016**, *16* (19), 3777–3787.
(65) Mitamura, K.; Shimizu, H.; Yamazaki, M.; Ichikawa, M.; Nagai, K.; Katada, J.; Wada, A.; Kawakami, C.; Sugaya, N. *J. Virol. Methods* **2013**, *194* (1–2), 123–128.
(66) Holstein, C. A.; Griffin, M.; Hong, J.; Sampson, P. D. *Anal. Chem.* **2015**, *87* (19), 9795–9801.
(67) Evaluation of 11 Commercially Available Rapid Influenza Diagnostic Tests — United States, 2011–2012 https://www.cdc.gov/mmwr/preview/mmwrhtml/mm6143a3.htm (accessed Mar 6, 2018).
(68) Huang, S.; Abe, K.; Bennett, S.; Liang, T.; Ladd, P. D.; Yokobe, L.; Anderson, C. E.; Shah, K.; Bishop, J.; Purfield, M.; Kauffman, P. C.; Paul, S.; Welch, A. E.; Strelitz, B.; Follmer, K.; Pullar, K.; Sanchez-Erebia, L.; Gerth-Guyette, E.; Domingo, G.; Klein, E.; Englund, J. A.; Fu, E.; Yager, P. *Anal. Chem.* **2017**, *89* (11), 5776–5783.
(69) Chan, K. H.; Lai, S. T.; Poon, L. L. M.; Guan, Y.; Yuen, K. Y.; Peiris, J. S. M. *J. Clin. Virol.* **2009**, *45* (3), 205–207.

(70) Knipe, D. *FIELDS VIROLOGY*, 6th ed.; Lippincott Williams & Wilkins : Philadelphia, PA, 2013.
(71) Hermanson, G. T. *Bioconjugate techniques*, Third edit.; Elsevier/Academic Press: Amsterdam, 2013.
(72) FAHIMI, H. D.; HERZOG, V. *J. Histochem. Cytochem.* **1973**, *21* (5), 499–502.
(73) Ye, Q.; Krug, R. M.; Tao, Y. J. *Nature* **2006**, *444* (7122), 1078–1082.
(74) Sambrook, J.; Russell, D. *Molecular Cloning: A Laboratory Manual*; Cold Spring Harbor Laboratory Press, 2001.
(75) Panpradist, N.; Toley, B. J.; Zhang, X.; Byrnes, S.; Buser, J. R.; Englund, J. A.; Lutz, B. R. *PLoS One* **2014**, *9* (9), e105786.
(76) Morin, I.; Schaeffer, P. M. *Anal. Biochem.* **2012**, *420* (2), 121–126.
(77) Holstein, C. A.; Chevalier, A.; Bennett, S.; Anderson, C. E.; Keniston, K.; Olsen, C.; Li, B.; Bales, B.; Moore, D. R.; Fu, E.; Baker, D.; Yager, P. *Anal. Bioanal. Chem.* **2016**, *408* (5), 1335–1346.
(78) Rohrman, B.; Richards-Kortum, R. *Anal. Chem.* **2015**, *87* (3), 1963–1967.
(79) He, J.; Evers, D. L.; O'Leary, T. J.; Mason, J. T. *J. Nanobiotechnology* **2012**, *10* (1), 26.
(80) Zhang, H.; Xu, Y.; Huang, Q.; Yi, C.; Xiao, T.; Li, Q. *Chem. Commun.* **2013**, *49* (36), 3778.
(81) Bu, D.; Zhuang, H.; Yang, G.; Ping, X. *Anal. Methods* **2015**, *7* (1), 99–106.
(82) Monjezi, R.; Tan, S. W.; Tey, B. T.; Sieo, C. C.; Tan, W. S. *J. Virol. Methods* **2013**, *187* (1), 121–126.
(83) Kuczius, T.; Becker, K.; Fischer, A.; Zhang, W. *Anal. Biochem.* **2012**, *431* (1), 4–10.
(84) Adler, M.; Schulz, S.; Fischer, R.; Niemeyer, C. M. *Biochem. Biophys. Res. Commun.* **2005**, *333* (4), 1289–1294.
(85) Lee, K.; Hur, B.; Chua, K.; Kuo, I.; Song, S.; Cha, S. *Immune Netw.* **2008**, *8* (3), 82.
(86) Kakizaki, E.; Yoshida, T.; Kawakami, H.; Oseto, M.; Sakai, T.; Sakai, M. *Lett. Appl. Microbiol.* **1996**, *23* (2), 101–103.
(87) van Buggenum, J. A. G. L.; Gerlach, J. P.; Eising, S.; Schoonen, L.; van Eijl, R. A. P. M.; Tanis, S. E. J.; Hogeweg, M.; Hubner, N. C.; van Hest, J. C.; Bonger, K. M.; Mulder, K. W. *Sci. Rep.* **2016**, *6* (1), 22675.
(88) Azar, M. M.; Landry, M. L. *J. Clin. Microbiol.* **2018**, *56* (7), e00367-18.
(89) Stellrecht, K. A. *J. Clin. Microbiol.* **2018**, *56* (3), e01531-17.
(90) Strauch, E.-M.; Bernard, S. M.; La, D.; Bohn, A. J.; Lee, P. S.; Anderson, C. E.; Nieusma, T.; Holstein, C. A.; Garcia, N. K.; Hooper, K. A.; Ravichandran, R.; Nelson, J. W.; Sheffler, W.; Bloom, J. D.; Lee, K. K.; Ward, A. B.; Yager, P.; Fuller, D. H.; Wilson, I. A.; Baker, D. *Nat. Biotechnol.* **2017**, *35* (7), 667–671.
(91) Anderson, C. E.; Holstein, C. A.; Strauch, E.-M.; Bennett, S.; Chevalier, A.; Nelson, J.; Fu, E.; Baker, D.; Yager, P. *Anal. Chem.* **2017**, *89* (12), 6608–6615.
(92) Seki, M.; Kim, C.-K.; Hayakawa, S.; Mitarai, S. *Eur. J. Clin. Microbiol. Infect. Dis.* **2018**, *37* (8), 1405–1410.
(93) Puri, L.; Oghor, C.; Denkinger, C. M.; Pai, M. *Lancet Glob. Heal.* **2016**, *4* (2), e94–e95.
(94) Rodriguez-Manzano, J.; Chia, P. Y.; Yeo, T. W.; Holmes, A.; Georgiou, P.; Yacoub, S. *Curr. Infect. Dis. Rep.* **2018**, *20* (8), 25.
(95) Lim, J. K.; Alexander, N.; Di Tanna, G. L. *BMC Health Serv. Res.* **2017**, *17* (1), 850.
(96) Kolluri, N.; Klapperich, C. M.; Cabodi, M. *Lab Chip* **2018**, *18* (1), 75–94.
(97) UNITAID hosted by the World Health Organization. *Malaria Diagnostics Technology*

Landscape semi-annual update; 2012.
(98) Kelly, H.; Coltart, C. E. M.; Pant Pai, N.; Klausner, J. D.; Unemo, M.; Toskin, I.; Peeling, R. W. *Sex. Transm. Infect.* **2017**, *93* (S4), S22–S30.
(99) Rivard, K. R.; Dumkow, L. E.; Draper, H. M.; Brandt, K. L.; Whalen, D. W.; Egwuatu, N. E. *Diagn. Microbiol. Infect. Dis.* **2017**, *87*, 175–179.
(100) Singh, R. K.; Dhama, K.; Karthik, K.; Tiwari, R.; Khandia, R.; Munjal, A.; Iqbal, H. M. N.; Malik, Y. S.; Bueno-Marí, R. *Front. Microbiol.* **2018**, *8*, 2677.
(101) Pardee, K.; Green, A. A.; Takahashi, M. K.; Braff, D.; Lambert, G.; Lee, J. W.; Ferrante, T.; Ma, D.; Donghia, N.; Fan, M.; Daringer, N. M.; Bosch, I.; Dudley, D. M.; O'Connor, D. H.; Gehrke, L.; Collins, J. J. *Cell* **2016**, *165* (5), 1255–1266.
(102) Fourati, S.; Feld, J. J.; Chevaliez, S.; Luhmann, N. *J. Int. AIDS Soc.* **2018**, *21*, e25058.
(103) Honeycutt, A. A.; Harris, J. L.; Khavjou, O.; Buffington, J.; Jones, T. S.; Rein, D. B. *Public Health Rep.* **2007**, *122* (2_suppl), 55–62.
(104) Clark, D. J.; Tyson, J.; Sails, A. D.; Krishna, S.; Staines, H. M. *J. Clin. Virol.* **2018**, *103*, 27–36.
(105) Zeshan, B.; Redhuan, N. E. M.; Mohamed, M.; Daud, N. H. A. *J. Anim. plant Sci.* **2018**, *28* (2), 365–376.
(106) Texas A&M Veterinary Medical Diagnostic Laboratory. Equine Herpesvirus-1 (qPCR) https://tvmdl.tamu.edu/tests/equine-herpesvirus-1-qpcr/ (accessed Aug 15, 2018).
(107) Umesha, S.; Manukumar, H. M. *Crit. Rev. Food Sci. Nutr.* **2018**, *58* (1), 84–104.
(108) Goldberg, I.; Williams, R. A. *Biotechnology and food ingredients*; Springer US, 1991.

8 APPENDIX A: ABBREVIATIONS

Abbreviation	Description
AgE	Silver enhancement
AUC	Analytical ultracentrifugation
AuE	Gold enhancement
BSA	Bovine serum albumin
CMC	Critical micelle concentration
DAB	3,3'-diaminobenzidine
DLS	Dynamic light scattering
DNA	Deoxyribonucleic acid
FDA	Food and Drug Administration
FICT	Fluorescent immunochromatographic strip test
HA	Hemagglutinin
HRP	Horseradish peroxidase
ICT	Immunochromatographic test
IgG	Immunoglobulin G
IRR	International Reagent Resource
iSDA	Isothermal strand displacement amplification
LAMP	Loop mediated isothermal amplification
LFIA	Lateral flow immunoassay
LFT	Lateral flow test
LOD	Limit of detection
Mab	Monoclonal antibody
MolES	Molecular Engineering and Sciences
MW	Molecular weight
NAAT	Nucleic acid amplification test
PBS	Phosphate buffered saline
PBST	Phosphate buffered saline with tween 20
PCR	Polymerase chain reaction
POC	Point of care
RDT	Rapid diagnostic test
RNA	Ribonucleic acid
RT-PCR	Reverse transcription polymerase chain reaction
SPR	Surface plasmon resonance
TB	Tuberculosis
UTM	Universal transfer media

9 APPENDIX B: EVALUATION AND POTENTIAL IMPACT OF LFT-ISDA

Significance of LFT-iSDA:

Nucleic acid amplification tests (NAATs) have been used not only for diagnostics of human's and animal's pathogens but also for food analysis and a wide range of other applications. One of the advantages of NAATs is their near-single-molecule sensitivity. However, not all analytes are nucleic acids and rapid diagnostic tests (RDTs) still play a critical role as a rapid and inexpensive method. In addition, sample preparation to purify nucleic acids for NAATs can be time-consuming and costly. Point-of-care (POC) protein detection methods such as lateral flow tests (LFTs) can be rapid and less expensive. Therefore, improving the sensitivity of LFTs is important to develop an accurate and rapid POC diagnostic method. In the following section, we consider the relative importance of protein LFTs with today's NAAT tests.

Current status of influenza diagnostic at Seattle Children's Hospital:

The first section is based on communication with Dr. Janet Englund at Seattle Children's Hospital (collaborator in the Flu Project) on the current situation especially for influenza diagnostics. The following contents are about (1) current influenza diagnostic platforms in use at Seattle Children's Hospital, (2) the required turnaround time and cost for one assay, and (3) reasons to select LFT-iSDA rather than NAATs for clinicians/lab pathologist.

(1) Current influenza diagnostic platform at Seattle Children's Hospital

The Filmarray system (BioFire Diagnostics, a multiplex PCR system) was used as their primary influenza diagnostic, but is now used only for selected patients. The more rapid Cepheid

GeneXpert PCR-based test for RSV/FLU is now used for routine screening of patients at Seattle Children's Hospital. According to Dr. Englund, UW uses a 3M Flu/RSV PCR test. The Filmarray is not used for routine patients because it is too expensive (expected cost per test is $125 and expected charge to patient is probably about $600, depending on site, insurance, etc.).

(2) Expected feasible turnaround time and cost for an influenza assay

If LFT-iSDA can be as sensitive and specific as a PCR-based test (e.g. Filmarray), the expected feasible turnaround time is < 1 hour. In addition, expected feasible assay cost is < $35 with no need for highly-paid technical operator so that the hospital can bill about $100 to the patient. Currently, the cost of the Cepheid system is about $50~75 and the cost to the patient is about $200. In any case, they need to have the diagnostic test cost less than the cost for antibiotics.

(3) Expected reason to select LFT-iSDA rather than NAATs for clinicians/lab pathologist

If the LFT-iSDA can be rapid, sensitive, specific and less expensive than NAATs, it would not matter to clinicians/lab pathologist how pathogens are detected. Dr. Englund said, "If cost is lower, it would be a winner. If cost is higher, it won't go well".

In summary, Dr. Englund emphasized that the landscape for testing influenza is really changing rapidly and being driven a lot by cost. In LFT-iSDA, reagents for immunoassay[68] (~ $0.6) and amplification master mix[63,64] (~ $0.25, based on the catalog prices for the enzymes and the dNTPs that are the most expensive part of the reaction) can be less than $1 per test. The other costs for assay automation and heating are expected to be about $10 (based on the information from our laboratory's MD NAAT project, which was for heating and detection of NA targets using iSDA). Therefore, a less expensive assay compared to existing NAATs ($50~75) could be

developed. Real-time fluorescence detection in LFT-iSDA, which is under development, would take ~20 min for immunoassay and ~30 min for amplification and detection. Therefore, turnaround time of < 1 hour can be achieved. Thus, LFT-iSDA could have impact as an alternative method in the hospital as an inexpensive and rapid POCT for influenza.

Literature review of NAATs and rapid diagnostic tests (RDTs, including LFTs):

In addition to the comments from Dr. Englund, review articles about NAATs and RDTs were explored to understand the impact of sensitivity improvement of protein detection. The following 11 papers were picked up from the most recent 20 papers published between October 2017 and July 2018.

Influenza[88,89]:

Mutation is the critical factor to keep and/or improve the sensitivity of NAATs and RDTs. For example, MP gene detectable by NAATs would be a more conserved sequence than the other sequences, but the gene has been still changed/mutated. From the 2014–2015 influenza season, MP mutations of H3N2 viruses have been reported in Belgium, Germany, and USA. This mutations affected commercial assays; three of eight assays showed sensitivities ranging from 51% to 85% compared to conventional RT-PCR (e.g. the GeneXpert Flu System was reported to have sensitivity of 85%). It is important for manufacturers to keep updating/screening more feasible reagents not only for NAATs but also for RDTs (e.g. target gene sequences for NAATs and antibodies for RDTs). An alternative way to solve this issue is to design protein binder[90,91] and to update the design for mutations. The cost of the Cepheid system is about $50~75 per test (based on the communication with Dr. Englund).

Tuberculosis (TB)[92]:

Currently available methods for diagnosing TB are (1) smear microscopy with sputum samples, (2) culture-based technologies, (3) NAATs (e.g. COBAS TaqMan system), (4) novel NAATs (e.g. GeneXpert MTB/RIF system as the first TB POCT with ~2 h turnaround time, and GeneXpert MTB/RIF Ultra and OMNI), (5) TB-LAMP (manual NAAT with ~1 h turnaround time as POCT endorsed by WHO), (6) lateral flow urine lipoarabinomannan assay (LF-LAM, with ~25 min turnaround time). LF-LAM has the assay sensitivity lower than NAAT methods; LFT-iSDA could improve the sensitivity with < 1 h turnaround time. LODs of LF-LAM and Xpert MTB/RIF were 100,000 and 131 cfu/mL in specimen. The cost paid by private patients for Xpert MTB/RIF system in high burden countries is shown in Table 1.[93] The cost per test is about \$30 ~ > \$100. If LFT-iSDA (about \$10 per test) can improve the sensitivity 10^3~10^4-fold better than LF-LAM as well as our influenza nucleoprotein assay, LFT-iSDA can be an alternative method as a rapid and inexpensive POCT for TB diagnostic.

Table 7: Price paid by private patients for GeneXpert MTB/RIF in high burden countries[93]

Country	Mean price for Xpert MTB/RIF	Range
Kenya	\$80.60	\$51-\$171
India (IPAQT member laboratories)	\$30.26	Fixed price
India (rest of private sector)	\$52.82	\$27.84-\$86.55
Pakistan	\$37.26	\$25.96-\$58.65
Philippines	\$155.44	\$128-\$183
Bangladesh	\$74.75	\$45.50-\$130
Afghanistan	\$50.00	N/A

Dengue[94]:

Current diagnostic methods are (1) NAATs, (2) serology tests for antigen, (3) ELISA, (4) plaque reduction and neutralization tests for antibodies, and (5) LFT. Novel methods are (6) nucleic acid

sequence-based amplification (NASBA), (7) RT-LAMP (within 30 min), (8) transcription-mediated amplification (TMA), and (9) RT recombinase polymerase amplification (RT-RPA). However, to date, only the Truelab Real-Time micro PCR System (Molbio Diagnostics) is commercially available as a NAAT system. The cost of representative RDT, Panbio RDT, is $6.90 per test.[95] Since the expected cost of LFT-iSDA is about $10, LFT-iSDA could be an alternative method with higher sensitivity as POCT for dengue diagnostic.

Malaria[96]:

To reach the goal of malaria elimination, diagnostic methods should be sensitive, inexpensive, portable, and available for mass screening. Current methods including (1) microscopy and (2) RDTs are not sufficiently sensitive. The parasite concentration that a LFT-iSDA could detect would be less than 2 parasites per μL if LFT-iSDA can improve the sensitivity 10^3~10^4-fold better than current RDTs as well as our influenza nucleoprotein assay. Less than 2 parasites per μL as LOD is the requirement suggested by WHO. Assay with < 1 h turnaround time would be feasible assay time as POC for malaria. Truelab micro PCR platform (Molbio Diagnostics), for example, would cost $12~$15 for a Truenat Pf chip[97]. Therefore, LFT-iSDA can be less expensive compared to existing NAAT system.

Urogenital *Chlamydia trachomatis* infections[98]:

Current protein detection does not have sufficient sensitivity. NAATs take ~90 min and are not inexpensive (representative PCR system is Xpert CT/NG System). Therefore, faster and less expensive assays are required. The cost of RDTs is about $19.[99] Since LFT-iSDA can be done within 1 h by ~$10 per test, LFT-iSDA could be alternative for Chlamydia diagnostic if the sensitivity can be improved as same as our influenza nucleoprotein assay.

Zika[100]:

Cost and assay time are important factors to provide accurate and rapid POCTs. IgM/IgG LFT (Nicolini et al., 2017) showed no cross-reactivity with other arboviruses, but it was expensive. NASBA has exceptional sensitivity to low-level infections and the technique is about $5~$20/test.[101]

Hepatitis C virus (HCV)[102]:

The overall diagnostic methods are still too expensive. The expected cost was $54 for true positive injection drug user who returned for diagnostic results.[103] If the assay can be done within 1 h, sensitive LFT-iSDA could be an alternative detection method.

Filovirus[104]:

PCR, LAMP, sequencing, and other 8 new technologies including glycoprotein (GP) and nucleoprotein (NP) detection are currently available. NAATs have the greatest potential for early detection so far because only a small amount of sample is required for detection and typing of virus. WHO suggested that the expected cost for Ebola diagnostic using PCR-based assay was about $100. Therefore, less expensive LFT-iSDA can be an alternative method. In our previous project, Ebola Project, our lab investigated LFT-iSDA for secreted GP (sGP) detection. However, it was assumed that the antibodies did not have enough affinity to develop highly sensitive LFT-iSDA comparable to our influenza nucleoprotein assay. Therefore, screening antibodies or designing high affinity binder would be required to develop a feasible LFT-iSDA.

Equine herpesvirus (EHV)[105]:

Currently available methods are (1) virus isolation, (2) serology-based assay, (3) ELISA, (4) virus neutralization test, (5) complement fixation to detect antibody such as IgM, (6)

immunofluorescence, (7) PCR (estimated cost per test is $30[106]), and (8) LAMP. If LFT-iSDA can be fast (< 1 h) and less expensive (~$10), LFT-iSDA can be an alternative.

Food analysis[107]:

Currently available immunoassays (e.g. 3M Tecra) take 2 ~ 50 h as the turnaround time. NAATs (e.g. GENE-TRAK Systems) take 1 ~ 50 h as the turnaround time. The expected cost of GENE-TRAK test for *Salmonella* is about $10.[108] If LFT-iSDA can be done within 1 h for food-born pathogens, LFT-iSDA could be an alternative method.

Conclusion:

If LFT-iSDA can be developed with (1) a turnaround time of less than 1 h, (2) the cost that is less than 10 USD per assay, and (3) the improvement of protein detection sensitivity that is the same as our influenza nucleoprotein assay (i.e. 10^3 ~ 10^4-fold better LOD than conventional LFTs), LFT-iSDA can be an alternative method for rapid and inexpensive POCT for the applications described above.

10 APPENDIX C: SIDE PROJECT (PAPER-BASED IEF)

The following contents are to report the side project (SP) that we investigated in addition to the primary works described above.

SP title: Separation and concentration of proteins by isoelectric focusing on paper-based analytical device

Keywords: Isoelectric focusing / Nitrocellulose / Paper-based device / Protein

SP abstract: This section presents a simple isoelectric focusing (IEF) technique without carrier ampholytes to produce stable pH gradients in paper substrates for the fabrication of paper-based analytical devices suitable for complex biological samples. To design the custom-built IEF apparatus, two types of electrode were employed: spring-loaded gold-plated contacts and silver-coated wire electrodes; the distance between anode and cathode was 8~10 mm. These electrodes provided a non-invasive and reliable electrical connection to the surface of a commercially available porous nitrocellulose membrane (20~60 mm × 13~15 mm). Applied potentials could be higher than 2.5 V, indicating the ability of paper substrates to release electrolysis bubbles out of the membrane due to their pores being open to the outside environment. Applying a potential to the electrodes resulted in electrolysis, which, in turn, generated a pH gradient within the intervening electrolyte without the need for ampholytes. Mapping the pH gradients that develop over time and space positions were quantitatively evaluated using a pH indicator and image processing. Concentration and separation of sample biological analytes were also performed with continuous sample flow to demonstrate the potential of paper-based IEF for use in sample pre-conditioning systems.

SP1. Introduction: Sample pre-conditioning is a key function in microfluidic devices for POC analytical devices for biological and chemical samples. In such a system, an analyte of interest is separated from other interfering compounds, followed by concentration and enrichment for subsequent analyses. Electrophoretic methods including isoelectric focusing (IEF), a separation method on the basis of isoelectric points (*pI*) of analytes, have been demonstrated as popular and powerful separation tools [1, 2]. IEF requires the use of localized buffers, usually either fixed or electrophoretically-active mobile "carrier ampholytes," to develop pH gradients in the gap separating two electrodes. Amphoteric compounds migrate to the region corresponding to their *pI* due to their zero net charge in the region, resulting in the concentration of each compound. IEF is known as a good separation technique because of its high loading capacity and potential to park and refocus compounds of interest [3]. The fractionation process of IEF can also be adjusted rapidly and easily by controlling parameters such as the voltage [4]. Therefore, the IEF technique is applicable to both high-throughput analysis and multidimensional separation of complex biological analytes, such as proteins.

Although IEF is regarded as a powerful tool for the reproducible high-resolution differentiation of complex protein mixtures, improvements can be made in some areas. The needs for successful proteomics include (1) increased resolving power, (2) simplification and automation of the electrophoresis procedure, and (3) simple, inexpensive, rapid, sensitive and reliable protein quantification [5]. A decade ago our lab engaged in converting IEF into a microfluidic technique by demonstrating the creation of stable pH gradients in ducts with electrodes on two walls perpendicular to flow [4, 6-8]. However, it was found that if one is to use IEF effectively in

traditional microfluidic channels, preventing and/or isolating bubbles caused by electrolysis is one of the most challenging issues [4]. Generated bubbles in microfluidic channels can interfere with the position of concentrated analytes, resulting in decreasing electrophoretic resolution. Furthermore, the result of IEF in microfluidic channels can be affected by undesired driven flow which is known as electroosmotic pumping [9, 10], which is complicated since the electroosmosis depends on the electric field and pH, factors which vary along the microfluidic channel [10]. Because of those parasitic effects, it is challenging to apply a high voltage to increase resolving power in a conventional microfluidic system. Thus, simple and inexpensive IEF techniques that enable increased resolving power are still required.

Paper-based microfluidic devices have recently attracted significant attention, especially for POC diagnostics [11, 12]. Paper-based analytical devices are regarded as rapid, easy to use, low-cost, portable and disposable tools with the use of small volumes of expensive reagents and without external power sources. Such simple and inexpensive microfluidic analytical devices have been demonstrated for the primary diagnosis in low-resource settings and home healthcare settings (e.g. detection of pH, total protein, glucose, cholesterol, adenosine, etc.) [13-15]. However, since paper-based devices move fluids simply by a capillary pressure, most of these devices are not capable of all of the protein fractionation methods available in conventional instrumentation. Therefore, the development of more powerful separation techniques that could be integrated with paper-based devices would be helpful.

Electrochemical analytical methods are one of the promising approaches for highly sensitive and selective detection when appropriate potentials and electrode materials are chosen [16, 17].

Electrochemical detection on paper-based analytical device has been demonstrated in recent studies [18]. For IEF, several types of porous material including a polymeric sponge [19] and paper strips [20] have been demonstrated as well as commercially available immobilized pH gradient (IPG) strips. However, such membrane-based IEF approaches employed fixed or non-fixed ampholytes and/or gel with IPG as the separation medium. A nonwoven fabric was employed for IEF without carrier ampholytes, but the system requires a peristaltic pump and/or a cooling box, which could be limitations in terms of simplification of the system [21-23]. Combining paper-based analytical devices with electrophoretic techniques could be a powerful, rapid, and low-cost analysis method; simpler IEF systems without carrier ampholytes or gel with IPG could further improve the ability of paper-based analytical devices.

This work represents an attempt to produce stable pH gradients without carrier ampholytes or gel-based IPG as a simple IEF technique using a paper substrate. Since paper substrates have membrane pores open to the outside environment, electrolysis bubbles would not be trapped in the membrane. Furthermore, the results indicate that the effect of electroosmotic pumping does not have a significant impact on IEF in a nitrocellulose membrane under the current experimental conditions. Such paper-based IEF technology can be used not only as a basic proteomic analytical tool but also as an on-line sample pre-conditioning system feasible for POC diagnosis of complex biological samples in both low-resource and home healthcare settings.

In this work, we demonstrated the applicability of a simple paper-based IEF technique using a porous nitrocellulose membrane. The generation of pH gradients under static conditions was

quantified using acid-base indicators. Concentration and separation of proteins were also demonstrated with continuous sample flow using fluorescent protein conjugates.

SP2. Materials and methods

SP2.1. Materials: All chemicals were used as purchased without further purification. Phenol red (Sigma, pKa=7.9) was used as an acid-base indicator to monitor pH gradient formation. The concentration of the indicator in aqueous solution was 0.5 mM. Na_2SO_4 (Thermo Fisher Scientific, Waltham, MA) was employed as the supporting electrolyte. As the amphoteric buffer, 2-(4-morpholino)ethanesulfonic acid (MES; Sigma) was used. The initial pH values of the buffer were adjusted from pH 3.63 to pH 8.19 using 0.1 mM NaOH. The pH values were measured with a pH meter (Beckman, model 340). Tween 20 (Thermo Fisher Scientific, Waltham, MA) was used as the blocking agent. Bovine serum albumin (BSA) and avidin conjugated with different fluorescent dyes were used as examples of biological analytes. Two protein conjugates were used: BSA Alexa Fluor 594 and avidin Alexa Fluor 488 (Life Technologies, Carlsbad, CA). As paper-based substrates, porous nitrocellulose membranes with a backing (HF135; Millipore, Billerica, MA) were used. Membranes were cut to appropriate shapes on a CO_2 laser cutting system (Universal Laser Systems, Scottsdale, AZ).

SP2.2. Instrumentation: In brief, the custom-built IEF apparatus consisted of spring-loaded gold-plated contacts (DigiKey Corp., Thief River Falls, MN) as electrodes supported by a printed circuit board (PCBexpress®) (SP Figure 1A-1). The top view of the membrane and electrodes is illustrated in SP Figure 1A-2. The gap between each contact was 2.54 mm (x coordinate) and the distance between the anode and cathode rows was 10 mm (y coordinate). The spring-loaded

contacts were placed on a nitrocellulose membrane (20 mm × 15 mm), providing a reliable electrical connection on the surface of the membrane. The contact electrodes were centered between the edges of the nitrocellulose membrane in the x coordinate. In all experiments, the anode was located at the y coordinate origin. Silver-coated copper wire electrodes were also compared with the aforementioned spring-loaded Au contacts. Silver was used as a component of electrode because it is fairly inert, and inexpensive compared to Au and Pt. A pair of wires was mounted on an acrylic plate to provide an electrical connection on the surface of the nitrocellulose membrane, which was mounted on another acrylic plate (SP Figure 1B). Acrylic plates were screwed together so that wires could connect uniformly to the membrane. The distance between anode and cathode was 8~10 mm (y coordinate). Likewise, the anode was located at the y coordinate origin in all experiments.

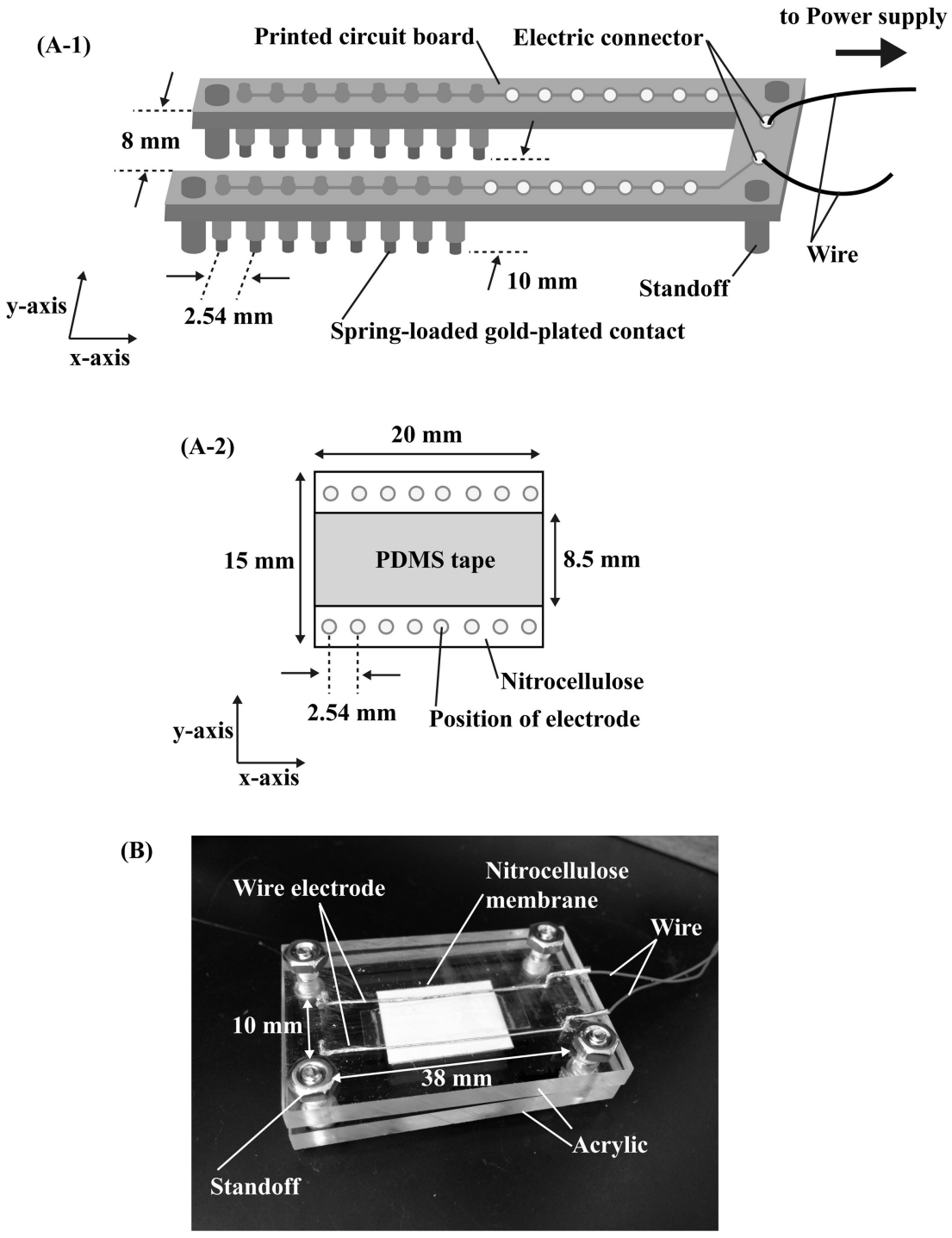

SP Figure 1. The two custom-build IEF apparati. (A-1) Schematic diagram of spring-loaded gold-plated contacts and (A-2) top view of the membrane, electrodes, and PDMS tape. (B) Photograph of the wire-electrode IEF apparatus.

SP2.3. Experimental conditions: Each type of electrode was mounted to ensure its electrical connection to the fluid-filled nitrocellulose membrane. Using a DC power supply (Hewlett-Packard, model 6209B), a constant potential was applied across the two sets of electrodes. PDMS (polydimethylsiloxane) tape (ARclad® 7876; Adhesives Research, Glen Rock, PA, which is actually a PDMS layer supported by a moisture-impermeable Mylar film) was cut and contacted with the upper surface of the membrane between anode and cathode to suppress evaporation of sample solutions. After setting up of the PDMS tape and electrodes, sample solutions were added to the membrane by pipetting. The performance of the paper-based IEF was verified by applying 50~400 μl of mixed sample solutions of MES buffer (0~200 mM), Na_2SO_4 (0~20 mM) and pH indicator or protein conjugates in most cases.

SP2.4. Image analysis: A web camera (Logitech, Fremont, CA) and accompanying PC software (Azcendant Software, Tempe, AZ) were used to acquire image data. The color changes on the membrane were tracked manually from the camera at one frame per 10 seconds using Image J. Standard fluorescence filter sets (ex. 455~460 nm, 520~535 nm; em. 550-nm-long pass, 590-nm-long pass) were used for fluorescence measurements.

SP3 Results and discussion:

SP3.1. pH gradient formation by IEF: To demonstrate pH gradient formation within the membrane, phenol red was used as a pH indicator at an initial pH of 7.18 (SP Figure 2). Applying a potential of greater than 2.0 V at this pH results in the electrolytic decomposition of water, forming H^+ and OH^-. As the electrodes are connected by the electrolyte, the result is the formation of a pH gradients [7, 24]. As a result, phenol red becomes bright red (pH 8.2~) near

the cathode by OH^- (SP Figure 2). H^+ formed at the anode caused the color change to pale yellow (~pH 6.8). SP Figure 2 shows that the positions of these color fronts (i.e. front of alkali and acid) shifted toward each other and reached steady-state locations, due to a combination of diffusion and electrophoresis (of species including the charged forms of the indicator dyes). As shown in SP Figure 2, color fronts using the wire electrodes (SP Figure 2B) were flatter than that using the spring-loaded contacts (SP Figure 2A). This could be due to the shape of electric field caused by the geometry of each electrode. Since pH gradients formed by the wire electrodes spread uniformly, the wire-electrode IEF apparatus was employed in the following experiments.

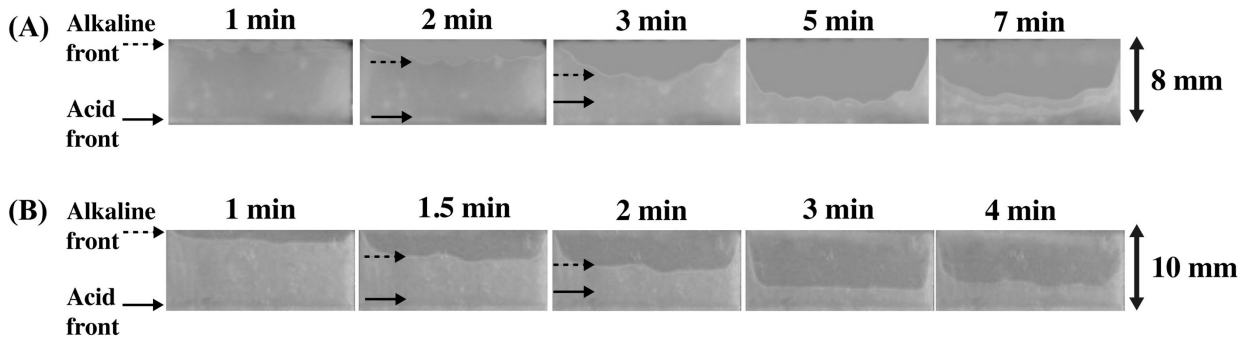

SP Figure 2. Optical images of pH changes of a 0.5 mM solution of phenol red in 15 mM MES and 10 mM Na_2SO_4; an initial pH of 7.18, applied potential of 6.0 V using (A) the spring-loaded contacts and (B) the wire electrodes. Arrows and dashed arrows indicate acid fronts and alkaline fronts, respectively.

To obtain optimal conditions for the pH gradient formation, concentrations of MES buffer and Na_2SO_4 were varied. Addition of MES buffer influenced the shift of the color fronts, contributing to their flatness. Na_2SO_4 is commonly used as electrolyte for electrolytic decomposition of water because (1) SO_4^{2-} has higher standard electrode potential than hydroxide and (2) Na^+ has lower standard electrode potential than a hydrogen ion. To demonstrate pH gradient formation, Na_2SO_4 was used as a supporting electrolyte to observe color changes with pH indicators. So far, a

combination of 15 mM MES and 10 mM Na_2SO_4 was effective for the generation of pH gradients without any other charged species such as proteins. Since electroosmotic pumping is one of the potential factors that could affect the formation of pH gradient, the effect of electroosmotic pumping was evaluated using Rhodamine B as a neutral dye indicator (data not shown). After addition of a solution of 100 mM MES and 0.5% Tween 20 (i.e. same condition for the protein separation) on the membrane, Rhodamine B in the same concentration of the solution was added to monitor the migration of the dye during IEF. The temperature rose at higher potential, leading to evaporation of the sample solution (40 V~). The effect of electroosmotic pumping does not have a significant impact on the migration of the dye during IEF at currents up to 1.3 mA. This result illustrates a potential of the paper-based IEF to reduce undesired driven flow, although further studies are required to confirm detailed phenomena.

SP3.2. Effect of initial pH conditions: The specific locations of the "alkaline front" (i.e. the boundary between moderately red (pH<8.2) and bright red (pH>8.2)) in each time increment were observed at different initial pH values (SP Figure 3), demonstrating the basic quantitative analysis by simple means. For each initial pH value, a steady state was reached by 300 s after voltage application. SP Figure 3 demonstrates that the steady-state positions of the alkaline front were closer to the anode when there were higher initial pH values. This result is consistent with previous research in open ducts, illustrating that the final position of the color fronts depends on the initial pH [7]. Experiments shown above were in nonflowing conditions without the continuous supply of sample solutions. Therefore, transverse IEF with continuous sample flow was performed in the following section.

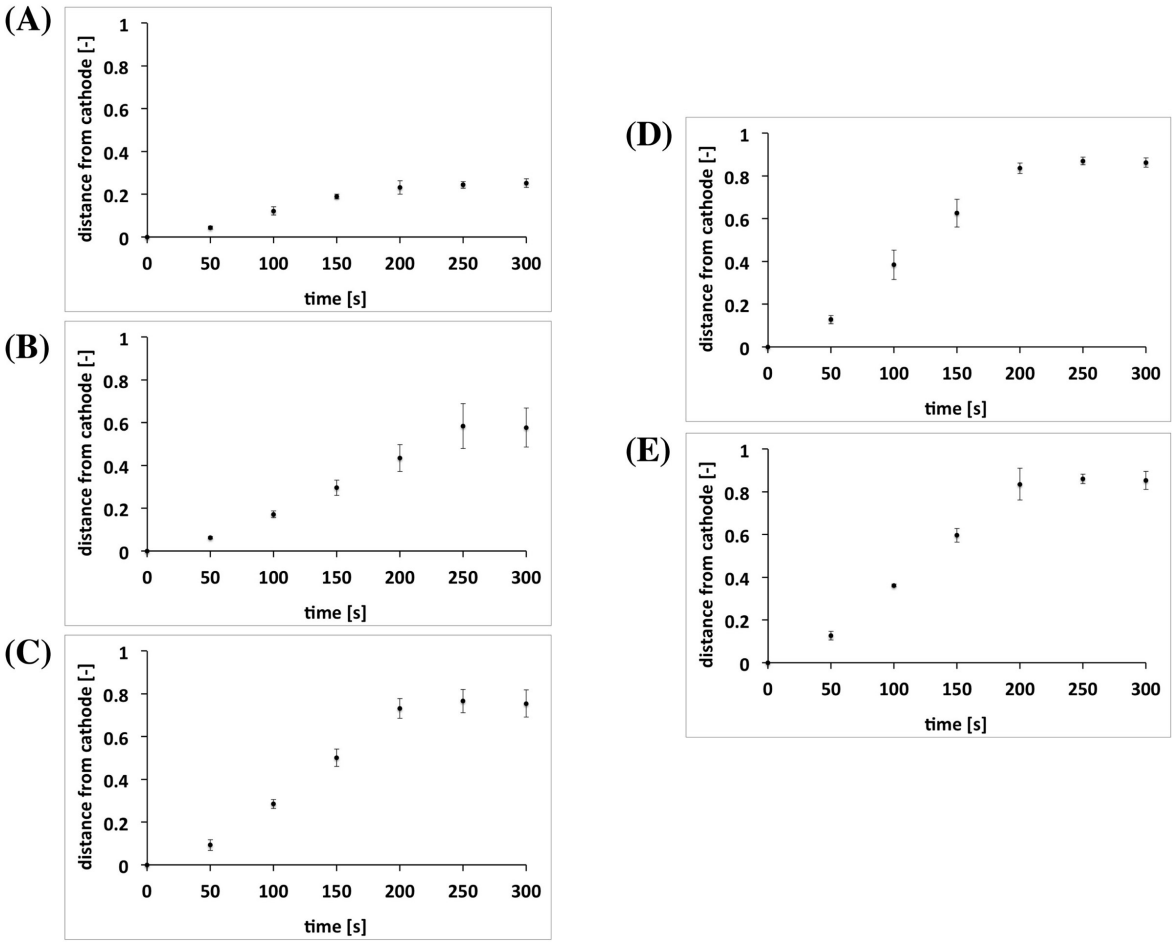

SP Figure 3. The effect of initial pH on pH gradient formation using wire electrodes. Specific pH positions for alkaline front of phenol red at the initial pH of (A) 3.47, (B) 5.07 (C) 6.25, (D) 7.05 and (E) 8.00. A 0.5 mM solution of phenol red in 15 mM MES and 10 mM Na_2SO_4 was used; applied potential of 6.0 V.

SP3.3. IEF for concentration of BSA: To demonstrate the separation and concentration of target proteins by IEF on the paper substrate, a commercially available conjugate of bovine serum albumin (BSA) with the fluorescent dye Alexa Fluor was used because the BSA conjugate has intense fluorescence and resistance to photobleaching. Furthermore, it has been described elsewhere that the covalent attachment of fluorescent dyes (e.g. rhodamine isothiocyanate or

fluorescein isothiocyanate) to BSA does not considerably influence the *pI* of BSA, which is 4.6 [7, 25].

For initial pH values higher than 7.0, the BSA conjugate was not entirely focused (data not shown). This could be due to the fact that higher ionic strength caused by addition of NaOH leads to lower field strength between the electrodes, resulting in decreased resolving power [4]. Therefore, the BSA conjugate was concentrated with an initial pH of 6.03 (SP Figure 4A). In this case, concentration of 3 μM of the BSA conjugate without continuous sample flow was demonstrated. A 10 mM sodium sulfate solution and a 15 mM MES solution were also used as a supporting electrolyte and a buffer solution, respectively. Since BSA has relatively large molecular weight (66 kDa), the BSA conjugate may move slower than the alkaline front observed by IEF using pH indicator shown in SP Figure 2 and 3. This could be the reason that applying a potential of lower than 6.0 V resulted a faint focused band of the BSA conjugate; sample solutions started to dry before reaching steady-state locations (data not shown). Therefore, a potential of 7.5 V was applied to increase resolving power. As a result, the BSA conjugate focused into one tight band (SP Figure 4A).

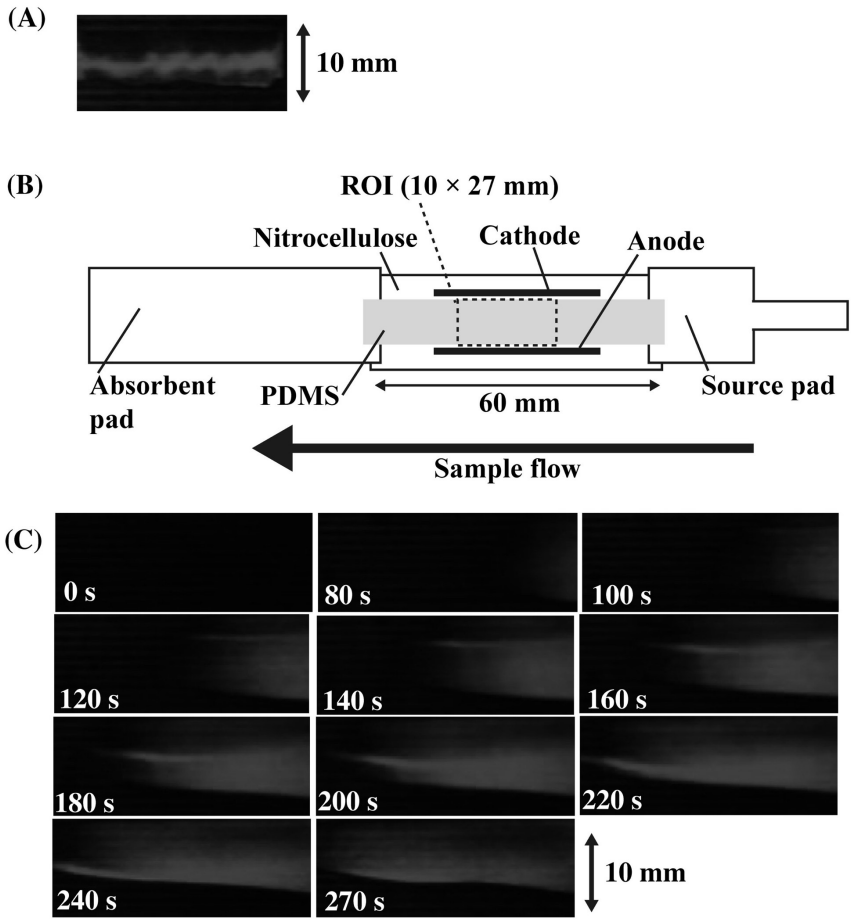

SP Figure 4. IEF of 3.0 μM BSA conjugate in 15 mM MES and 10 mM Na_2SO_4; applied potential of 7.0 V, measured current of 0.4 mA, an initial pH of 6.03. (A) Fluorescence image of BSA conjugate 200 s after applying a potential without continuous sample flow. (B) Schematic diagram of membranes, electrodes, PDMS, and ROI (region of imaging) for IEF with continuous sample flow. (C) Fluorescence images of BSA conjugate with continuous sample flow.

In a conventional microfluidic system, application of a high voltage (2.5 V~) using electrodes in the channel causes bubble formation. However, the electrolysis bubbles caused by applying a potential of higher than 2.5 V would not be trapped in the membrane due to its pore structure being open to the outside environment where the electrodes contact the paper. This result showed a potential of the paper-based membrane to apply higher voltages for increased resolving power.

Paper substrates for IEF, however, could have limitations regarding evaporation and heat. For example, sample solutions started to dry up before pH gradient reached steady-state locations when no covering material was used on the membrane. Subsequently, Mylar-backed PDMS films were used to cover the membrane and suppress evaporation. Heat produced by applying a high potential could lead to denaturation of proteins and nitrocellulose. This can be avoided by sandwiching the membrane between thermal conductors.

To demonstrate IEF on the membrane with continuous sample flow, nitrocellulose membrane was cut (60 × 15 mm) and cellulose membrane (C083 Cellulose Fiber Sample Pad; Millipore, Billerica, MA) was used as source and absorbent pads (SP Figure 4B). The wire electrodes were used to apply a potential. SP Figure 4C shows optical images of continuous flow of 3 μM solution of BSA conjugate on nitrocellulose membrane in each time increment. 10 mM sodium sulfate and 15 mM MES were used with the initial pH of 6.03. At the initial state (~100 s), the sample solution flowed uniformly along a strip. The BSA conjugate was then gradually concentrated at a certain location between anode and cathode. A steady state was reached before 300 s of voltage application, which is similar to the result without continuous sample flow.

SP3.4 IEF for separation of protein conjugates: To demonstrate the separation of protein conjugates, we chose BSA conjugate and avidin conjugate because of their clearly separated *pI* (BSA: 4.6, avidin: 10.5). Several parameters, such as applied voltage and initial pH, were varied to obtain optimal conditions for separations. It was experimentally confirmed that one of the problems was the nonspecific adsorption of protein conjugates to the nitrocellulose membrane.

To address this issue, Tween 20, a common blocking agent for lateral flow test strips, was used. It was also confirmed that Tween 20 (~0.5%) does not lead to background fluorescence.

One of the most important factors to effectively separate proteins is the slope of the pH gradient, which should be shallow enough to allow separation. Concentration of MES was varied from 15 mM to 200 mM to investigate optimal buffer concentration for the effective separation of BSA and avidin conjugates. 15~50 mM MES resulted in slightly separated BSA and avidin conjugates while a majority of them were overlapped. 150~200 mM MES led to the separation of them although BSA was not highly concentrated, which could be due to the high ionic strength. Raising the ionic strength of the solution can lower the field strength across the nitrocellulose membrane. This effect reduces the efficiency of the focusing process, resulting in decreasing the rate of the concentrated band formation [4, 26].

SP Figure 5 shows fluorescence images of continuous flow (from right to left) of a protein mixture (3 μM BSA conjugate and 3 μM avidin conjugate) in 100 mM MES and 0.5% Tween 20 in each time increment. Images were captured every 10 seconds and each set of fluorescent LED and long pass filter was switched every 20~40 seconds. A potential was applied after the entire membrane was wet with the mixture of protein solution. The mixture of BSA and avidin conjugates gradually separated and avidin was concentrated near the cathode, resulting in a tight band 100 s after applying a potential. BSA conjugate was observed as a broader band, indicating that the pH gradient was not uniformly distributed. In addition, BSA is well known as a blocker for a nitrocellulose membrane and thus nonspecific interaction with the membrane (e.g. physical

and electrostatic adsorption) could affect the band formation and diffusion during IEF. In further studies, different combinations of proteins and buffers should be investigated.

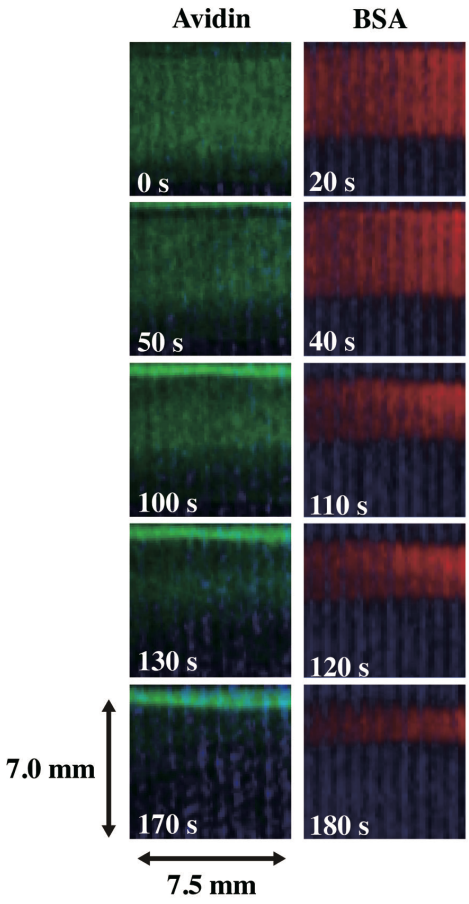

SP Figure 5. IEF of the mixture of BSA conjugate and avidin conjugate; fluorescence images of BSA and avidin conjugates with continuous sample flow. Experimental conditions: 3.0 µM BSA Alexa Fluor 594 conjugate and 3.0 µM avidin Alexa Fluor 488 conjugate in 100 mM MES with initial pH of 5.15; applied potential of 7.0 V; measured current of 0.8 mA; concentration of Tween 20 was 0.5% (v/v).

In this work, we have been able to demonstrate that a nitrocellulose membrane can be used for the simple IEF not only as a basic proteomic analytical tool but also as an on-line sample pre-conditioning system. However, for future applications, significant improvements are still

necessary. Approaches could include the use of a mixture of buffers with different pKa to get a shallower pH gradient, thermal conductors to suppress the heat produced by a high potential, and different material and geometrical arrangements to avoid the evaporation.

SP4 Concluding remarks: It is demonstrated in this work that IEF without carrier ampholytes or gel with IPG can be simply performed on commercially available porous nitrocellulose membranes. Applying a potential to the membranes resulted in pH gradients generated by the electrolysis of water in the supporting electrolyte and/or other charged species such as proteins. It is possible to increase resolving power compared to closed microfluidic devices since electrolysis bubbles generated at the electrodes are not trapped in the membrane due to its porous structures being open to the outside environment. This method does not require a peristaltic pump to load the sample due to capillary force of the membrane, indicating a potential for the simplification of the system.

For the separation and concentration of the tested protein conjugates, the required times were about 2~5 min and condensed bands were observed at the region corresponding to the respective *pI* values of the protein conjugates. Although more concentrated tight bands should be formed for effective IEF systems, this work represents an initial attempt to demonstrate a simple and inexpensive method for the differentiation of complex biological samples in a nitrocellulose membrane. In further studies, the paper-based IEF technique will be tested to develop a sample pre-conditioning system of a paper-based analytical device.

SP5 Acknowledgements: Research reported in this work was supported by NIAID of the National Institutes of Health under award number 1R01AI096184-01. The content is solely the responsibility of the authors and does not necessarily represent the official views of the National Institutes of Health. This study was also supported by the Japan Student Services Organization.

SP6 References:

[1] Giordano, B. C., Burgi, D. S., Hart, S. J., Terray, A., *Anal. Chim. Acta* **2012**, 718, 11-24.

[2] Sommer, G. J., Hatch, A. V., *Electrophoresis* **2009**, 30, 742-757.

[3] Lion, N., Rohner, T. C., Dayon, L., Arnaud, I. L., et al., *Electrophoresis* **2003**, 24, 3533-3562.

[4] Macounova, K., Cabrera, C. R., Yager, P., *Anal. Chem.* **2001**, 73, 1627-1633.

[5] Görg, A., Obermaier, C., Boguth, G., Harder, A., et al., *Electrophoresis* **2000**, 21, 1037-1053.

[6] Cabrera, C. R., Yager, P., *Electrophoresis* **2001**, 22, 355-362.

[7] Macounova, K., Cabrera, C. R., Holl, M. R., Yager, P., *Anal. Chem.* **2000**, 72, 3745-3751.

[8] Cabrera, C. R., Finlayson, B., Yager, P., *Anal. Chem.* **2000**, 73, 658-666.

[9] Thormann, W., Caslavska, J., Mosher, R. A., *Journal of Chromatography A* **2007**, 1155, 154-163.

[10] Steinmann, L., Mosher, R. A., Thormann, W., *Journal of Chromatography A* **1996**, 756, 219-232.

[11] Yetisen, A. K., Akram, M. S., Lowe, C. R., *Lab Chip* **2013**, 13, 2210-2251.

[12] Martinez, A. W., Phillips, S. T., Whitesides, G. M., Carrilho, E., *Anal. Chem.* **2010**, 82, 3-10.

[13] Carrilho, E., Martinez, A. W., Whitesides, G. M., *Anal. Chem.* **2009**, 81, 7091–7095.

[14] Zhao, W., Ali, M. M., Aguirre, S. D., Brook, M. A., Li, Y., *Anal. Chem.* **2008**, 80, 8431–8437.

[15] Martinez, A. W., Phillips, S. T., Butte, M. J., Whitesides, G. M., *Angew. Chem., Int. Ed.* **2007**, 46, 1318-1320.

[16] Dungchai, W., Chailapakul, O., Henry, C. S., *Anal. Chem.* **2009**, 81, 5821-5826.

[17] Holcomb, R. E., Kraly, J. R., Henry, C. S., *Analyst* **2009**, 134, 486-492.

[18] Tobjörk, D., Österbacka, R., *Advanced Materials* **2011**, 23, 1935-1961.

[19] Harrington, M. G., Lee, K. H., Bailey, J. E., Hood, L. E., *Electrophoresis* **1994**, 15, 187-194.

[20] Seshi, B., Raja, K., Chandramouli, K., *Clinical Proteomics* **2011**, 8, 10.

[21] Duša, F., Šlais, K., *Electrophoresis* **2013**, 34, 1519-1525.

[22] Duša, F., Křenková, J., Moravcová, D., Kahle, V., Šlais, K., *Electrophoresis* **2012**, 33, 1687-1694.

[23] Stastna, M., Slais, K., *Electrophoresis* **2010**, 31, 433-439.

[24] Corstjens, H., Billiet, H. A. H., Frank, J., Luyben, K., *Electrophoresis* **1996**, 17, 137-143.

[25] McDonagh, P. F., Williams, S. K., *Microvascular Research* **1984**, 27, 14-27.

[26] Wehr, T., Rodriguez-Diaz, R., Zhu, M., Chromatographic Science Series, Marcel Dekker, New York **1999**, Vol. 80, pp 131-233.

VITA

KOJI ABE

EDUCATION

Ph.D., Bioengineering, August 2018, University of Washington, Seattle, WA, USA
"Increased sensitivity for lateral flow immunoassays through signal amplification methods"

M.S., Analytical Chemistry, March 2010, Keio University, Yokohama, Japan
"Inkjet-printed paperfluidic sensing device"

B.S., Applied Chemistry, March 2008, Keio University, Yokohama, Japan
"Inkjet-printed microfluidic multianalyte chemical sensing paper"

RESEARCH EXPERIENCE

Ph.D. Research, Department of Bioengineering, University of Washington
Seattle, WA September 2012 – present

Medical device development, Department of Catheter Development, Terumo Corporation
Shizuoka, Japan April 2010 – May 2012

M.S. and B.S. Research, Department of Applied Chemistry, Keio University
Yokohama, Japan April 2007 – March 2010

PUBLICATIONS

- **K. Abe** et al., "Increased sensitivity for lateral flow tests through signal amplification by isothermal strand displacement amplification (LFT-iSDA)", *PLOS ONE*, under review.
- KG. Shah, **K. Abe** et al., "Mobile phone ratiometric imaging enables highly sensitive fluorescence lateral flow immunoassays without external optical filters", *Anal. Chem.*, **2018**, 90 (11), 6967.
- S. Huang, **K. Abe** et al., "Disposable Autonomous Device for Swab-to-Result Diagnosis of Influenza", *Anal. Chem.*, **2017**, 89 (11), 5776.
- **K. Abe** et al., "Inkjet-Printed Paperfluidic Immuno-Chemical Sensing Device", *Anal. Bioanal. Chem.*, **2010**, 398(2), 885.
- **K. Abe** et al., "Inkjet-Printed Microfluidic Multianalyte Chemical Sensing Paper", *Anal. Chem.*, **2008**, 80, 6928.

SELECTED ORAL PRESENTATION AT PROFESSIONAL MEETINGS

- MicroTAS 2016 Dublin, Ireland, October 9-13, 2016, "A disposable swab-to-result influenza rapid test device based on a 2-dimensional paper network".

SELECTED AWARDS

- 2010, "outstanding graduate research activities", Graduate School of Integrated Design Engineering at Keio University